UCSF
UC San Francisco Electronic Theses and Dissertations

Title
Extrathymic Aire-Expressing Cells

Permalink
https://escholarship.org/uc/item/74m9h40d

Author
Gardner, James Morgan

Publication Date
2010

Peer reviewed|Thesis/dissertation

eScholarship.org Powered by the California Digital Library
University of California

Extrathymic *Aire*-Expressing Cells

by

James Morgan Gardner

DISSERTATION

Submitted in partial satisfaction of the requirements for the degree of

DOCTOR OF PHILOSOPHY

in

Genetics

in the

GRADUATE DIVISION

of the

[redacted]

Acknowledgements

I would like to thank my parents for their unconditional love and support.

Mark Anderson, for his generous and enthusiastic guidance, patience, and thoughtful mentorship.

Art Weiss and Jason Cyster for their wisdom and kindness.

The members of the Anderson Lab for help, advice, and friendship; in particular Todd Metzger, who contributed significantly to many experiments.

And Helen, for everything else.

Portions of Chapter I are modified from"The Mouse Model of APS-1," J.M. Gardner and M.S. Anderson, from *Immunoendocrinology: Scientific and Clinical Aspects*, ed. G. Eisenbarth, 1st. ed. 2010.

Chapter II is modified from "Deletional tolerance mediated by extrathymic Aire-expressing cells" J.M. Gardner et al., *Science* 2008;321: 843-7

Chapter III is a modified from "Prevention of Autoimmune Diabetes by Self-Antigen Expression in Extrathymic Aire-Expressing Cells" J.M. Gardner et al., submitted manuscript.

Extrathymic *Aire*-Expressing Cells

James Morgan Gardner

Abstract

Clonal diversity within the adaptive immune system, while endowing organisms with the ability to respond to a broad range of potential pathogens, presents a substantial risk for autoimmunity. Numerous complementary mechanisms have evolved to prevent such deleterious outcomes, and to establish and maintain appropriate tolerance to self. Medullary epithelial cells of the thymus play an essential role in this process by displaying a diverse set of tissue-specific antigens via a mechanism dependent on the Autoimmune regulator (*Aire*) gene. Here we describe a discrete population of extrathymic *Aire*-expressing cells (eTACs) in the secondary lymphoid organs. We show that *Aire* regulates a diverse range of tissue-specific antigen genes in eTACs distinct from those presented in the thymus. To define a potential role for this population in immune tolerance, we demonstrate that self-antigen expression in eTACs is sufficient to prevent T cell-mediated autoimmune diabetes mediated by CD4+ or CD8+ T cells. We demonstrate that such tolerance is established via anergic or deletional mechanisms for CD4+ or CD8+ cells, respectively, and does not require the presence or induction of regulatory populations. Further, we show that tolerance induction by eTACs is highly resistant to conversion to immunogenicity. Finally, we describe the development of a novel transgenic mouse model for depletion of mTECs and eTACs, and suggest that the absence of these populations predisposes to autoimmunity. Together this work identifies self-antigen expressing eTACs as a population with potential significance in both physiologic and therapeutic maintenance of self-tolerance.

Table of Contents

Title Page i

Chapter I: *Aire* and Immune Self-Tolerance 1

- Adaptive immunity and self-tolerance 2
- *Aire* is essential for immune self-tolerance 6
- The mechanism of *Aire* deficiency 17
- Extrathymic *Aire* and TSA expression 37

Chapter II: Identification and Characterization of Extrathymic Aire-Expressing Cells 48

- Introduction 49
- Results 49
- Discussion 77
- Materials and Methods 79

Chapter III: Self-Antigen Expression in eTACs Prevents Autoimmunity 91

- Introduction 92
- Results 94
- Discussion 131
- Materials and Methods 137

Chapter IV: The *AireDTR* Mouse and Autoimmunity 149

- Introduction 150
- Results 151

Discussion 172
Materials and Methods 177
Chapter V: Discussion 181
eTACs exist in the secondary lymphoid organs and express diverse TSAs 183
eTAC interactions with T cells are tolerogenic and prevent autoimmunity 185
The *AireDTR* mouse: a tool for the study of immune tolerance 186
The mechanism of eTAC-mediated T-cell tolerance 188
eTACs and Tregs 191
The role of Aire in eTACs 192
The identity and origin of eTACs 194
Why eTACs? 195
Theraputic self-antigen expression in eTACs? 197
Appendix: Selected Protocols 203
Thymectomy/Thymic Transplant/Bone Marrow Chimerism 204
Stromal Preparation for FACS 218

List of Tables

Table S2.1: Genes significantly upregulated in *Aire*$^{+/+}$ vs. *Aire* $^{-/-}$ eTACs 67

Table S2.2: Genes significantly downregulated in *Aire*$^{+/+}$ vs. *Aire* $^{-/-}$ eTACs........ 69

List of Figures

Chapter 1

Figure 1.1. The mouse and human Aire protein and gene 8

Figure 1.2. Histology of *Aire*-knockout tissues shows multiorgan lymphocytic infiltrate and tissue destruction 12

Figure 1.3. Organ-specific disease incidence in APS-1 patients and characterized *Aire*-deficient mouse strains 15

Figure 1.4. *Aire* regulates TSA expression in mTECs, preventing escape of tissue-specific autoreactive thymocytes 21

Chapter 2

Figure 2.1. The *Adig* transgene recapitulates *Aire* expression in the thymus and mediates negative selection of autoreactive T cells 50

Figure S2.1. The Aire-driven *Igrp-Gfp* transgene introduces a novel antigen into the thymus which faithfully reflects thymic *Aire* expression and causes deletion of cognate T cells 53

Figure 2.2. *Aire*-expressing cells exist in the secondary lymphoid organs 56

Figure S2.2. Extrathymic *Aire* BAC-driven *Igrp-gfp* is expressed selectively in lymphoid structures 58

Figure S2.3. Transgenic *Igrp-gfp* is expressed by both hematopoietic and radioresistant populations in the secondary lymphoid organs 60

Figure S2.4. eTACs do not express markers characteristic of other lymphoid stroma 62

Figure 2.3. *Aire* regulates the expression of a unique set of tissue-specific antigens in eTACs 65

Figure 2.4. eTACs directly interact with autoreactive lymphocytes and mediate deletional tolerance 73

Figure S2.5. The relative absence of 8.3 T cells after adoptive transfer into *Adig* transgenic mice is not due to egress 75

Chapter 3

Figure 3.1. The *Adbig* transgene recapitulates *Aire* expression in mTECs and eTACs 96

Figure S3.1. GFP+ mTECs and eTACs from *Adbig* mice are significantly enriched for *Aire* transcript 99

Figure 3.2. eTACs directly interact with CD4+ T cells and induce functional T-cell unresponsiveness 102

Figure S3.2. Efficiency of reconstitution in wildtype and *Adbig* NOD mice lethally irradiated and reconstituted with MHC II-/- bone marrow 104

Figure 3.3. Cognate antigen expression in eTACs prevents BDC2.5-mediated insulitis and autoimmune diabetes 108

Figure 3.4. eTAC-induced self-tolerance in BDC2.5 T cells is cell-intrinsic and does not require the presence of regulatory T cell populations 111

Figure S3.3. Effeciency of depletion of FoxP3+ regulatory T cells in FoxP3-DTR BDC2.5 mice 114

Figure 3.5. eTAC-mediated tolerance induction in BDC2.5 T cells is not abrogated by CD40/TLR stimulus or PD-L1 blockade 117

Figure S3.4. Anti-PD-L1 treatment regimen induces rapid diabetes onset in wildtype NOD mice 120

Figure 3.6. αDEC1040 treatment induces proliferation but not tolerance of BDC2.5 T cells 123

Figure 3.7. IGRP expression in eTACs leads to peripheral deletion of 8.3 T cells and prevention of CD8-mediated diabetes 127

Figure S3.5. Efficiency of reconstitution in *Adig* mice lethally irradiated and reconstituted with Thy1.1+ *8.3* bone marrow 129

Chapter 4

Figure 4.1. The *AireDTR* transgene is expressed in mTECs and eTACs 153

Figure 4.2. DT administration induces effective depletion of *AireDTR* transgene-expressing cells in the thymus and secondary lymphoid organs 156

Figure 4.3. Kinetics of DT depletion and recovery 159

Figure 4.4. Continuous depletion of *Aire*-expressing cells in the thymus induces complete loss of medullary epithelium and architecture 164

Figure 4.5. Thymocyte profile is globally normal in “amedullary” *AireDTR* thymi, but shows decreased CD4+ Tregs 167

Figure 4.6. *AireDTR* NOD mice treated with DT from weeks 1-3 do not show growth retardation or mortality but are predisposed to autoimmunity 170

Chapter I

Aire and Immune Self-Tolerance

I resist any thing better than my own diversity,

Breathe the air but leave plenty after me

-Walt Whitman, Song of Myself

1. Adaptive immunity and self-tolerance

Multicellularity in living organisms permits astounding degrees of specialization, but requires a continuous negotiation between individual cells tethered to a common fate. One of the most important challenges for multicellular organisms is to define the collective "self," and to defend that self from invasion by "non-self" pathogens in order to avoid destruction by parasitism, neoplasm, and infection. The immune system is responsible identifying and neutralizing such non-self agents, while trying to avoid attacking one's own diverse and specialized tissues. The immune system thus serves to protect organisms from external microbial threats, while remaining "tolerant" of its own varied constitutive parts. Furthermore, while increasing size, complexity, and longevity among multicellular organisms provide numerous advantages, they also pose unique problems: as an organism's lifespan increases, the number and diversity of pathogens it may encounter, and the number of generations during which those pathogens may evolve in the organism's lifetime increase dramatically. Long-lived organisms thus suffer an acute adaptive handicap with regard to defense against the organisms that try to invade them—they lack the ability to evolve quickly, and therefore to adapt genetically to the incredible and ever-changing diversity of potential pathogens.

The adaptive immune system represents an elegant solution to this problem—the ability to generate islands of genetic hypervariability within specific populations of somatic cells, and then select from these variants—that allows the system both to generate staggering diversity and to constantly adapt to novel microbial variants. While many organisms ranging from plants to insects have some forms of innate immune protection involving phagocytic cells with fixed receptor specificity, it appears that only vertebrates seem to have evolved such a complex system for responding to the ever-changing microbial environment *(1)*.

Functionally, the adaptive immune system consists of clonal populations of antigen-specific cells each with their own unique cell-surface receptor. Two principal cell types constitute the adaptive immune system, B and T cells. B cells recognize antigen through membrane-bound immunoglobulin in the form of the B-cell receptor (BCR), and upon activation they proliferate and produce antibodies, generating a soluble immune response against free (extracellular) pathogens. T cells recognize antigen through the T-cell receptor (TCR), and in contrast to B cell-generated immunoglobulins which recognize free soluble antigen, the TCR recognizes antigen displayed in the context of specialized antigen presentation molecules termed multiple histocompatibility (MHC) proteins. T cells thus respond principally to intracellular pathogens or to pathogens that have been consumed, processed, and presented by other antigen-presenting cells (APCs).

The singular feature of adaptive immunity which endows it with the ability to respond to such an diverse range of potential pathogens is that the genes encoding the BCR and TCR are themselves composed of multiple cassettes, and these cassettes undergo somatic and permanent BCR or TCR gene rearrangement during B and T cell development, respectively. A number of complementary mechanisms aid in generating additional and truly random diversity in the antigen-binding regions of the BCR and

TCR during gene rearrangement *(2)*, the end result of which is random and irreversible gene rearrangement endowing each T or B cell with a unique receptor. The system as a whole therefore generates a population of immune cells with an almost limitless diversity of antigen-specificity, composed of individual B and T cell clones each with the ability to recognize a single unique antigen. As these cells are selected to survive, divide, and differentiate, they and all their daughter cells retain the same receptor, and thus the same antigen-specificity. This "clonal selection" paradigm, which developed gradually through the work of numerous investigators ranging from Paul Erlich *(3)*, to Niels Jerne *(4)*, David Talmadge *(5)*, and F. Macfarlane Burnet *(6)*, has come to centrally define our understanding of adaptive immunity and immunologic tolerance.

However it is precisely this combinatorial diversity within the adaptive immune system that also constitutes the most substantive risk for autoimmunity. While random somatic generation of B- and T-cell receptors affords the immune system with the ability to respond to diverse pathogens, it also generates an enormous number of B and T cells with potentially autoreactive receptors that recognize some component of the host organism itself. Thus, in addition to the complex machinery needed to generate this receptor diversity, the adaptive immune system also requires an equally complex set of mechanisms to properly educate immune cells how to distinguish "self" from "nonself." For B cells this education occurs initially in the bone marrow, but for T cells, the primary site of this education is the thymus.

T-cell progenitors derived from bone marrow hematopoietic stem cells migrate to the thymus, a mediastinal organ essential for T-cell development and maturation. In the thymus, individual T-cell progenitors (called thymocytes) sequentially rearrange their TCR genes to generate a random receptor and undergo selection, both positively to select *for* those cells that have generated a functional MHC-binding receptor, and negatively to select *against* those T cells whose functional receptors strongly recognize self-antigen. The process of negative selection takes place preferentially in the medulla, where thymocytes with self-reactive TCRs encounter self-antigen on specialized antigen-presenting cells (APCs) and either die or become repurposed as regulatory T cells. While negative selection of self-reactive thymocytes has been characterized and understood for quite some time, until recently it was unknown precisely how this process might account for the breadth of immune self-tolerance against the entire diversity of the body's proteome. For example, while this process might effectively delete developing thymocytes specific for ubiquitous self-antigens (like actin or ribosomal subunit proteins) present in all cells, it was more challenging to imagine how the same process might occur for T cells reactive against one of an organism's diverse and specialized tissue-specific antigens (TSAs) like insulin, thyroglobulin or interphotoreceptor binding protein (IRBP) whose expression are highly restricted to single peripheral tissues in the body.

This suggested that perhaps many potentially autoreactive T cells escaped thymic negative selection simply because of the absence of exposure to cognate antigen during thymic development, and thus that the burden of maintaining immune tolerance fell principally to peripheral mechanisms like second-signal requirement for activation, the presence of inhibitory co-stimulatory molecules, regulatory T cells, and antigen sequestration in sites of immune privilege.

While such mechanisms are clearly indispensible for the maintenance of tolerance, recently a number of lines of evidence have converged to suggest that expression of diverse TSAs in centralized sites of T-cell education might also play an essential role in the maintenance of tolerance. Surprisingly, the principal set of findings that codified this paradigm were related to the genetic mapping of a rare monogenic autoimmune disease in humans, and the resultant discovery of the essential role played by this gene in human and mouse immunologic self-tolerance.

2. *Aire* is essential for immune self-tolerance

A. APS-1 in humans: a monogenic autoimmune disease caused by *AIRE* mutations

Autoimmune polyglandular syndrome type 1 (APS-1) is a rare autoimmune disease characterized principally by immune-mediated destruction of the endocrine organs. Clinically, the diagnosis is made by meeting two of the following three criteria—hypoparathyroidism, adrenal insufficiency, and mucocutaneous candidiasis. In addition, most APS-1 patients exhibit a diverse range of other autoimmune symptoms including type I diabetes, gonadal atrophy, hypothyroidism, autoimmune hepatitis, and autoimmune pneumonitis, among others *(7, 8)*. The disease generally manifests during childhood, but the diverse symptoms may emerge throughout a patient's life. Though the precise manifestations vary from individual to individual, and even between siblings *(7)*, the overall clinical picture is one of a profound failure in the immune system's ability to properly distinguish self- from non-self-tissues, and a consequently devastating attack on primarily the endocrine organs.

While the manifestations of this disease are diverse, the genetics are uniquely simple. APS-1 is an autosomal recessive disease caused by mutations in a single gene, the autoimmune regulator (*AIRE*). Though rare, with an estimated total of 500 cases worldwide, APS-1 has uniquely elevated frequency among genetically isolated groups including Sardinians (1/14,400), Iranian Jews (1/9000), and Finns (1/25000) *(9)*. Linkage analysis of families with the disorder led to the identification of *AIRE (10, 11)*, with almost all affected APS-1 patients containing either homozygous or compound heterozygous mutations of the gene. To date over 40 such mutations have been identified, the majority of which are either premature stop codons or large exon deletions *(12)*.

The *AIRE* gene itself encodes a ~57-kDa protein of 545 amino acids comprised of multiple domains common to transcriptional regulators and nuclear proteins **(Figure 1.1)**. Located on chromosome 21 in humans and chromosome 10 in mice, *Aire* is a single-copy gene whose orthologues have been identified in all gnathostome (jawed vertebrate) classes except the cartilaginous fish, and whose sequence and structure is broadly conserved between these classes *(13)*. Suggestively, this places the emergence of the *Aire* gene approximately 500 million years ago, roughly coincident with the

Figure 1.1. The mouse and human Aire protein and gene.

Figure 1.1

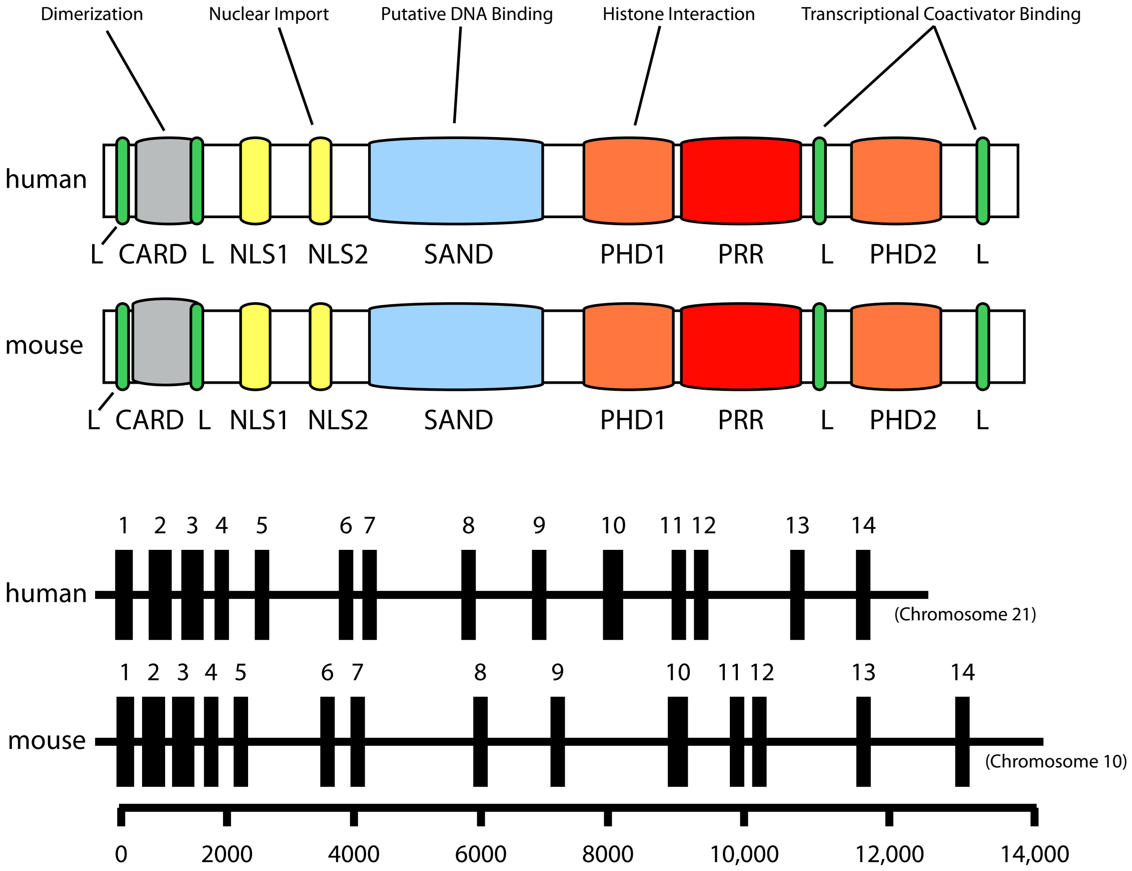
Dimerization
Nuclear Import
Putative DNA Binding
Histone Interaction
Transcriptional Coactivator Binding
human
L
CARD
L
NLS1
NLS2
SAND
PHD1
PRR
L
PHD2
L
mouse
L
CARD
L
NLS1
NLS2
SAND
PHD1
PRR
L
PHD2
L
1
2
3
4
5
6
7
8
9
10
11
12
13
14
human
(Chromosome 21)
1
2
3
4
5
6
7
8
9
10
11
12
13
14
mouse
(Chromosome 10)
0
2000
4000
6000
8000
10,000
12,000
14,000

emergence of the adaptive immune system *(14)*. This relationship between *Aire* and the adaptive immune system may speak to its central role in maintaining self-tolerance in the adaptive immune system.

The murine *Aire* gene, in particular, is highly homologous to the human gene, sharing all major protein domains, all exons, and having 71% nucleotide and 73% amino-acid sequence homology **(Figure 1.1)** *(15, 16)*. As such, and because the mouse is such a well characterized system for the study of the immunology, it has proven an attractive candidate for modeling human APS-1, and for studying the mechanisms of *Aire* biology and immune self-tolerance in general.

B. The mouse model of APS-1 broadly recapitulates the autoimmunity observed in human APS-1

Due to the significant interest in the mechanisms underlying APS-1 upon the identification of the *AIRE* gene and its murine homologue *Aire*, a number of independent groups generated *Aire*-knockout mice. In all cases, these mice exhibited significant autoimmunity including multi-organ lymphocytic infiltration, autoreactive antibodies in serum, and tissue destruction, though the precise phenotypes differed somewhat depending on the strain and the influence of genetic background.

The first *Aire*-knockout mouse was generated by insertion of a termination codon in exon 6, replicating a common mutation observed in APS-1 patients *(17)*. This knockout, though generated in a relatively autoimmune-resistant Sv/129/C57BL/6 mixed background, still exhibited both multiorgan lymphocytic infiltration and the presence of autoreactive antibodies in serum, as well as infertility among both males and females. Specific endocrine organs including the ovaries and liver showed distinct lymphocytic infiltrates, and consistent with human APS-1, adrenal glands were absent in a significant portion of the *Aire*-knockout mice suggesting their complete destruction. Further, *Aire*-knockout mouse serum demonstrated antibody reactivity against the liver, testis, pancreas, and adrenal glands. A second *Aire*-knockout mouse, also in the Sv/129/C57BL/6 mixed background, was generated by targeted deletion of exon 2 of the murine *Aire* gene which resulted in a frameshift early termination *(18)*. These mice demonstrated lymphocytic infiltrates of the salivary gland, ovary, retina, thyroid, liver, and stomach, and serum autoantibodies were also detected against the salivary gland, ovary, retina, thyroid, pancreas, and stomach **(Figure 1.2)**. Further, this study showed a distinct correlation between organ-specific autoantibodies and lymphocytic infiltrates of that organ. Finally a third group generated a unique *Aire* knockout by targeted deletion of a region spanning from exon 5 to exon 12, removing the sequences coding for the SAND domain as well as both PHD domains *(19)*. This third knockout showed a similar phenotype of infertility and autoimmune lymphocytic infiltrates of the salivary and lacrimal glands, as well as some infiltration of the pancreas and stomach.

Overall, these overlapping models suggest a consistent picture of the *Aire*-knockout mouse as predisposed to autoimmunity that generally resembles the diverse but organ-specific autoimmunity seen in APS-1 patients. As in APS-1 patients, *Aire*-

Figure 1.2. Histology of *Aire*-knockout tissues shows multiorgan lymphocytic infiltrate and tissue destruction (***images courtesy of J. DeVoss***).

Figure 1.2

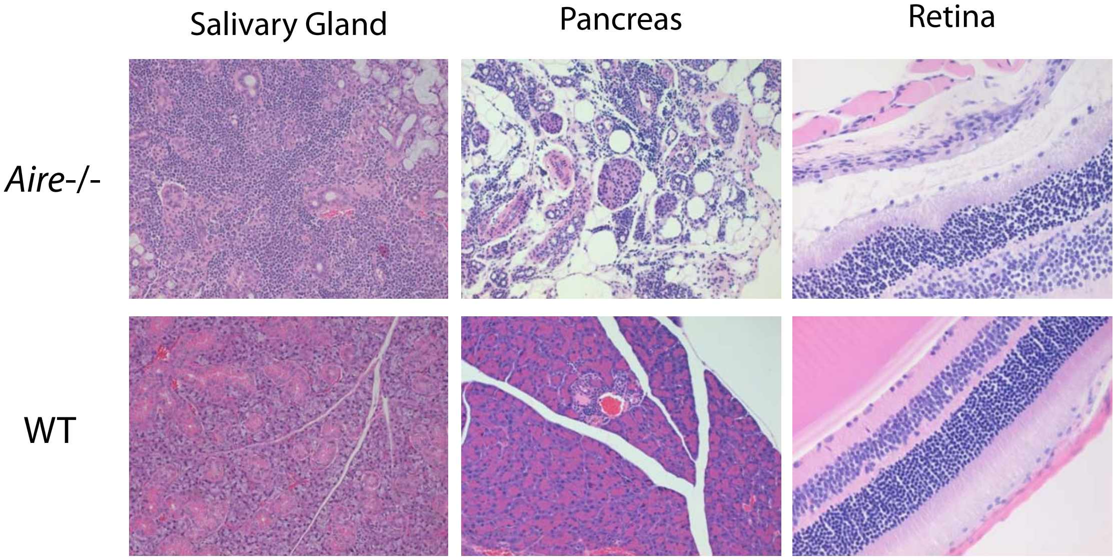
Salivary Gland
Pancreas
Retina
Aire-/-
WT

knockout mice begin with relatively mild disease that spreads in both the number of targeted organs and the severity of tissue damage. Further, the disease seen in *Aire*-knockout mice is both disseminated and organ-specific—while numerous and diverse organs can be targeted, specific organs are affected while others are spared, and the organs targeted differ from individual to individual or strain to strain.

The influence of genetic modifier loci on the disease phenotype of *Aire*-knockout mice was further demonstrated when the *Aire* mutation was backcrossed into diverse genetic backgrounds ***(20)***. In autoimmune-prone strains like the non-obese diabetic (NOD) mouse, for example, lymphocytic infiltration affects a diverse set of organs including the retina, cornea, stomach, salivary gland, lung, liver, prostate, ovary, pancreas, and thyroid gland, while only a small subset of these organs (retina, salivary gland, lung, and prostate) are infiltrated in the autoimmune-resistant C57BL/6 strain **(Figure 1.3)**. Further, *Aire*-knockout NOD mice experience wasting and die by 15 weeks of age, while *Aire*-knockout C57BL/6 mice do not waste and have survival curves similar to wildtype. Thus, the presence or absence of other genetic modifiers affects both the spectrum of organs targeted and the severity of tissue damage.

In this sense, the *Aire*-knockout mouse broadly reflects the heterogeneity of disease manifestations in human APS-1, where genetic modifiers and environmental factors likely influence the spectrum of affected organs (though it should be noted that the exacerbation or elimination of innate immune stimuli appears to have little to no discernable effect on the spectrum of disease in *Aire*-knockout mice ***(21)***). However,

Figure 1.3. Organ-specific disease incidence in APS-1 patients and characterized *Aire*-deficient mouse strains ***(7, 8, 20, 50, 89, 90; M. Su, J. DeVoss, M. Cheng, T. Shum, personal communication)***.

Figure 1.3

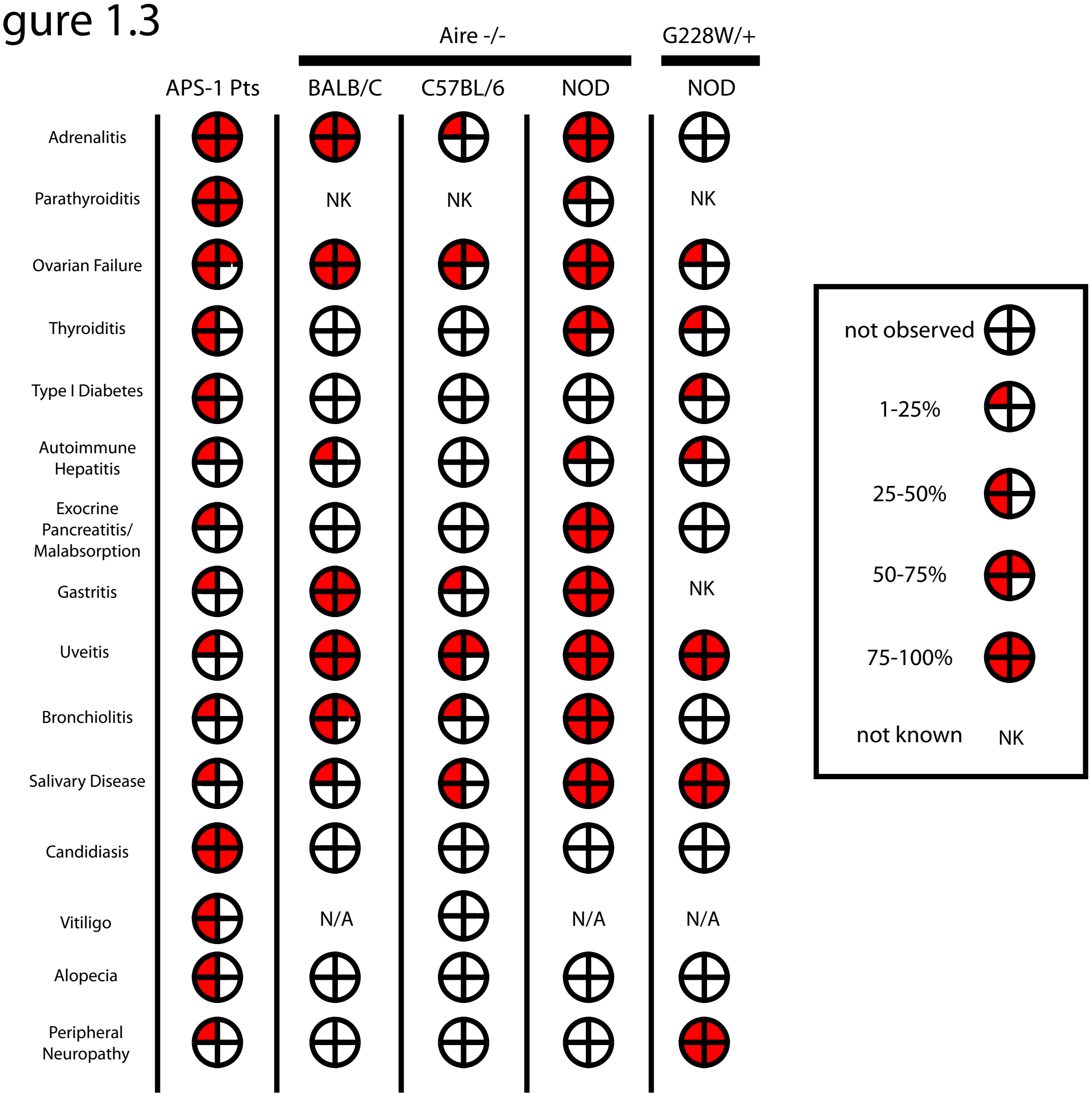
Aire -/-
G228W/+
APS-1 Pts
BALB/C
C57BL/6
NOD
NOD
Adrenalitis
Parathyroiditis
Ovarian Failure
Thyroiditis
Type I Diabetes
Autoimmune Hepatitis
Exocrine Pancreatitis/ Malabsorption
Gastritis
Uveitis
Bronchiolitis
Salivary Disease
Candidiasis
Vitiligo
Alopecia
Peripheral Neuropathy
NK
N/A
not observed
1-25%
25-50%
50-75%
75-100%
not known
NK

some of the targeted organs clearly seem to differ between humans and mice; for example, the endocrine pancreas is targeted in many APS-1 patients but spared in mice, while the retina is targeted in mice but rare in humans. Indeed even among those organs that are shared between man and mouse, the precise antigens recognized may in fact differ between the species *(22)*. Some disease manifestations of APS-1 in humans are never observed in mice, for example mucocutaneous Candidiasis, though this may be partly explained by the fact that Candida is a commensal organism in humans but not in mice *(23, 24)*. Regardless of these differences, however, the mouse model of APS-1 provides a broad recapitulation of the autoimmunity seen in the human disease, and therefore presents an invaluable tool to learn about both the pathogenesis of this disease as well as more fundamental mechanisms of immune self-tolerance.

3. The mechanism of *Aire* deficiency

Aire's expression in the thymus provides clues to its function

While the phenotypic characterization of *Aire*-knockout mice demonstrated a broad recapitulation of the autoimmunity seen in APS-1, this still did not provide immediate answers to the fundamental pathogenesis of the disease. Indeed, while the described *Aire*-knockout mouse models all reported autoimmune sequellae, they also reported few or no detectable changes in the immune system itself. The number of thymocytes and lymphocytes, the ratios of CD4+ and CD8+ T cells and B cells, the activation and death of thymocytes, the responsiveness of T cells to *in vitro* stimulation, and the number and function of regulatory T cells are all grossly normal in *Aire*-knockout mice *(17-19)*.

One clue to *Aire*'s function, however, lay in its highly tissue-restricted expression pattern. While early attempts to characterize this expression were somewhat discordant, all concurred that *Aire* was most highly expressed in the thymus *(15, 25, 26)*. As the organ in which T cells develop and are selected, the thymus plays an important role in shaping a T-cell repertoire. As discussed, because the adaptive immune system generates individual receptors for each T-cell precursor essentially at random through V(D)J recombination, many T-cell precursors are born with either a completely nonfunctional receptor or with a receptor that recognizes self. One of the principal functions of the thymus, therefore, is to provide permissive signals for those developing T cells that express a functional T-cell receptor (positive selection), while eliminating those that recognize self-antigen (negative selection), or diverting such self-reactive T cells to a regulatory lineage *(27, 28)*.

As discussed, the thymus therefore shoulders a heavy burden in trying to prevent the development of self-reactive effector T cells—it must eliminate not just T cells that recognize ubiquitous self-antigens expressed in all cells, but also those T cells that might recognize tissue-specific antigens (TSAs). Without some mechanism to account for this, T cells specific for such antigens might escape thymic negative selection simply because the self-antigen was sequestered in the target organ. Numerous complementary systems could, and do, exist to prevent the development and activation of such tissue-specific autoreactive T cells, including the migration of antigen-presenting cells from the periphery back to the thymus *(29)*, the peripheral development of regulatory T cells *(30)*, and the inactivation or anergy of those naïve T cells that undergo inappropriate activation upon exposure to self-antigen *(reviewed in 31)*. However the thymus also contributes to tolerance against TSAs through an elegant mechanism partially dependent on *Aire.*

Aire-expressing medullary thymic epithelial cells are unique sources of TSA expression

Unlike most epithelium, thymic epithelial cells (TECs) do not form a continuous barrier or define a topological space; rather, they are interdigitated among the developing T-cell precursors throughout the entire parenchyma of the thymus. Broadly speaking, cortical thymic epithelial cells (cTECs) play an important role in the positive selection of T cell precursors, while medullary epithelial cells (mTECs) play a role in the negative selection of those T cells that recognize self antigen *(reviewed in 14)*. While ectopic expression of individual tissue-specific antigens like insulin in the thymus was first described more than a decade ago *(32, 33)*, until recently the scope of such TSA expression, its physiologic significance, and the cell populations responsible were unknown. Thus, the discovery that mTECs were in fact the principal cell population responsible for this thymic TSA expression, and that mTECs expressed thousands of such TSAs *(34)*, suggested that these cells might play an important role not only in tolerizing the immune system against ubiquitous antigens but also against many tissue-restricted ones as well. However this theory, while compelling, lacked evidence of physiologic relevance as no direct examples of autoimmunity caused by defects in thymic TSA expression were known.

The contemporaneous discoveries that APS-1 was caused by mutations in the *AIRE* gene, that mTECs were the source of TSA expression in the thymus, and that *AIRE* was highly expressed in mTECs led investigators to hypothesize that perhaps the autoimmunity observed in APS-1 patients and *Aire*-knockout mice resulted from a failure of tissue-specific antigen expression in the thymus *(18, 34)*. Indeed, using microarrays and quantitative PCR to compare TSA expression in mTECs from *Aire*-wildtype and *Aire*-knockout mice it was shown that *Aire* is required for mTECs to produce this diverse set of TSAs, and in the absence of *Aire* this reduction in expression of "peripheral self" in the thymus leads to autoimmunity in these mice *(18)*. Thus in *Aire*-knockout mice, mTECs are unable to promiscuously transcribe tissue-specific antigens like insulin, thyroglobulin, and interphotoreceptor retinoid-binding protein, and therefore T cells reactive against these antigens can escape thymic negative selection without ever seeing these antigens **(Figure 1.4)**. Further, loss of *Aire* in the thymic epithelium is sufficient to cause this autoimmunity, as transplantation of *Aire*-deficient thymic stroma into Nude mice (which lack a thymus due to mutation of the *FoxN1* gene) causes these mice to develop autoimmunity *(18)*.

To confirm that loss of thymic TSA expression in *Aire*-knockout mice leads directly to autoimmunity, additional studies have been done using *Aire*-dependent tissue-specific antigen promoters to drive expression of exogenous neo-antigens in the thymus and study negative selection of T-cell receptor transgenic T cells specific for those antigens in the presence and absence of *Aire*. For example, investigators used the insulin

Figure 1.4. *Aire* regulates TSA expression in mTECs, preventing escape of tissue-specific autoreactive thymocytes.

Figure 1.4

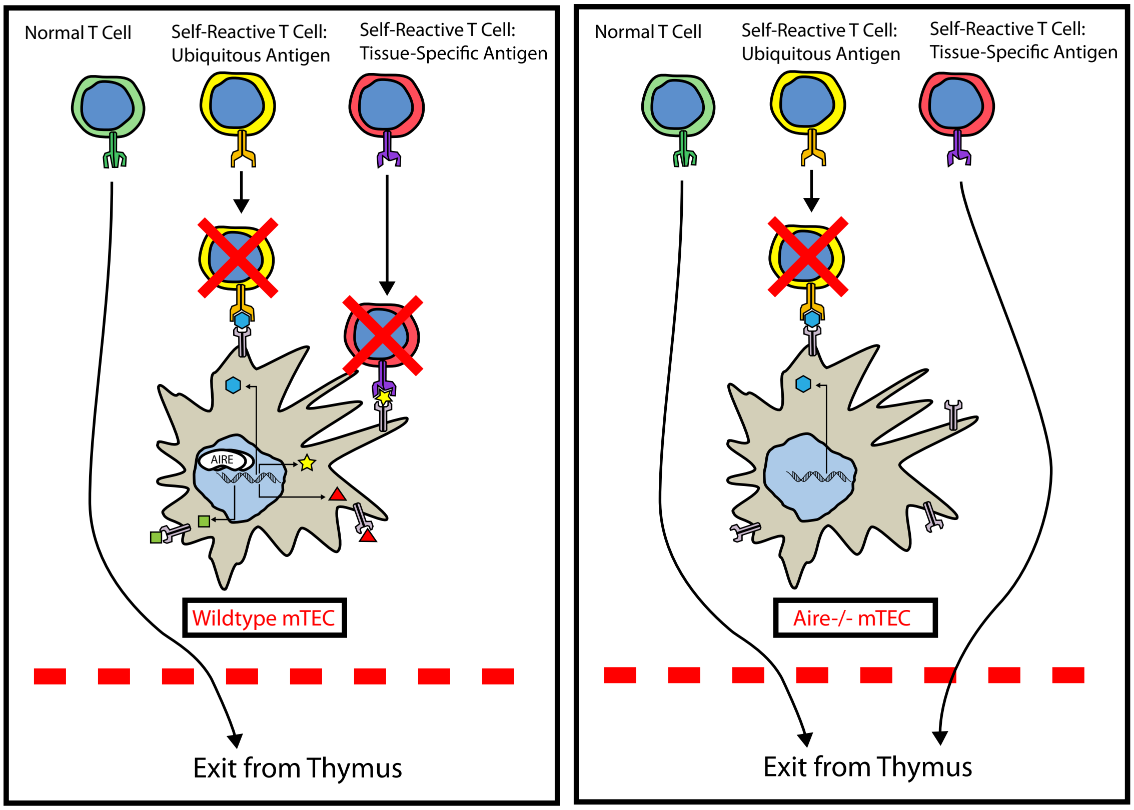
Normal T Cell
Self-Reactive T Cell: Ubiquitous Antigen
Self-Reactive T Cell: Tissue-Specific Antigen
AIRE
Wildtype mTEC
Exit from Thymus
Normal T Cell
Self-Reactive T Cell: Ubiquitous Antigen
Self-Reactive T Cell: Tissue-Specific Antigen
Aire-/- mTEC
Exit from Thymus

promoter to drive expression of hen egg lysozyme (HEL) in both the pancreas and the thymus, and then examined the thymic negative selection of HEL-specific T cells in *Aire*-wildtype and *Aire*-knockout mice *(35, 36)*. Because mTECs normally transcribe insulin at low levels in an *Aire*-dependent manner, these transgenic mice produce insulin promoter-driven HEL within the thymus, and when HEL-specific T cell precursors are introduced, they are negatively selected and die before leaving the thymus. However in the absence of *Aire*, mTECs no longer produce this insulin-driven HEL, and thus HEL-specific T cells do not undergo negative selection in the *Aire*-knockout thymus. Instead, these cells now mature normally and exit the thymus, encountering HEL protein in the pancreatic islets and causing autoimmune diabetes. Such transgenic approaches provide mechanistic insight into the breakdown of tolerance that occurs in the absence of *Aire*, offering clear evidence that autoimmunity in *Aire*-knockout mice can result from failures in thymic TSA expression.

It is important to note that while promiscuous expression of tissue-specific antigens in the thymus represents a large sample of the body's transcriptome, and *Aire* regulates a significant percentage of these TSAs, it is also clear that both these sets are incomplete—that some TSAs, like islet-specific glucose-6-phosphatase related protein (IGRP), a major autoantigen in type I diabetes, are not expressed at all in mTECs *(37)*, while others like C-reactive protein (CRP) from the liver, are clearly expressed in mTECs but in an *Aire*-independent fashion *(18)*. Indeed, mature mTECs themselves appear to promiscuously express at least 3000 TSA genes, of which *Aire* regulates perhaps

250-1000, in addition to other, non-TSA genes *(18, 38, 39)*. Thus *Aire* appears to regulate the thymic expression of a subset of the TSAs expressed in mTECs, and these TSAs themselves represent a subset of the body's total transcriptome. This incredibly diverse but incomplete representation of self in the thymus suggests, not surprisingly, that other complementary mechanisms must also be in place to help reinforce self-tolerance.

Such transcriptional de-regulation is itself a remarkable feat, as it requires uncoupling the normally tissue-restricted expression program of specific genes, allowing them all to be simultaneously expressed in this one remarkable cell population. Precisely how *Aire* functions to accomplish this is still not completely understood, though the molecular mechanism of Aire's action has been the subject of significant recent study.

The molecular mechanism of Aire function

Even before *Aire* was implicated as a regulator of tissue-specific antigen gene transcription in mTECs, the homology of its predicted domains to other known proteins **(Figure 1.1)** led investigators to speculate that it might act as a transcriptional regulator *(10, 11)*. Like other transcriptional regulators, Aire contains a nuclear localization sequence which is necessary *(40)* and sufficient *(41)* to target it to the nucleus; a caspase recruitment domain (CARD) involved in homodimerization *(42)*; four LXXLL nuclear receptor boxes that mediate interaction with transcriptional coactivators *(43)*; a SAND (Sp100, Aire, NucP41/P75, and Deaf1) domain whose other family members have

DNA-binding ability *(44)*; and two zinc-finger containing plant homeodomains (PHD1 and 2) that may be involved in histone binding *(45, 46)*.

The subcellular localization of Aire also provides clues that suggest it might act to regulate transcription. Immunofluorescent staining shows that Aire in mTECs localizes to the nucleus, specifically into punctate nuclear bodies *(47, 48)* that may associate with the nuclear matrix *(49)*. More specifically, Aire appears to localize within or adjacent to nuclear speckles, which are often sites of splicing, polyadenylation, capping, and other RNA processing, as well as sites of RNA polymerase II stabilization and elongation *(50)*. Indeed, Aire has been suggested to play a role in transcriptional elongation through recruitment of P-TEFb, a positive elongation factor *(51)*. Further, in *in vitro* assays Aire has been shown to interact with the transcriptional coactivator CBP, and to have direct and cooperative transcriptional transactivation capabilities *(52, 53)* as well as direct DNA-binding activity *(45, 54)*. However the relevance of these *in vitro* findings to Aire's function *in vivo* is still uncertain, and its role in directly binding to *cis*-acting regulatory sequences of target genes remains unclear. Further, genomic analyses of the thousands of *Aire*-regulated gene promoters have failed to identify any common sequence elements that might define a consensus binding site for Aire.

Because Aire exerts such large-scale effects on transcription of diverse genes across the genome, it has also been suggested that it may exert its effects epigenetically, perhaps by interacting with and modifying chromatin. Indeed, a number of groups have observed that *Aire*-regulated genes cluster into groups within a chromosome *(39, 55)*.

However, the clustering of *Aire*-regulated genes is not a simple case of broad transcriptional derepression. For example, in the casein gene cluster (normally expressed in mammary epithelium of lactating females but also in *Aire*-expressing mTECs), individual *Aire*-repressed genes sit between groups of *Aire*-induced genes, while other genes within the same cluster are unaffected by the presence or absence of *Aire* *(39)*. This suggests that while Aire may mediate large-scale epigenetic changes such as chromatin remodeling, such changes alone are not sufficient to explain its transcriptional regulatory effects.

Recent reports have also described potentially significant interaction between Aire's PHD1 domain and unmethylated histones. The importance of the PHD1 domain to Aire's function is underscored by the fact that it is highly conserved between species *(13)*, and is also the site of a number of deleterious point mutations in human APS-1 patients *(56)*. Furthermore, other PHD domains have been found in chromatin-associated proteins and these domains appear to bind histones in a manner that is sensitive to the methylation status of specific lysine residues on the histone *(57, 58)*. Indeed, these reports have now shown that the PHD1 domain of mouse and human Aire bind directly to Histone H3 and that methylation of this histone on lysine 4 inhibits interactions with Aire and Aire's ability to bind chromatin-associated DNA *(46, 59)*. Importantly, these groups have shown that transfected Aire directly binds to and upregulates expression of a number of TSA genes *in vitro*, that this effect is dependent on the histone-binding residues of its PHD1 domain, and that those genes upregulated by

Aire also show a higher ratio or unmethylated to methylated histone H3K4. This interaction provides an attractive rudimentary model for Aire's function, as unmethylated H3K4 is generally associated with sites of transcriptional repression. Thus, perhaps Aire employs histone methylation status to aid in targeting it to quiescent genomic regions to upregulate transcription of otherwise repressed TSA genes.

This hypothesis was supported and extended by a recent study extensively describing the binding partners of Aire through immunoprecipitation and mass spectroscopy *(60)*. While Aire binds to histones themselves, it also appears to interact with large multimolecular complexes that include chromatin modifying enzymes, transcriptional regulation machinery , DNA manipulation and repair enzymes (e.g. DNA-PK, TOP2a), nuclear transport proteins, and splicing/pre-mRNA processing machinery. The relative contributions of each of these components to Aire's regulation of TSA gene transcription has yet to be fully dissected, but these results provide a number of suggestive clues to Aire's potential function. The association with chromatin-modification enzymes suggests that in addition to Aire reading the local chromatin environment for signs of transcriptional repression, Aire may also modify this same chromatin to promote transcription. The association with DNA manipulation and repair enzymes like Top2a and DNA-PK, which are also involved in transcriptional elongation and processivity, suggests that Aire binding may promote transcription through the introduction and repair of double-stranded breaks (DSBs) in DNA. In support of this, DNA-PK deficient mice have reduced thymic TSA expression (relative to Rag-/-

controls), Aire appears to induce such DSBs in transfected cells, and artificial introduction of DSBs upregulates expression of certain TSA genes in vitro *(60)*. Finally, association with pre-mRNA processing machinery suggests that Aire may be involved in stabilizing RNA splicing of TSA transcripts. In support of this, while Aire clearly upregulates the level of spliced TSA transcripts in mTECs, analysis of pre-spliced levels of the same candidate TSA transcripts shows no difference between Aire-wildtype and Aire-deficient thymi. The generalizability of this finding to all Aire-regulated TSAs remains to be determined, but if valid, it suggests that pre-mRNA processing may play a central role in Aire function. Indeed, it is interesting to speculate that if this hypothesis is generally true (that Aire wildtype and Aire-deficient thymi have equivalent levels of all pre-spliced transcripts and only differ in the levels of post-spliced transcripts), it implies that stabilization of pre-mRNA splicing may be the primary role for Aire in unregulating gene expression. Indeed, this suggests that all the other suggested chromatin/DNA modification/transcriptional stabilization components of Aire function that generate pre-spliced mRNA may not play a significant role in promoting TSA expression if the pre-spliced mRNA levels are equivalent even in the absence of Aire. Clearly, the analysis of Aire's binding partners has provided many new insights into its function, but it is clear that such association methods produce a complex picture of the mechanistic reality.

In addition to this recent surplus of data regarding Aire's binding partners, there is also growing evidence that Aire may regulates transcription of individual genes in a stochastic manner, turning on certain genes in some mTECs and other genes in others. It is believed that only mature, postmitotic mTECs make *Aire* *(61)*, and these mature mTECs collectively express by far the greatest number of TSAs of the thymic cell populations *(39)*. However, there is substantial mouse-to-mouse variability in transcription of Aire-regulated genes in the thymus between mice of the same background, and even significant variability between the two thymic lobes of individual animals *(62)*. Furthermore, single-cell sorting of *Aire*-expressing mTECs has shown similar variability between individual cells, suggesting that each mature mTEC may only produce a small number of these TSAs *(63, 64)*. Within an Aire-regulated locus like the casein gene cluster, for example, one mTEC will express one casein gene and not others, while another mTEC will express different casein genes or none at all. Single-cell sorting also reveals that the TSAs expressed in each mTEC do not appear to follow any tissue-specific regulatory pattern—a cell that expresses some lactation genes like the caseins will simultaneously express genes from other tissues, like insulin. This stochastic mechanism even applies at the individual gene level; whereas autosomal genes in differentiated tissues are normally expressed biallelically, in single mTECs there is often expression of only one allele *(64)*. Together, these data suggest that while Aire acts to globally stimulate transcription of a wide range of genes in mTECs, in any one cell it appears to activate only a small and random subset of these genes.

Finally, some additional insight has been gained into Aire's function through the study of a novel autosomal dominant inheritance pattern of *AIRE* mutations in an Italian kindred. This disease manifested a unique phenotype including predominant thyroiditis as well as some of the conventional hallmarks of APS-1, but all affected family members were reported to be heterozygotes with one functional *AIRE* allele *(65)*, and one allele carrying a missense mutation causing substitution of a tryptophan for a glycine at amino acid 228, within the putative DNA-binding SAND domain. Consequently, we recently knocked this G228W mutation into the *Aire* locus to generate a mouse model of this APS-1-like disease *(50)*. As in humans, G228W heterozygous mice developed spontaneous autoimmunity targeting a diverse range of organs including the lacrimal and salivary glands, as well as background-dependent infiltration of the retina, exocrine pancreas, thyroid gland, and sciatic nerve **(Figure 1.3)**.

In addition to confirming the unique genetics of this mutation, two interesting observations have arisen out of the generation of this mouse. First, this study suggests a link between Aire's subnuclear localization and its function, because the introduction of the G228W allele causes Aire, which is normally distributed in nuclear dots, to form large, ubiquitin-containing aggregates within the nucleus that resemble nuclear inclusion bodies. Second, this G228W system provides unique insight into the levels of thymic TSA expression that are required to maintain self-tolerance. For each *Aire*-regulated TSA gene examined, the presence of the heterozygous G228W mutation reduced but did not abolish expression of that gene in mTECs, whereas complete *Aire*-knockout mice showed undetectable or nearly undetectable expression. For example the retinal antigen IRBP, which is both necessary and sufficient to prevent autoimmunity against the target organ, was still expressed in mTECs of the G228W mouse but at lower levels. In the complete absence of thymic IRBP, all examined strains develop uveitis, but in the G228W mouse, this lower level of IRBP expression led to uveitis only certain, autoimmune-prone backgrounds like the NOD mouse *(50)*. This finding suggests that not only do the presence of absence of thymic TSAs matter, but the levels of expression may be critically important as well. Such results are also indirectly supported in certain human autoimmunity, where it has been found that type I diabetes is associated with decreased levels of intrathymic insulin expression *(66, 67)*.

Recent evidence has thus provided many clues to understand Aire's function at the molecular level, from description of its binding partners to the molecular biology of target gene transcription. However we remain far from understanding the fundamental nature of Aire's function, from decoding the Aire regulation of specific genes, or ultimately from being able to understand or predict which genes are Aire-regulated. Furthermore, in addition to its role in regulating TSA expression, there is also evidence that Aire may play other roles in mTECs including affecting development and facilitating antigen presentation of or negative selection against non Aire-regulated antigens *(55, 68, 69)*. Much work therefore remains in order to resolve the basic molecular biology of Aire function, and to understand how a single protein exerts such broad-ranging but pleiotropic transcriptional effects. In contrast, much more is now known about the cellular mechanisms of disease.

Cellular mechanisms of disease in *Aire*-deficient mice

While early studies of *Aire*-knockout mice implicated TSA expression in the thymic stroma as playing a causative role in disease pathogenesis, the cellular mechanisms of the resulting disease were not immediately clear. One question that arose was whether the disease resulted from a failure to delete autoreactive effector T cells that destroyed self-tissue, or a failure to produce autoreactive regulatory T cells that protected self-tissue. Indeed, the thymic development of regulatory T cells is indispensable in maintaining self-tolerance *(28)*, and the expression of a self-antigen within the thymus does lead to the development of regulatory T cells specific for that antigen *(70, 71)*.

Aire-deficient mice, however, appear to have no gross defects in regulatory T cells, as the number and percent of FoxP3+ Tregs are unchanged in *Aire*-knockout animals from multiple strains *(18, 19)*. Further, the ability of Tregs to suppress proliferation of effector T cells in a dose-dependent manner, a classic hallmark of Treg function, is equivalent in *Aire*-wildtype and *Aire*-knockout mice, as is the ability to rescue immunodeficient recipients from Treg-depleted adoptive transfer mediated autoimmunity *(19, 68)*. Because the tolerance mediated by regulatory T cells is a dominant form of tolerance which can be transferred, experiments have also been done to combine equal numbers of *Aire*-wildtype and *Aire*-knockout thymi or splenocytes and determine whether the presence of *Aire*-wildtype Tregs can therefore complement the tolerance defect observed in *Aire*-knockout animals. In all such cases, the presence of *Aire*-wildtype thymic stroma or *Aire*-wildtype splenocytes does not prevent the autoimmunity caused by the *Aire*-knockout counterpart, suggesting that the autoimmunity in the *Aire*-knockout could not be rescued by replacing the regulatory T cell compartment *(68)*. Finally, crossing the *Aire* knockout onto the Scurfy knockout strain, which lacks FoxP3 and therefore functional regulatory T cells, accelerates disease over either individual knockout alone *(72)*, suggesting that the defects are complementary and not redundant. Thus, while an altered regulatory T-cell repertoire may still play some role in the pathogenesis of autoimmunity in *Aire*-knockout mice, it appears secondary to a defect in negative selection of autoreactive effector T cells.

The effector cells themselves that mediate disease in *Aire*-knockout mice have also been characterized. Since the initial description of the *Aire*-knockout mouse it has been known that the transfer of bulk lymphocytes from an *Aire*-deficient mouse into an immunodeficient recipient causes autoimmunity in the recipient, and therefore that lymphocytes themselves are sufficient to mediate disease *(18)*. Histological examination of affected organs in *Aire*-knockout mice also shows a clear lymphocytic infiltrate, with a preponderance of CD4+ T cells but also some CD8+ T cells and B cells *(73, 74)*, with the relative ratios depending on the tissue targeted and the severity of the lesion. Further, the pathogenesis of disease has been shown to require T cells, as *Aire*-knockout mice that lack T cells do not develop autoimmunity *(74)*. Among T cell subsets, CD4+ T cells appear to play the most important role, as depletion of CD4+ T cells, but not CD8+ T cells, before transfer of *Aire*-deficient bulk lymphocytes, prevents autoimmunity. The CD4+ T cells isolated from the infiltrated tissues of *Aire*-knockout mice show a distinct skewing toward a Th1-like phenotype, and produce high levels of INF-γ and TNF-α but low levels of Th2 or Th17 cytokines like IL-4, IL-10, and IL-17 *(74)*. In support of the relevance of Th1-skewing in the pathogenesis of *Aire*-deficiency, *Aire*-knockout mice lacking the *Stat4* gene, which is necessary for Th1-like polarization, exhibit significantly reduced autoimmunity, while those lacking the *Stat6* gene, which is necessary for Th2-like polarization, exhibit in some cases worse disease.

The role of CD4+ T cells in the pathogenesis of autoimmunity in *Aire*-knockout mice is further supported by the fact that treatment with a depleting anti-CD4 antibody dramatically reduces the tissue infiltration and organ destruction across a range of organs from the eye to the liver, lung, pancreas and salivary glands *(74)*. As in other models of autoimmune disease *(75)*, treatment with a depleting anti-CD4 antibody appears to largely prevent the severe manifestations of disease in *Aire*-knockout mice, and may be of future therapeutic interest in the treatment of APS-1. The role of B cells in the model is currently less clear *(74, 76)*. Sera transfers are unable to promote autoimmunity, suggesting a limited role for autoantibodies. However, B-cell depletion with Rituximab appears to ameliorate disease in the mouse model *(76)*. Taken together, these results suggest that B cells may serve as a contributor through their APC function, but more detailed study is needed.

Defining the antigen-specific response in *Aire*-knockout mice: identification of disease-relevant autoantigens

While the role of B cells and antibodies in the pathogenesis of disease in the *Aire*-knockout mouse appears to be limited, these autoantibodies can be used as tools to identify disease-relevant autoantigens. One such example from the *Aire*-knockout mouse is the identification of the retinal antigen interphotoreceptor retinoid-binding protein (IRBP), whose *Aire*-dependent thymic expression is both necessary and sufficient to prevent retinal autoimmunity in mice *(73)*. Using serum from *Aire*-deficient mice as a tool, the investigators found a ~150kD protein that was the target of consistent antibody reactivity in *Aire*-knockout mice, and identified this protein as IRBP. To test whether IRBP expression in the thymus was required to prevent uveitis, thymic tissue from IRBP-knockout mice (which still retain functional *Aire*) was then transplanted into athymic recipient mice, and surprisingly it was found that these mice did in fact develop retinal autoimmunity. Thus, IRBP presents both a promising model antigen to study central tolerance and a potentially exciting therapeutic target for antigen-specific therapy of autoimmune uveitis.

Additional organ-specific antigens have also been identified in *Aire*-knockout mice using similar techniques. A stomach antigen, Mucin 6, was shown to be the target of autoantibodies in *Aire*-knockout serum and to be *Aire*-regulated in the thymic stroma *(77)*. Other organ-specific autoantigens identified include an exocrine pancreatic protein, protein disulfide isomerase, PDIp *(78)*, and as well as a salivary antigen, α-fodrin *(19)*, though these last two are not *Aire*-regulated in the thymus, and their causative role in the pathogenesis of organ-specific autoimmunity is therefore less clear. It is perhaps surprising, given the vast array of self-antigens regulated by *Aire* in the thymus, that only a restricted number of organs are targeted in *Aire*-knockout mice and in APS-1 patients, and within those organs only specific antigens are recognized. The reason for this telescoping, oligoclonal immune response to self is not entirely clear, but may reflect the limited autoreactive T-cell repertoire in the model.

Finally it is important to note that there may be some differences in autoantibody reactivity profiles between APS-1 patients and *Aire*-knockout mouse strains ***(22)***. Indeed, some of the proteins recognized by APS-1 patient serum may be different than those targeted in *Aire*-knockout mice; this would, in fact, not be surprising given the significant divergence in MHC molecules observed between the two species. However some overlap clearly exists, as evidenced by the recent identification of the NALP5 protein as an important parathyroid antigen in APS-1, and the parallel reactivity to NALP5 seen in *Aire*-knockout mouse serum ***(79, and T. Shum, M. Cheng, O. Kampe, M. Anderson, unpublished results)***.

The mechanism of *Aire* deficiency: important questions remain

Studies to date have thus firmly established the relevance of *Aire*-mediated thymic TSA expression in the maintenance of immunologic tolerance, and have begun to shed light on the mechanisms by which Aire may accomplish this. Naturally, however, this model remains incomplete, and numerous questions remain. For example, although thymic expression of many disease-relevant TSA genes like insulin are clearly *Aire*-dependent

(18), *Aire*-deficient mice fail to develop autoimmunity against the target organs of many of these antigens (e.g. insulitis or diabetes; *(17-19)*), suggesting that perhaps peripheral mechanisms are acting to prevent disease despite the absence of thymic negative selection. Conversely, while an incredible diversity of TSAs are expressed in the thymus, many are entirely absent, and yet mice generally do not develop autoimmune disease against such antigens. Finally, while many antigens identified in *Aire*-knockout mice are in fact regulated in the thymus, these mice also develop autoreactivity to non-Aire-dependent antigens *(19)*, though epitope spreading may account for some such reactivity. Numerous overlapping systems exist which could help explain why such autoimmunity fails to develop, but one intriguing possibility is that perhaps lymphocyte self-education continues even after thymic egress. To this end it is tantalizing to note that there is a growing body of evidence for expression of both *Aire* and TSA transcripts outside the thymus.

4. Extrathymic *Aire* and TSA expression

In addition to its established role in thymic tolerance, there is recent evidence that *Aire* and tissue-specific antigens may also be expressed outside the thymus in the secondary lymphoid organs. Indeed the original report identifying the *AIRE* gene showed Northern blot data detecting *AIRE* transcript in both the thymus and lymph nodes *(10)*. Subsequent attempts to characterize the distribution of *Aire* expression in mouse and human tissues by PT-PCR analysis found detectable levels of transcript in the thymus, spleen and lymph nodes (as well as the gonads *(18, 25)*). However the identification and characterization of specific populations of genuine *Aire*-expressing cells outside the thymus has remained difficult. A number of studies have described *Aire* transcript expression in dendritic cells in both the thymus and the secondary lymphoid organs *(25, 80)*, and another recent study described a cell-intrinsic effect of *Aire* on dendritic cell production of the tumor necrosis family member BAFF *(81)*. Conversely, *Aire* transcript has also been described as enriched among CD45- non-hematopoietic stromal fractions in the secondary lymphoid organs *(82)*, while still other reports have described expression among lymphocytes *(48, 83)* and even in non-lymphoid populations such as the hepatocytes and Purkinje cells of the cerebellum *(17)*. Furthermore, it remains controversial whether such reports of *Aire* transcript outside the thymus correlate with the presence of functional protein, and one recent report suggested specifically that *Aire* protein was only observed in the thymus, and was not made in the secondary lymphoid organs *(84)*. Thus the presence, identity, and function of extrathymic *Aire*-expressing cells remains an area of significant uncertainty.

Recent evidence has also begun to suggest that the secondary lymphoid organs may be sites of promiscuous TSA expression. These studies have generally shown that a particular tissue-specific antigen gene is expressed or can drive transgene expression in the secondary lymphoid organs, and that such self-antigen expression leads to deletion of naïve T cells specific for that antigen. One such report employed a transgenic system in which ovalbumin (OVA) was expressed under the control of the intestinal fatty-acid binding protein (iFABP) promoter *(82)*. Upon adoptive transfer of CFSE-labeled OVA-specific OT-I CD8+ T cells, they observed proliferation of OT-I cells not only in mesenteric lymph nodes draining known (intestinal) sites of iFABP expression, but also in distant peripheral lymph nodes, and found that this early proliferation ultimately led to deletion of adoptively transferred OT-I cells. Using β2M-deficient bone marrow to reconstitute transgenic adoptive transfer recipients, the authors argued that radioresistant cells were sufficient to induce this OT-I proliferation and deletion in peripheral lymph nodes. This CD45-negative population was also shown to have detectable levels of both *Aire* and other TSA transcripts.

A subsequent report *(85)* employing a TCR-transgenic mouse designated "FH," reactive to the melanocyte antigen tyrosinase in the context of a humanized class I MHC, discovered that albino FH mice (which lack tyrosinase) had increased tetramer-positive T cells relative to wildtype FH mice. Surprisingly, however, reciprocal thymic transplant experiments revealed that such T cells were not undergoing thymic negative selection, and that tyrosinase expression in the secondary lymphoid organs mediated this apparent deletion. Indeed adoptive transfer of FH cells showed antigen-specific CFSE dilution in all secondary lymphoid organs at three days post-transfer, and antigen-specific deletion of FH cells by two weeks. B2M -/- bone-marrow chimeras further suggested that this deletion was mediated by a radioresistant population of cells. Other studies have described expression of both *Aire* and Insulin2 (*Ins2*) transcripts in the lymph nodes *(86)*, and one recent report *(87)* described detection of *Ins2* and a number of other islet specific

TSA transcripts in the pancreatic lymph nodes, finding that the expression of these TSAs correlated chronologically with diabetes progression in NOD mice.

There is also some limited evidence suggesting that TSA expression may occur in subpopulations of hematopoietic cells. Zheng et al. *(88)*, using TRAMP mice in which the promoter of mouse *Probasin (mPb),* a prostate-specific antigen, drives expression of SV40 T-antigen (SV40Tag), found that in addition to thymic expression of SV40Tag, which induced negative selection of cognate TG-B CD8+ T cells, they observed mice reconstituted with TRAMP+ bone marrow caused activation-induced cell death of TG-B T cells. Similarly, Garcia et al. *(89)* identified a population of dendritic cells in the thymus, spleen, and peripheral blood which they suggest both display proinsulin peptides on their surface and endogenously express the insulin gene. Collectively, these studies suggest that some expression of both *Aire* and certain tissue-specific antigens may be occurring in the secondary lymphoid organs. However the very presence and certainly the identity of *Aire*–expressing cells outside the thymus, and their relationship to tissue-specific antigen expression, have remained largely unclear, as has the role of Aire and the contribution of such populations to the maintenance of self-tolerance.

The following chapters directly examine the nature and function of extrathymic *Aire*-expressing cells (eTACs). Chapter two describes the identification of this population containing both *Aire* transcript and protein, and examines the nature of Aire-regulated TSA expression in these cells. It then describes the ability of eTACs to interact directly with autoreactive CD8+ T cells, and the outcome of such interactions. Chapter three examines the ability of self-antigen expression in eTACs to directly prevent autoimmune disease. In the process it identifies direct interaction between eTACs and CD4+ T cells, and begins to define the mechanism by which these cells induce tolerance in both CD4+ and CD8+ T cell populations. Finally, chapter four describes preliminary results developing a mouse model to selectively deplete mTECs and eTACs and better define their contribution to the physiologic maintenance of self-tolerance. Together these results will aim to define the population of extrathymic *Aire*-expressing cells, and suggest a role that this population may play in the maintenance of immunologic self-tolerance.

References

1. Boehm T, Bleul CC. The evolutionary history of lymphoid organs. Nat Immunol 2007;8:131-5.
2. Tonegawa S. Somatic generation of antibody diversity. Nature 1983;302:575-81.
3. Ehrlich P, Bolduan C. Collected studies on immunity. 1st ed. New York,: J. Wiley & sons; [etc.; 1906.
4. Jerne NK. The Natural-Selection Theory of Antibody Formation. Proc Natl Acad Sci U S A 1955;41:849-57.
5. Talmage DW. Allergy and immunology. Annu Rev Med 1957;8:239-56.
6. Burnet FM. A Modification of Jerne's Theory of Antibody Production using the Concept of Clonal Selection. The Australian Journal of Science 1957;20:67-9.
7. Perheentupa J. Autoimmune polyendocrinopathy-candidiasis-ectodermal dystrophy. J Clin Endocrinol Metab 2006;91:2843-50.
8. Perheentupa J. APS-I/APECED: the clinical disease and therapy. Endocrinol Metab Clin North Am 2002;31:295-320, vi.
9. Peterson P, Peltonen L. Autoimmune polyendocrinopathy syndrome type 1 (APS1) and AIRE gene: new views on molecular basis of autoimmunity. J Autoimmun 2005;25 Suppl:49-55.

10. Nagamine K, Peterson P, Scott HS, et al. Positional cloning of the APECED gene. Nat Genet 1997;17:393-8.
11. An autoimmune disease, APECED, caused by mutations in a novel gene featuring two PHD-type zinc-finger domains. Nat Genet 1997;17:399-403.
12. Heino M, Peterson P, Kudoh J, et al. APECED mutations in the autoimmune regulator (AIRE) gene. Hum Mutat 2001;18:205-11.
13. Saltis M, Criscitiello MF, Ohta Y, et al. Evolutionarily conserved and divergent regions of the autoimmune regulator (Aire) gene: a comparative analysis. Immunogenetics 2008;60:105-14.
14. Kyewski B, Klein L. A central role for central tolerance. Annu Rev Immunol 2006;24:571-606.
15. Blechschmidt K, Schweiger M, Wertz K, et al. The mouse Aire gene: comparative genomic sequencing, gene organization, and expression. Genome Res 1999;9:158-66.
16. Mittaz L, Rossier C, Heino M, et al. Isolation and characterization of the mouse Aire gene. Biochem Biophys Res Commun 1999;255:483-90.
17. Ramsey C, Winqvist O, Puhakka L, et al. Aire deficient mice develop multiple features of APECED phenotype and show altered immune response. Hum Mol Genet 2002;11:397-409.
18. Anderson MS, Venanzi ES, Klein L, et al. Projection of an immunological self shadow within the thymus by the aire protein. Science 2002;298:1395-401.
19. Kuroda N, Mitani T, Takeda N, et al. Development of autoimmunity against transcriptionally unrepressed target antigen in the thymus of Aire-deficient mice. J Immunol 2005;174:1862-70.
20. Jiang W, Anderson MS, Bronson R, Mathis D, Benoist C. Modifier loci condition autoimmunity provoked by Aire deficiency. J Exp Med 2005;202:805-15.
21. Gray DH, Gavanescu I, Benoist C, Mathis D. Danger-free autoimmune disease in Aire-deficient mice. Proc Natl Acad Sci U S A 2007;104:18193-8.
22. Pontynen N, Miettinen A, Arstila TP, et al. Aire deficient mice do not develop the same profile of tissue-specific autoantibodies as APECED patients. J Autoimmun 2006;27:96-104.
23. Lacasse M, Fortier C, Trudel L, Collet AJ, Deslauriers N. Experimental oral candidosis in the mouse: microbiologic and histologic aspects. J Oral Pathol Med 1990;19:136-41.
24. Phillips AW, Balish E. Growth and invasiveness of Candida albicans in the germ-free and conventional mouse after oral challenge. Appl Microbiol 1966;14:737-41.

25. Heino M, Peterson P, Sillanpaa N, et al. RNA and protein expression of the murine autoimmune regulator gene (Aire) in normal, RelB-deficient and in NOD mouse. Eur J Immunol 2000;30:1884-93.

26. Zuklys S, Balciunaite G, Agarwal A, Fasler-Kan E, Palmer E, Hollander GA. Normal thymic architecture and negative selection are associated with Aire expression, the gene defective in the autoimmune-polyendocrinopathy-candidiasis-ectodermal dystrophy (APECED). J Immunol 2000;165:1976-83.

27. Kim JM, Rasmussen JP, Rudensky AY. Regulatory T cells prevent catastrophic autoimmunity throughout the lifespan of mice. Nat Immunol 2007;8:191-7.

28. Sakaguchi S, Yamaguchi T, Nomura T, Ono M. Regulatory T cells and immune tolerance. Cell 2008;133:775-87.

29. Bonasio R, Scimone ML, Schaerli P, Grabie N, Lichtman AH, von Andrian UH. Clonal deletion of thymocytes by circulating dendritic cells homing to the thymus. Nat Immunol 2006;7:1092-100.

30. Apostolou I, von Boehmer H. In vivo instruction of suppressor commitment in naive T cells. J Exp Med 2004;199:1401-8.

31. Schwartz RH. T cell anergy. Annu Rev Immunol 2003;21:305-34.

32. Jolicoeur C, Hanahan D, Smith KM. T-cell tolerance toward a transgenic beta-cell antigen and transcription of endogenous pancreatic genes in thymus. Proc Natl Acad Sci U S A 1994;91:6707-11.

33. Smith KM, Olson DC, Hirose R, Hanahan D. Pancreatic gene expression in rare cells of thymic medulla: evidence for functional contribution to T cell tolerance. Int Immunol 1997;9:1355-65.

34. Derbinski J, Schulte A, Kyewski B, Klein L. Promiscuous gene expression in medullary thymic epithelial cells mirrors the peripheral self. Nat Immunol 2001;2:1032-9.

35. Liston A, Gray DH, Lesage S, et al. Gene dosage--limiting role of Aire in thymic expression, clonal deletion, and organ-specific autoimmunity. J Exp Med 2004;200:1015-26.

36. Liston A, Lesage S, Wilson J, Peltonen L, Goodnow CC. Aire regulates negative selection of organ-specific T cells. Nat Immunol 2003;4:350-4.

37. Gardner JM, Devoss JJ, Friedman RS, et al. Deletional tolerance mediated by extrathymic Aire-expressing cells. Science 2008;321:843-7.

38. Kyewski B, Derbinski J. Self-representation in the thymus: an extended view. Nat Rev Immunol 2004;4:688-98.

39. Derbinski J, Gabler J, Brors B, et al. Promiscuous gene expression in thymic epithelial cells is regulated at multiple levels. J Exp Med 2005;202:33-45.

40. Ilmarinen T, Melen K, Kangas H, Julkunen I, Ulmanen I, Eskelin P. The monopartite nuclear localization signal of autoimmune regulator mediates its nuclear import and interaction with multiple importin alpha molecules. FEBS J 2006;273:315-24.

41. Pitkanen J, Vahamurto P, Krohn K, Peterson P. Subcellular localization of the autoimmune regulator protein. characterization of nuclear targeting and transcriptional activation domain. J Biol Chem 2001;276:19597-602.

42. Meloni A, Fiorillo E, Corda D, Perniola R, Cao A, Rosatelli MC. Two novel mutations of the AIRE protein affecting its homodimerization properties. Hum Mutat 2005;25:319.

43. Savkur RS, Burris TP. The coactivator LXXLL nuclear receptor recognition motif. J Pept Res 2004;63:207-12.

44. Bottomley MJ, Collard MW, Huggenvik JI, Liu Z, Gibson TJ, Sattler M. The SAND domain structure defines a novel DNA-binding fold in transcriptional regulation. Nat Struct Biol 2001;8:626-33.

45. Purohit S, Kumar PG, Laloraya M, She JX. Mapping DNA-binding domains of the autoimmune regulator protein. Biochem Biophys Res Commun 2005;327:939-44.

46. Org T, Chignola F, Hetenyi C, et al. The autoimmune regulator PHD finger binds to non-methylated histone H3K4 to activate gene expression. EMBO Rep 2008;9:370-6.

47. Heino M, Peterson P, Kudoh J, et al. Autoimmune regulator is expressed in the cells regulating immune tolerance in thymus medulla. Biochem Biophys Res Commun 1999;257:821-5.

48. Bjorses P, Pelto-Huikko M, Kaukonen J, Aaltonen J, Peltonen L, Ulmanen I. Localization of the APECED protein in distinct nuclear structures. Hum Mol Genet 1999;8:259-66.

49. Tao Y, Kupfer R, Stewart BJ, et al. AIRE recruits multiple transcriptional components to specific genomic regions through tethering to nuclear matrix. Mol Immunol 2006;43:335-45.

50. Su MA, Giang K, Zumer K, et al. Mechanisms of an autoimmunity syndrome in mice caused by a dominant mutation in Aire. J Clin Invest 2008;118:1712-26.

51. Oven I, Brdickova N, Kohoutek J, Vaupotic T, Narat M, Peterlin BM. AIRE recruits P-TEFb for transcriptional elongation of target genes in medullary thymic epithelial cells. Mol Cell Biol 2007;27:8815-23.

52. Pitkanen J, Doucas V, Sternsdorf T, et al. The autoimmune regulator protein has transcriptional transactivating properties and interacts with the common coactivator CREB-binding protein. J Biol Chem 2000;275:16802-9.

53. Pitkanen J, Rebane A, Rowell J, et al. Cooperative activation of transcription by autoimmune regulator AIRE and CBP. Biochem Biophys Res Commun 2005;333:944-53.

54. Kumar PG, Laloraya M, Wang CY, et al. The autoimmune regulator (AIRE) is a DNA-binding protein. J Biol Chem 2001;276:41357-64.

55. Johnnidis JB, Venanzi ES, Taxman DJ, Ting JP, Benoist CO, Mathis DJ. Chromosomal clustering of genes controlled by the aire transcription factor. Proc Natl Acad Sci U S A 2005;102:7233-8.

56. Halonen M, Kangas H, Ruppell T, et al. APECED-causing mutations in AIRE reveal the functional domains of the protein. Hum Mutat 2004;23:245-57.

57. Li H, Ilin S, Wang W, et al. Molecular basis for site-specific read-out of histone H3K4me3 by the BPTF PHD finger of NURF. Nature 2006;442:91-5.

58. Pena PV, Davrazou F, Shi X, et al. Molecular mechanism of histone H3K4me3 recognition by plant homeodomain of ING2. Nature 2006;442:100-3.

59. Koh AS, Kuo AJ, Park SY, et al. Aire employs a histone-binding module to mediate immunological tolerance, linking chromatin regulation with organ-specific autoimmunity. Proc Natl Acad Sci U S A 2008;105:15878-83.

60. Abramson J, Giraud M, Benoist C, Mathis D. Aire's partners in the molecular control of immunological tolerance. Cell;140:123-35.

61. Gray D, Abramson J, Benoist C, Mathis D. Proliferative arrest and rapid turnover of thymic epithelial cells expressing Aire. J Exp Med 2007;204:2521-8.

62. Venanzi ES, Melamed R, Mathis D, Benoist C. The variable immunological self: genetic variation and nongenetic noise in Aire-regulated transcription. Proc Natl Acad Sci U S A 2008;105:15860-5.

63. Derbinski J, Pinto S, Rosch S, Hexel K, Kyewski B. Promiscuous gene expression patterns in single medullary thymic epithelial cells argue for a stochastic mechanism. Proc Natl Acad Sci U S A 2008;105:657-62.

64. Villasenor J, Besse W, Benoist C, Mathis D. Ectopic expression of peripheral-tissue antigens in the thymic epithelium: probabilistic, monoallelic, misinitiated. Proc Natl Acad Sci U S A 2008;105:15854-9.

65. Cetani F, Barbesino G, Borsari S, et al. A novel mutation of the autoimmune regulator gene in an Italian kindred with autoimmune polyendocrinopathy-candidiasis-ectodermal dystrophy, acting in a dominant fashion and strongly cosegregating with hypothyroid autoimmune thyroiditis. J Clin Endocrinol Metab 2001;86:4747-52.

66. Pugliese A, Zeller M, Fernandez A, Jr., et al. The insulin gene is transcribed in the human thymus and transcription levels correlated with allelic variation at the INS VNTR-IDDM2 susceptibility locus for type 1 diabetes. Nat Genet 1997;15:293-7.

67. Vafiadis P, Bennett ST, Todd JA, et al. Insulin expression in human thymus is modulated by INS VNTR alleles at the IDDM2 locus. Nat Genet 1997;15:289-92.

68. Anderson MS, Venanzi ES, Chen Z, Berzins SP, Benoist C, Mathis D. The cellular mechanism of Aire control of T cell tolerance. Immunity 2005;23:227-39.

69. Yano M, Kuroda N, Han H, et al. Aire controls the differentiation program of thymic epithelial cells in the medulla for the establishment of self-tolerance. J Exp Med 2008;205:2827-38.

70. Jordan MS, Boesteanu A, Reed AJ, et al. Thymic selection of CD4+CD25+ regulatory T cells induced by an agonist self-peptide. Nat Immunol 2001;2:301-6.

71. Aschenbrenner K, D'Cruz LM, Vollmann EH, et al. Selection of Foxp3+ regulatory T cells specific for self antigen expressed and presented by Aire+ medullary thymic epithelial cells. Nat Immunol 2007;8:351-8.

72. Chen Z, Benoist C, Mathis D. How defects in central tolerance impinge on a deficiency in regulatory T cells. Proc Natl Acad Sci U S A 2005;102:14735-40.

73. DeVoss J, Hou Y, Johannes K, et al. Spontaneous autoimmunity prevented by thymic expression of a single self-antigen. J Exp Med 2006;203:2727-35.

74. Devoss JJ, Shum AK, Johannes KP, et al. Effector mechanisms of the autoimmune syndrome in the murine model of autoimmune polyglandular syndrome type 1. J Immunol 2008;181:4072-9.

75. Makhlouf L, Grey ST, Dong V, et al. Depleting anti-CD4 monoclonal antibody cures new-onset diabetes, prevents recurrent autoimmune diabetes, and delays allograft rejection in nonobese diabetic mice. Transplantation 2004;77:990-7.

76. Gavanescu I, Benoist C, Mathis D. B cells are required for Aire-deficient mice to develop multi-organ autoinflammation: A therapeutic approach for APECED patients. Proc Natl Acad Sci U S A 2008;105:13009-14.

77. Gavanescu I, Kessler B, Ploegh H, Benoist C, Mathis D. Loss of Aire-dependent thymic expression of a peripheral tissue antigen renders it a target of autoimmunity. Proc Natl Acad Sci U S A 2007;104:4583-7.

78. Niki S, Oshikawa K, Mouri Y, et al. Alteration of intra-pancreatic target-organ specificity by abrogation of Aire in NOD mice. J Clin Invest 2006;116:1292-301.

79. Alimohammadi M, Bjorklund P, Hallgren A, et al. Autoimmune polyendocrine syndrome type 1 and NALP5, a parathyroid autoantigen. N Engl J Med 2008;358:1018-28.

80. Kogawa K, Nagafuchi S, Katsuta H, et al. Expression of AIRE gene in peripheral monocyte/dendritic cell lineage. Immunol Lett 2002;80:195-8.

81. Lindh E, Lind SM, Lindmark E, et al. AIRE regulates T-cell-independent B-cell responses through BAFF. Proc Natl Acad Sci U S A 2008;105:18466-71.

82. Lee JW, Epardaud M, Sun J, et al. Peripheral antigen display by lymph node stroma promotes T cell tolerance to intestinal self. Nat Immunol 2007;8:181-90.

83. Suzuki E, Kobayashi Y, Kawano O, et al. Expression of AIRE in thymocytes and peripheral lymphocytes. Autoimmunity 2008;41:133-9.

84. Hubert FX, Kinkel SA, Webster KE, et al. A specific anti-Aire antibody reveals aire expression is restricted to medullary thymic epithelial cells and not expressed in periphery. J Immunol 2008;180:3824-32.

85. Nichols LA, Chen Y, Colella TA, Bennett CL, Clausen BE, Engelhard VH. Deletional self-tolerance to a melanocyte/melanoma antigen derived from tyrosinase is mediated by a radio-resistant cell in peripheral and mesenteric lymph nodes. J Immunol 2007;179:993-1003.

86. Kont V, Laan M, Kisand K, Merits A, Scott HS, Peterson P. Modulation of Aire regulates the expression of tissue-restricted antigens. Mol Immunol 2008;45:25-33.

87. Yip L, Su L, Sheng D, et al. Deaf1 isoforms control the expression of genes encoding peripheral tissue antigens in the pancreatic lymph nodes during type 1 diabetes. Nat Immunol 2009;10:1026-33.

88. Zheng X, Yin L, Liu Y, Zheng P. Expression of tissue-specific autoantigens in the hematopoietic cells leads to activation-induced cell death of autoreactive T cells in the secondary lymphoid organs. Eur J Immunol 2004;34:3126-34.

89. Garcia CA, Prabakar KR, Diez J, et al. Dendritic cells in human thymus and periphery display a proinsulin epitope in a transcription-dependent, capture-independent fashion. J Immunol 2005;175:2111-22.

Chapter II

Identification and Characterization of Extrathymic *Aire*-Expressing Cells

Introduction

Mechanisms of central tolerance are mediated in part through the expression of a wide array of otherwise tissue-specific self-antigens (TSAs) in specialized medullary thymic epithelial cells (mTECs; *(1-3)*). The thymic expression of many of these TSAs is dependent on the *Autoimmune Regulator* (*Aire*) gene *(4, 5)*, and mutations in *Aire* lead to severe, multi-organ, tissue-specific autoimmunity in both mice *(4, 6)* and humans *(7, 8)*. Although these results reveal a role for thymic *Aire*, self-tolerance must continue to be enforced after T cells leave the thymus. Consistent with this, *Aire* expression is also detectable outside the thymus, notably in the secondary lymphoid tissues *(4, 9)*, although the identity and function of such extrathymic *Aire*-expressing cells remains unclear *(10, 11)*. Here we identify a population of extrathymic *Aire*-expressing cells and examine a potential role for *Aire* in maintaining peripheral tolerance.

Results

To accurately label *Aire*-expressing cells *in vivo,* we employed a bacterial artificial chromosome (BAC)-transgenic approach *(12)* using the murine *Aire* locus modified to drive expression of green fluorescent protein (*Gfp*) fused to an autoimmune diabetes-related self-antigen gene, islet-specific glucose-6-phosphatase related protein (*Igrp*, **Figure 2.1**A). IGRP is a pancreatic β-cell specific protein against which autoreactive CD8+ T cells are produced in both mouse and human autoimmune diabetes *(13-16)*. We

Figure 2.1. The *Adig* transgene recapitulates *Aire* expression in the thymus and mediates negative selection of autoreactive T cells. (**a**) Schematic of *Igrp-gfp* transgene targeting into the *Aire* BAC. Targeting replaces *Aire* exon 2, the coding portion of exon 1 and part of exon 3, such that the transgene does not make functional Aire (**b**) Immunofluorescent staining of GFP (green) and Aire (red) in thymic frozen sections of *Adig* mice. (**c**) Flow cytometry of CD45-, DAPI-, Ly51lo-gated thymic stromal cells from wildtype (left) and *Adig* (right) NOD mice. (**d**) Flow cytometry of CD45-, DAPI-, Ly51lo, EpCAM+ mTECs from *Adig* NOD mice gated as GFP- (yellow) or GFP+ (green) and stained for MHC II (left) and CD80 (right). (**e**) Thymocytes from *8.3* TCR-transgenic mice (top panels) or double-transgenic *8.3/Adig* mice (bottom panels) stained for CD4/CD8 (left panels), or pre-gated as CD4- CD8+ and stained for IGRP-mimetope (red) or mock (green) peptide/K^d tetramer reactivity (right panels). (**f**) Diabetes incidence curves for *8.3* TCR-transgenic mice (N=6) and *8.3/Adig* double-transgenic mice (N=10).

Figure 2.1

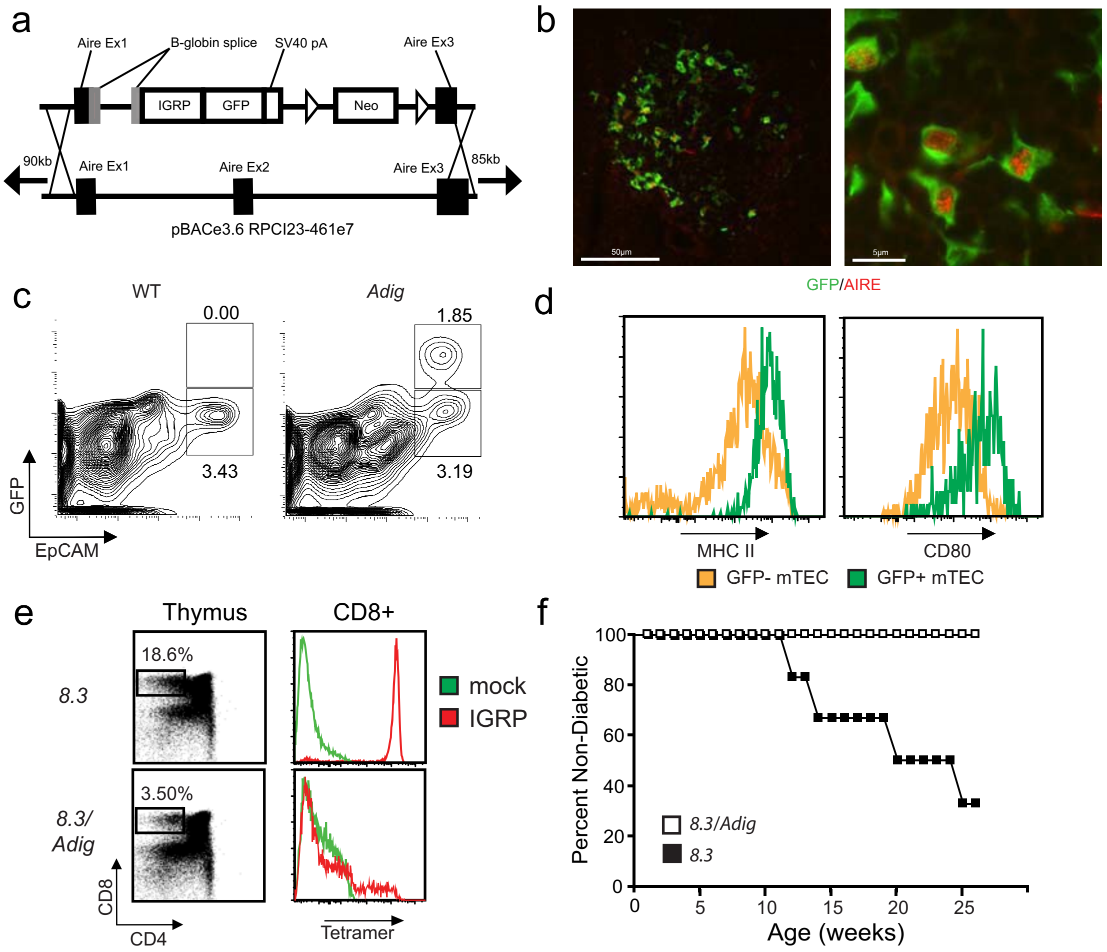

a
Aire Ex1
B-globin splice
SV40 pA
Aire Ex3
IGRP
GFP
Neo
90kb
Aire Ex1
Aire Ex2
Aire Ex3
85kb
pBACe3.6 RPCI23-461e7
b
50μm
5μm
GFP/AIRE
c
WT
Adig
0.00
3.43
1.85
3.19
GFP
EpCAM
d
MHC II
CD80
GFP- mTEC
GFP+ mTEC
e
Thymus
CD8+
8.3
18.6%
8.3/
Adig
3.50%
CD8
CD4
Tetramer
mock
IGRP
f
Percent Non-Diabetic
100
80
60
40
20
0
0
5
10
15
20
25
Age (weeks)
8.3/Adig
8.3

elected to include *Igrp* in our transgenic construct because it is not detectable in the thymus (**Figure S2.1A**) and because an IGRP-specific T-cell-receptor transgenic line (*8.3*; *(13)*) can be used to monitor interactions of *Igrp-Gfp*-expressing cells. To verify the fidelity of the BAC transgene in recapitulating endogenous *Aire* expression in the resultant *Adig* (*Aire*-Driven *Igrp-Gfp*) transgenic mice, thymic sections were co-stained for Aire and GFP, revealing thymic GFP expression highly restricted to *Aire*-expressing cells in the medulla (**Figure 2.1B, Figure S2.1B**). By flow cytometry GFP+ cells were detectable specifically within the mTEC compartment (**Figure 2.1C**), with approximately 30-40% of mTECs being GFP-positive. GFP+ mTECs expressed uniformly high levels of class II MHC and CD80 (**Figure 2.1D**), similar to previous studies of *Aire*-expressing mTECs *(3, 11, 17)*.

To test how the introduction of IGRP into the thymic medullary epithelium might affect T-cell selection, we compared *8.3* TCR-transgenic and *8.3/Adig* double-transgenic mice. Tetramer staining confirmed that the *8.3/Adig* double-transgenic mice showed a significant decrease in the percent and avidity of IGRP-specific CD8+ T cells in the thymus (**Figure 2.1E**) and in the periphery (**Figure S2.1C**). Further, while IGRP-reactive CD8+ T cells were readily detected in the polyclonal wildtype NOD background, they were completely absent in *Adig* NOD mice (**Figure S2.1D**). To test the functional impact of this negative selection, *8.3* and *8.3/Adig* mice were followed for diabetes incidence, and *8.3/Adig* mice were completely protected from disease (**Figure 2.1F**).

Figure S2.1. The *Aire*-driven *Igrp-Gfp* transgene introduces a novel antigen into the thymus which faithfully reflects thymic *Aire* expression and causes deletion of cognate T cells. (**a**) Real-time PCR analysis of *Aire*, *Igrp*, and *Ins1* transcripts in the thymus and pancreas. (**b**) Immunofluorescent per-cell quantitation of coexpression of Aire and GFP in mTECs from four independent founder lines (solid, empty, gray, striped), showing the percent of double-positive (Aire+/GFP+, DP) and single-positive (Aire+/GFP-, AireSP or Aire-/GFP+, GFPSP) cells among Aire+ or GFP+ cells of the thymus. (**c**) CD4/CD8 (top panels) and IGRP peptide/mock tetramer staining of pancreatic lymph nodes from nondiabetic wildtype (left), *8.3* (middle), and *8.3/Adig* (right) NOD mice gated on forward/side scatter (top panels) and CD4- CD8+ status (bottom panels). (**d**) CD8 and IGRP/K^d tetramer staining of thymus (top panels) and pancreatic lymph node (bottom panels) from nondiabetic wildtype (left and right panels) and *Adig* NOD mice (middle panel) gated on forward/side scatter and CD4- CD8+ status.

Figure S2.1

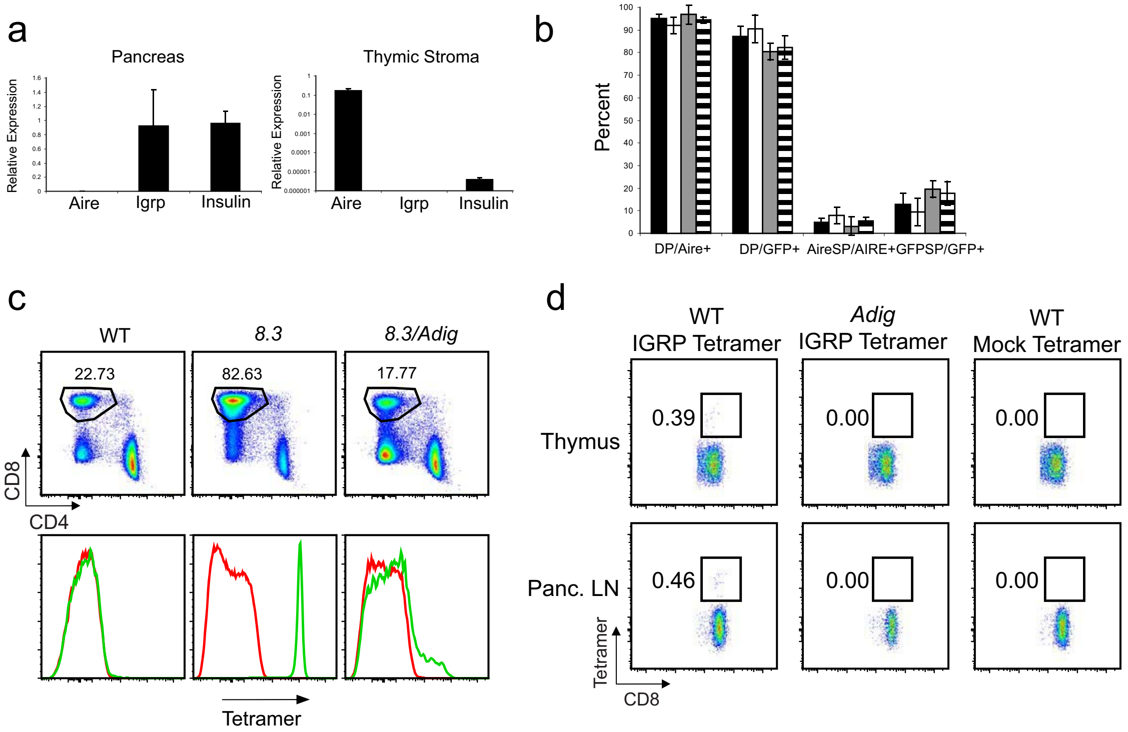
a
Pancreas
Relative Expression
1.6
1.4
1.2
1
0.8
0.6
0.4
0.2
0
Aire
Igrp
Insulin
Thymic Stroma
Relative Expression
1
0.1
0.01
0.001
0.0001
0.00001
0.000001
Aire
Igrp
Insulin
b
Percent
100
90
80
70
60
50
40
30
20
10
0
DP/Aire+
DP/GFP+
AireSP/AIRE+
GFPSP/GFP+
c
WT
8.3
8.3/Adig
22.73
82.63
17.77
CD8
CD4
Tetramer
d
WT
IGRP Tetramer
Adig
IGRP Tetramer
WT
Mock Tetramer
Thymus
0.39
0.00
0.00
Panc. LN
0.46
0.00
0.00
Tetramer
CD8

In a broad tissue survey using immunofluorescent anti-GFP staining, expression of the transgene was undetectable in most tissues, but distinct populations of extrathymic transgene-expressing cells were observed within the lymph nodes and spleen (**Figure S2.2A**). These extra-Thymic *Aire*-expressing Cells (eTACs) were generally confined to the T-cell zones of the secondary lymphoid organs and preferentially localized to T cell-B cell boundary regions (**Figure 2.2A, B**). Immunofluorescent costains showed these cells to be negative for B cell (B220), fibroblastic reticular cell (gp38, ERTR-7), and dendritic cell (CD11c) markers, but positive for class II MHC (**Figure 2.2A, B**). Reciprocal bone-marrow chimeras demonstrated that many of these cells were radioresistant (**Figure S2.3A**). Given this, we isolated secondary lymphoid stroma for flow cytometry and found that, as in the thymus, a unique population of GFP+ cells was present that was CD45-, MHC II+ (**Figure 2.2C**). These CD45-low eTACs shared some characteristics with mTECs (e.g. MHC II+, PDL1+, EpCAM+), but were distinct in that eTACs did not express the costimulatory molecules CD80 and CD86 (**Figure 2.2D**). While GFP+ eTACs represented a significant percentage of the EpCAM+ cells in the periphery (8.5% ±2.4%), eTACs failed to bind the mTEC marker UEA-I or the FRC marker gp38, suggesting they are distinct from previously described self-antigen-expressing stromal populations (*(9)*, **Figure S2.4**). eTACs also appeared to be ubiquitous in lymphoid organs, as they were detected in mesenteric lymph nodes, Peyer's patches (**Figure S2.2B**) and in the tertiary lymphoid structures that form in the infiltrated pancreatic islets of NOD mice (**Figure S2.2C**). By flow cytometry GFP+ cells were also detected in the

Figure 2.2. *Aire*-expressing cells exist in the secondary lymphoid organs. (**a and b**) Representative immunofluorescent costains of lymph node (a) and spleen (b) sections co-stained for GFP (green, all sections) and B220 (a-d), gp38 (e), ERTR-7 (f), CD11c (g), or MHC II (h; all red). Images a, b, and d-h are from *Adig* NOD mice, images c are from wildtype NOD mice. (**c**) Flow cytometric analysis and gating from *Adig* and wildtype NOD thymus, spleen, and lymph node stroma analyzed for CD45, DAPI, MHC II, and GFP. (**d**) Flow cytometric analysis of *Adig* NOD thymus (T), spleen (S), and lymph nodes (L), showing expression of indicated markers (red) or isotype staining (blue) in mTECs and eTACs respectively, defined as CD45-, DAPI-, MHC II+, GFP+. (**e**) Real-time PCR analysis of *Aire* expression relative to endogenous control in cell-sorted mTECs/eTACs (CD45-, PI-, MHC II+, CD11c-, EpCAM+) and DCs (CD45+, PI-, MHC II+, CD11c+, EpCAM-) of nontransgenic NOD thymus, spleen, and lymph node. (**f**) Immunofluorescent GFP (green)/Aire (red) costains of lymph nodes from *Adig* NOD mice.

Figure 2.2

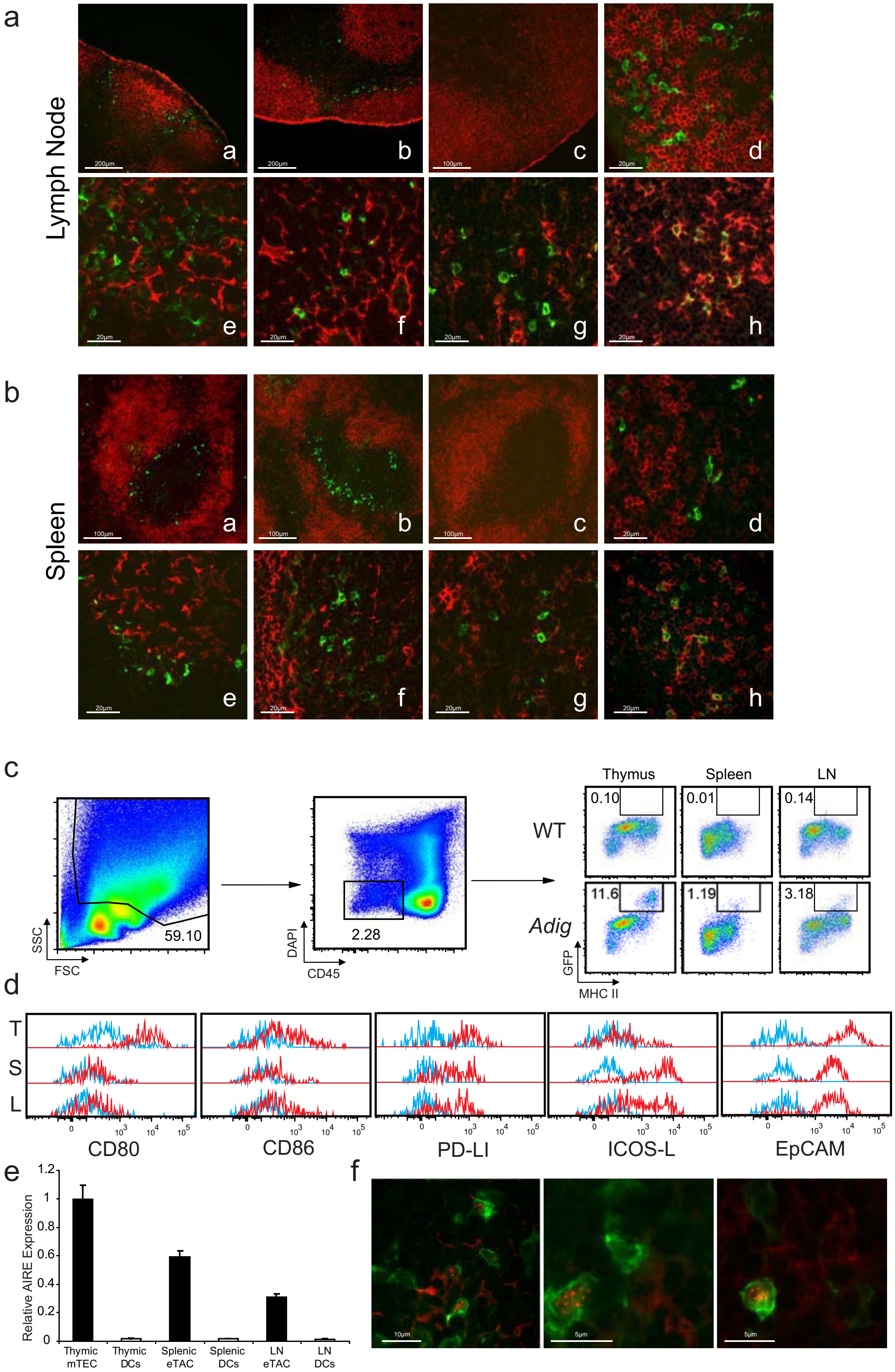
a
Lymph Node
200µm
a
200µm
b
100µm
c
20µm
d
20µm
e
20µm
f
20µm
g
20µm
h
b
Spleen
100µm
a
100µm
b
100µm
c
20µm
d
20µm
e
20µm
f
20µm
g
20µm
h
c
SSC
FSC
59.10
DAPI
CD45
2.28
Thymus
Spleen
LN
WT
0.10
0.01
0.14
Adig
11.6
1.19
3.18
GFP
MHC II
d
T
S
L
0
10^3
10^4
10^5
CD80
CD86
PD-LI
ICOS-L
EpCAM
e
Relative AIRE Expression
1.2
1
0.8
0.6
0.4
0.2
0
Thymic mTEC
Thymic DCs
Splenic eTAC
Splenic DCs
LN eTAC
LN DCs
f
10µm
5µm
5µm

Figure S2.2. Extrathymic *Aire* BAC-driven *Igrp-gfp* is expressed selectively in lymphoid structures. (**a**) Immunofluorescent tissue survey of indicated *Adig* NOD mouse organs stained with anti-GFP (left panel, green) and DAPI (right panel, blue). (**b**) Immunofluorescent staining of Peyer's patch from *Adig* (left) and wildtype NOD mice (right) with anti-B220 (red) and anti-GFP (green). (**c**) Immunofluorescent staining of lymphocyte-infiltrated islet with anti-B220 (red) and anti-GFP (green) from nondiabetic *Adig* (left) and wildtype (right) NOD mice.

Figure S2.2

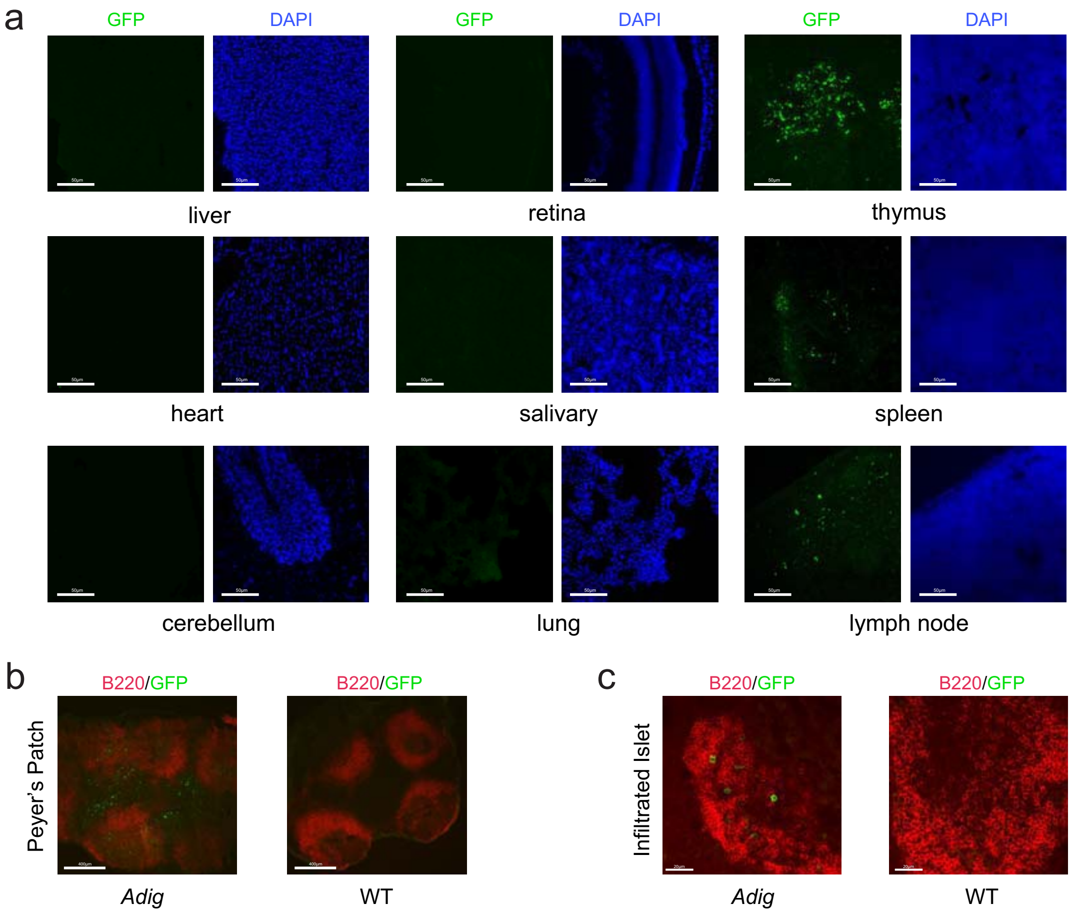
a
GFP
DAPI
GFP
DAPI
GFP
DAPI
liver
retina
thymus
heart
salivary
spleen
cerebellum
lung
lymph node
b
B220/GFP
B220/GFP
Peyer's Patch
Adig
WT
c
B220/GFP
B220/GFP
Infiltrated Islet
Adig
WT

Figure S2.3. Transgenic *Igrp-gfp* is expressed by both hematopoietic and radioresistant populations in the secondary lymphoid organs. (**a**) Immunofluorescent staining for B220 (red) and GFP (green) of bone-marrow chimeric lymph nodes from *Adig* mice reconstituted with wildtype bone marrow (WT→TG) or wildtype mice reconstituted with *Adig* bone marrow (TG→WT). (**b**) Flow cytometry of secondary lymphoid organs; representative pooled lymph node samples from a nontransgenic (upper panels) and an *Adig* NOD mouse (lower panels) are shown, with the common gating strategy shown for both in the top-most two panels. (**c**) Flow cytometric histogram showing distribution of CD11c expression among GFP+ cells in the stromal (blue; CD45-, DAPI-, MHC II+, GFP+) and hematopoietic (red; CD45+, DAPI-, MHC II+, GFP+) compartments of *Adig* NOD mice. (**d**) GFP fluorescence in hematopoietic GFP+ cells (red; CD45+, DAPI-, MHC II+, GFP+) relative to stromal GFP+ cells (blue; CD45-, DAPI-, MHC II+, GFP+), by flow cytometry. Representative of four independent experiments.

Figure S2.3

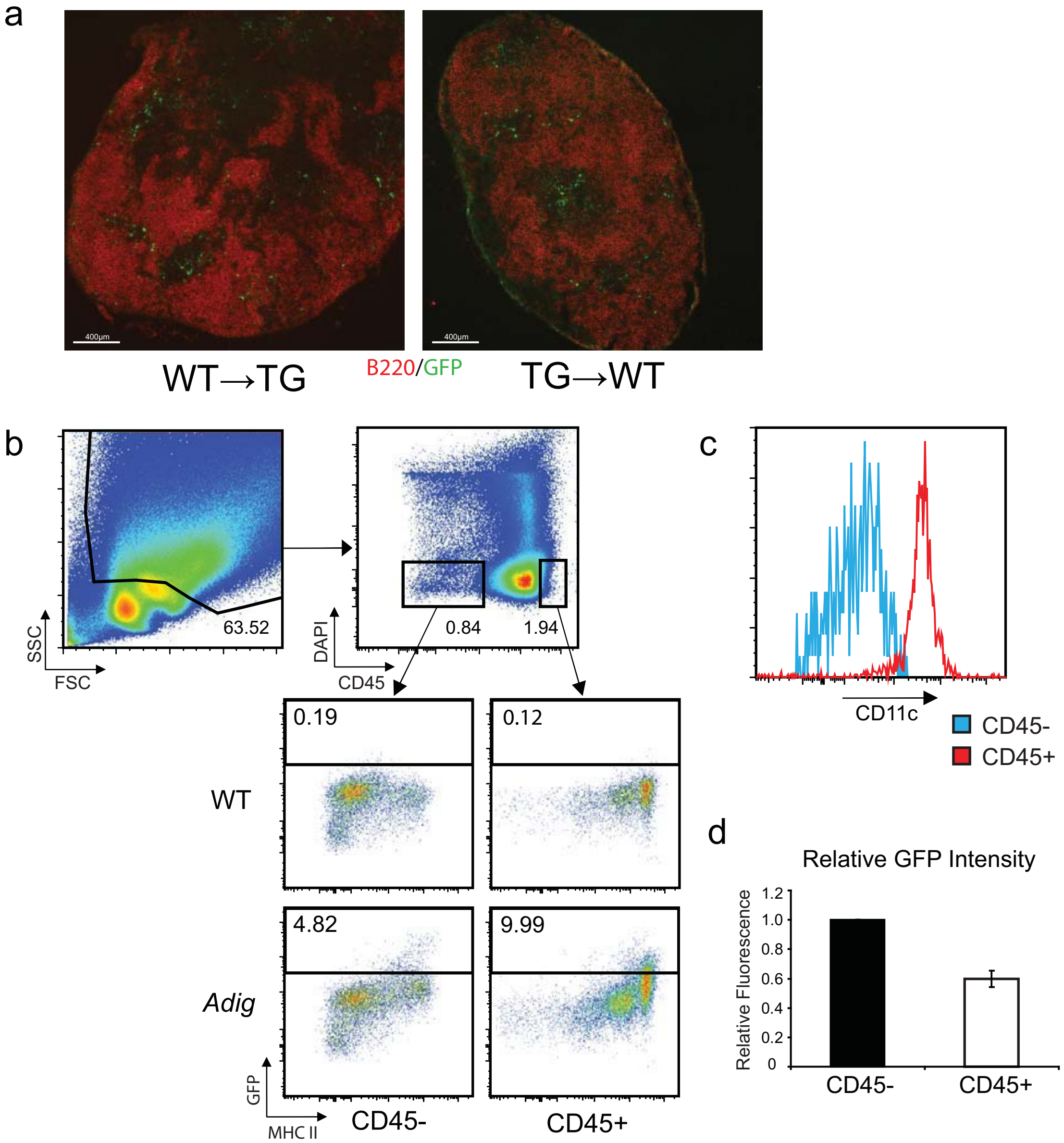
a
400μm
400μm
WT→TG
B220/GFP
TG→WT
b
63.52
SSC
FSC
0.84
1.94
DAPI
CD45
0.19
0.12
WT
4.82
9.99
Adig
GFP
MHC II
CD45-
CD45+
c
CD11c
CD45-
CD45+
d
Relative GFP Intensity
Relative Fluorescence
1.2
1.0
0.8
0.6
0.4
0.2
0
CD45-
CD45+

Figure S2.4. eTACs do not express markers characteristic of other lymphoid stroma. (**a**) Flow cytometry of thymus (T), spleen (S), and lymph node (L) mTECs (thymus, red) and eTACs (spleen and lymph node, red) and DCs (blue) from *Adig* mice stained with UEA-I. (**b**) Flow cytometry of spleen (S) and lymph node (L) eTACs and fibroblastic reticular cells (defined as CD45-, gp38+) from wildtype and Adig mice analyzed for expression of GFP (top) and gp38 (bottom).

Figure S2.4

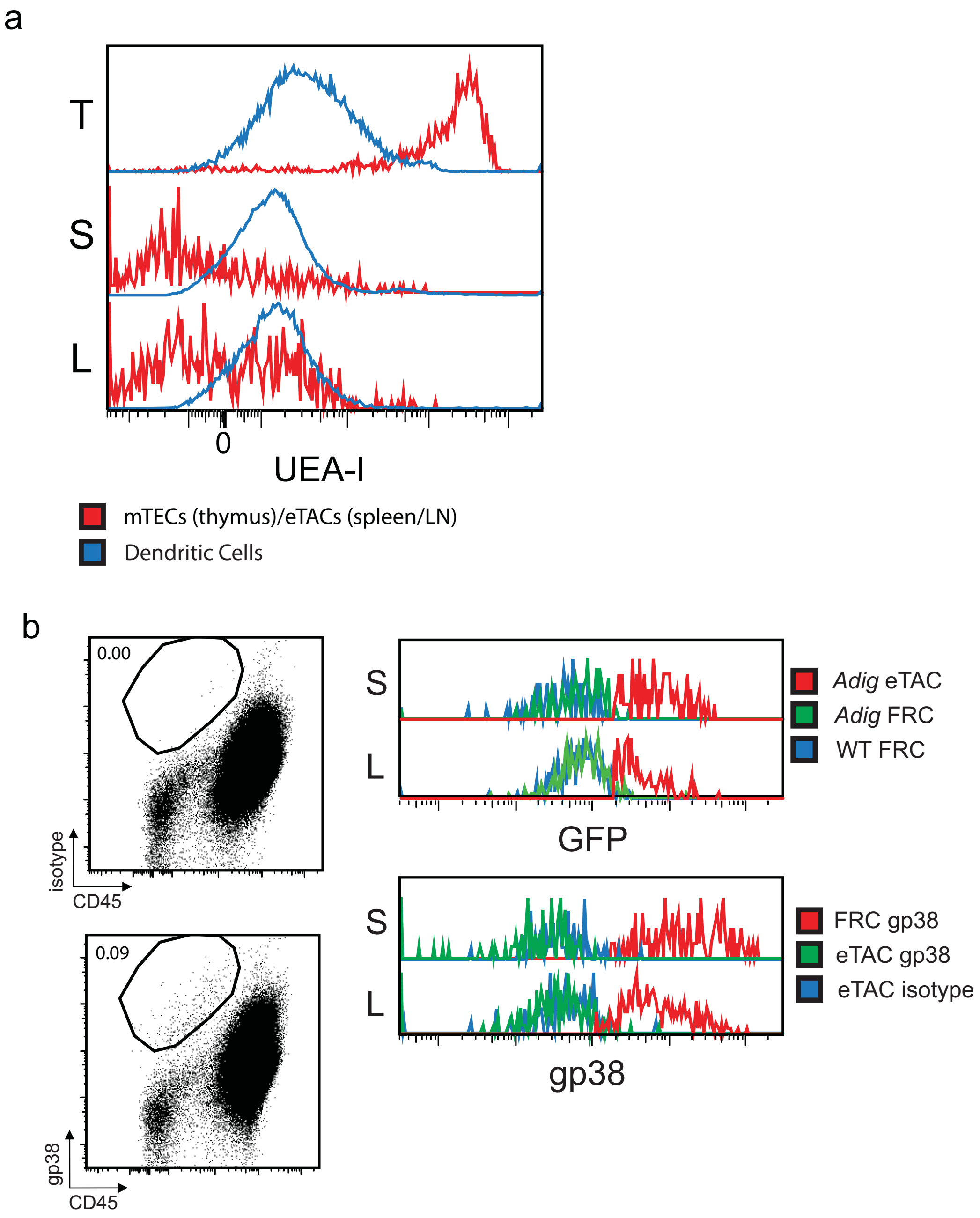
a
T
S
L
0
UEA-I
🟥 mTECs (thymus)/eTACs (spleen/LN)
🟦 Dendritic Cells
b
0.00
isotype
CD45
0.09
gp38
CD45
S
L
GFP
🟥 *Adig* eTAC
🟩 *Adig* FRC
🟦 WT FRC
S
L
gp38
🟥 FRC gp38
🟩 eTAC gp38
🟦 eTAC isotype

CD45+ compartment that expressed CD11c, although the level of GFP expression in these cells was significantly lower than in the CD45- cells and less enriched for *Aire* message (**Figure 2.2E, S2.4**).

To validate that *Igrp-Gfp* transgene expression in eTACs reflected endogenous *Aire* expression, the eTAC surface markers identified in *Adig* mice (CD45-, MHC II+, EpCAM+) were used to sort eTACs from non-transgenic mice, and *Aire* transcript was indeed found to be abundant in these cells, confirming that this population expressed high levels of *Aire* (**Figure 2.2E**). Co-staining of secondary lymphoid organs for Aire and GFP also demonstrated Aire protein localized to perinuclear speckles within a subset of eTACs (**Figure 2.2F**). The number of GFP+ cells in which Aire protein can be detected was smaller in the periphery (24.8% ±4.6%) than in the thymus (85.0% ±4.5%), and the Aire staining much weaker—near the limit of detection—which may explain why previous attempts to identify these cells in the absence of the transgenic reporter have been difficult ***(11)***.

Because Aire has been shown to play an important role in the transcriptional regulation of self-antigens in mTECs, we sought to define its function as a transcriptional regulator in eTACs. GFP+ eTACs were sorted for microarray analysis from the spleens and pooled lymph nodes of *Adig* mice crossed onto the $Aire^{+/+}$ or $Aire^{-/-}$ background. As in mTECs, the number of genes upregulated by Aire in eTACs was greater than the number downregulated (**Figure 2.3A**, **Tables S2.1, S2.2; array data available online at the Gene Expression Omnibus, record number GSE12388**). Both the

Figure 2.3. *Aire* regulates the expression of a unique set of tissue-specific antigens in eTACs. (**a**) Heat map and unsupervised clustering of *Aire*-regulated genes in eTACs. Pooled eTACs were sorted from lymph nodes and spleens from cohorts of 3-6-week-old *Adig Aire*$^{+/+}$ and *Adig Aire*$^{-/-}$ NOD mice. Each of the 8 arrays represents 3-5 pooled mice. (**b**) Schematic diagram of the unique and common genes regulated by *Aire* in eTACs and mTECs. (**c**) Classification of *Aire*-regulated genes in eTACs based on tissue-specificity, as compared to mTECs and to a random gene set. (**d**) Real-time PCR analysis of *Aire*-regulated TSAs in eTACs, normalized to endogenous control. eTACs were sorted from pooled nontransgenic *Aire*$^{+/+}$ (black bars) and *Aire*$^{-/-}$ (white bars) NOD spleens based on the surface marker profile CD45-, PI-, CD11c-, MHC II+, EpCAM+, and characterized for expression of glutamate receptor NMDA2C (*Grin2c*), ras-related associated with diabetes (*Rrad*), ladinin (*Lad1*), gulonolactone (L-) oxidase (*Gulo*), and desmoglein 1 alpha (*Dsg1a*) (**e**) Expression of antigen processing and presentation genes in eTACs relative to other lymphoid cell populations after median-centered normalization to the expression of all genes in each array. (**f**) Global expression profile similarity of eTACs (left) and mTECs (right) to other relevant cell types based on Pearson correlation values calculated for population-specific centroids.

Figure 2.3

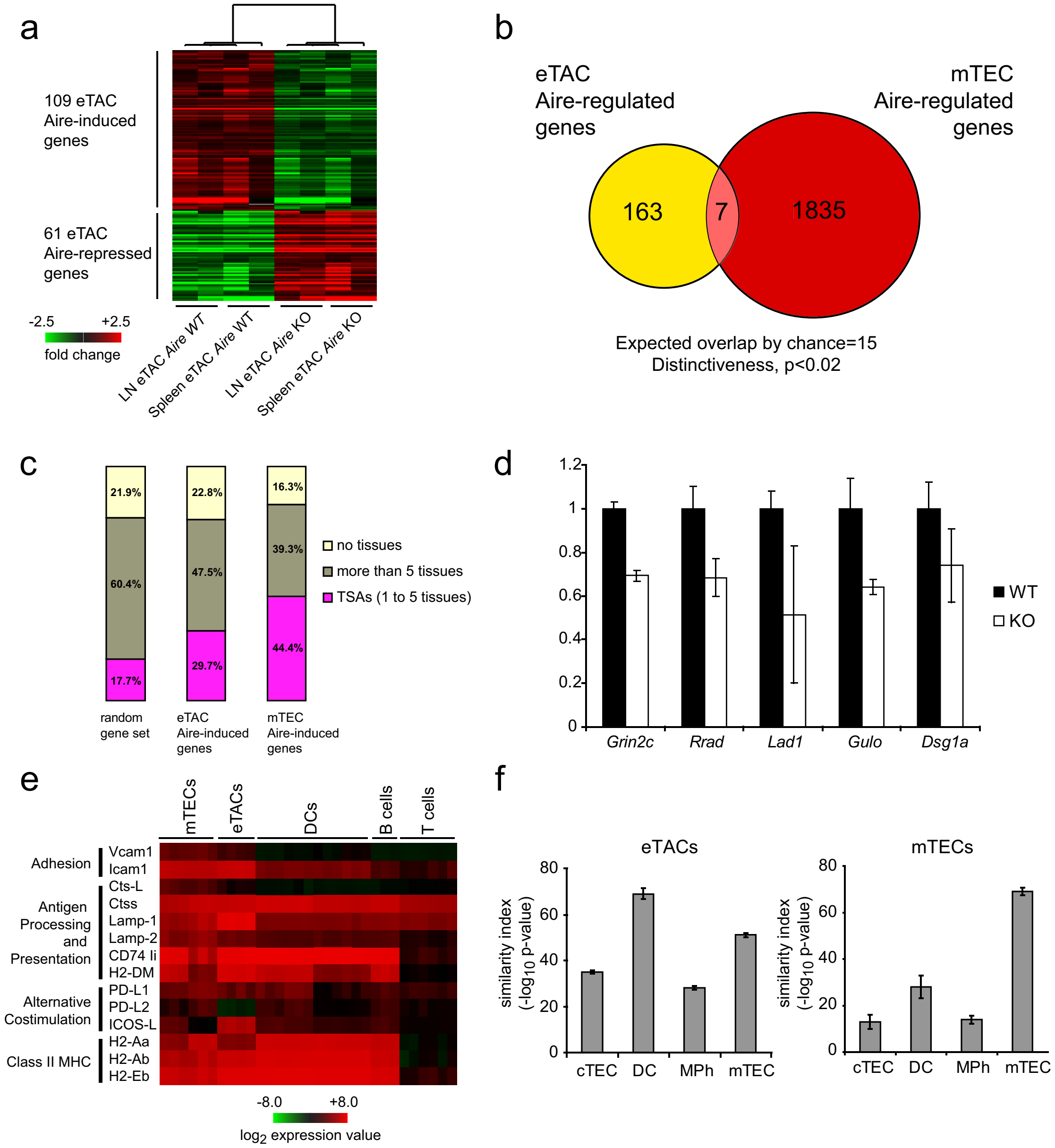
a
109 eTAC Aire-induced genes
61 eTAC Aire-repressed genes
-2.5
+2.5
fold change
LN eTAC Aire WT
Spleen eTAC Aire WT
LN eTAC Aire KO
Spleen eTAC Aire KO
b
eTAC Aire-regulated genes
mTEC Aire-regulated genes
163
7
1835
Expected overlap by chance=15
Distinctiveness, p<0.02
c
21.9%
60.4%
17.7%
22.8%
47.5%
29.7%
16.3%
39.3%
44.4%
no tissues
more than 5 tissues
TSAs (1 to 5 tissues)
random gene set
eTAC Aire-induced genes
mTEC Aire-induced genes
d
1.2
1
0.8
0.6
0.4
0.2
0
Grin2c
Rrad
Lad1
Gulo
Dsg1a
WT
KO
e
mTECs
eTACs
DCs
B cells
T cells
Adhesion
Vcam1
Icam1
Antigen Processing and Presentation
Cts-L
Ctss
Lamp-1
Lamp-2
CD74 Ii
H2-DM
Alternative Costimulation
PD-L1
PD-L2
ICOS-L
Class II MHC
H2-Aa
H2-Ab
H2-Eb
-8.0
+8.0
log2 expression value
f
eTACs
mTECs
similarity index (-log10 p-value)
80
60
40
20
0
cTEC
DC
MPh
mTEC

Table S2.1. Genes significantly upregulated in *Aire*$^{+/+}$ vs. *Aire* $^{-/-}$ eTACs. Genes are labeled according to accession number, gene symbol, and gene name, and ranked in descending order by fold change. Genes are color-coded according to whether they can be categorized as tissue-specific antigens (TSAs, pink), are below the detection threshold in all tissues (yellow), are housekeeping genes expressed in more than 5 tissues (gray), or were not accessible in the expression databases employed (white).

Table S2.1

🟪 TSA: 1-5 tissues
🟨 Below threshold in all tissues
⬛ Housekeeping: >5 tissues
☐ Not accessible

Aire-induced genes in eTACs

EntrezGeneID	**Gene Symbol**	**Gene Name**
67943	Mesdc2	mesoderm development candiate 2
192174	Rwdd4a	RWD domain containing 4A
12516	Cd7	CD7 antigen
239273	Abcc4	ATP-binding cassette, sub-family C (CFTR
73553	1700091H14Rik	RIKEN cDNA 1700091H14 gene
70356	St13	Suppression of tumorigenicity 13
56424	Stub1	STIP1 homology and U-Box containing protein 1
214854	Lincr	lung-inducible neuralized-related C3HC4 RING domain protein
11634	Aire	autoimmune regulator
17305	Mfng	manic fringe homolog (Drosophila)
12638	Cftr	cystic fibrosis transmembrane conductance regulator homolog
20353	Sema4c	sema domain, ig domain (Ig), tm domain (TM) and short cytoplasmic domain 4C
268756	Gulo	gulonolactone (L-) oxidase
67815	Sec14l2	SEC14-like 2 (S. cerevisiae)
54199	Ccrl2	chemokine (C-C motif) receptor-like 2
53876	Ear3	eosinophil-associated, ribonuclease A family, member 3
239554	Foxred2	FAD-dependent oxidoreductase domain containing 2
19659	Rbp1	retinol binding protein 1, cellular
217166	Nr1d1	nuclear receptor subfamily 1, group D, member 1
13026	Pcyt1a	phosphate cytidylyltransferase 1, choline, alpha isoform
78303	Hist3h2ba	histone cluster 3, H2ba
18166	Npy1r	neuropeptide Y receptor Y1
231637	Ssh1	slingshot homolog 1 (Drosophila)
328516	D430034N21	hypothetical protein D430034N21
11838	Arc	activity regulated cytoskeletal-associated protein
107766	Haao	3-hydroxyanthranilate 3,4-dioxygenase
67307	3110049J23Rik	RIKEN cDNA 3110049J23 gene
74137	Nuak2	NUAK family, SNF1-like kinase, 2
66790	Grtp1	GH regulated TBC protein 1
24115	Best1	bestrophin 1
109900	Asl	argininosuccinate lyase
75766	Tm7sf4	transmembrane 7 superfamily member 4
69632	Arhgef12	Rho guanine nucleotide exchange factor (GEF) 12
381409	Cdh26	cadherin-like 26
12778	Cxcr7	chemokine (C-X-C motif) receptor 7
17393	Mmp7	matrix metallopeptidase 7
109222	Rarres1	retinoic acid receptor responder (tazarotene induced) 1
207521	Dtx4	deltex 4 homolog (Drosophila)
67442	Retsat	retinol saturase (all trans retinol 13,14 reductase)
73280	1700028N14Rik	RIKEN cDNA 1700028N14 gene
11810	Apobec1	apolipoprotein B editing complex 1
70008	Ace2	angiotensin I converting enzyme (peptidyl-dipeptidase A) 2
17972	Ncf4	neutrophil cytosolic factor 4
13850	Ephx2	epoxide hydrolase 2, cytoplasmic
21366	Slc6a6	solute carrier family 6 (neurotransmitter transporter, taurine), member 6
53872	Caprin1	cell cycle associated protein 1
30933	Tor2a	torsin family 2, member A
20192	Ryr3	ryanodine receptor 3
60406	Sap30	sin3 associated polypeptide
14813	Grin2c	glutamate receptor, ionotropic, NMDA2C (epsilon 3)
16826	Ldb2	LIM domain binding 2
68067	3010026O09Rik	RIKEN cDNA 3010026O09 gene
103573	Xpo1	exportin 1, CRM1 homolog (yeast)
64058	Perp	PERP, TP53 apoptosis effector
102866	Pls3	plastin 3 (T-isoform)
223691	Eif3s6ip	eukaryotic translation initiation factor 3, subunit 6 interacting protein
67370	Zfp606	zinc finger protein 606
14466	Gba	glucosidase, beta, acid
20623	Snrk	SNF related kinase
14525	Gcet2	germinal center expressed transcript 2
93765	Ube2n	ubiquitin-conjugating enzyme E2N
319939	Tns3	tensin 3
11501	Adam8	a disintegrin and metallopeptidase domain 8
18641	Pfkl	phosphofructokinase, liver, B-type
97332	C87482	expressed sequence C87482
22339	Vegfa	vascular endothelial growth factor A
80288	Bcl9l	B-cell CLL
217666	L2hgdh	L-2-hydroxyglutarate dehydrogenase
54156	Egfl6	EGF-like-domain, multiple 6
110119	Mpi1	mannose phosphate isomerase 1
20519	Slc22a3	solute carrier family 22 (organic cation transporter), member 3
20815	Srpk1	serine
19012	Ppap2a	phosphatidic acid phosphatase 2a
56786	Tmem9b	TMEM9 domain family, member B
353187	Nr1d2	nuclear receptor subfamily 1, group D, member 2
19684	Rdx	radixin
14537	Gcnt1	glucosaminyl (N-acetyl) transferase 1, core 2
13510	Dsg1a	desmoglein 1 alpha
57319	Smpdl3a	sphingomyelin phosphodiesterase, acid-like 3A
15199	Hebp1	heme binding protein 1
320811	9430034N14Rik	RIKEN cDNA 9430034N14 gene
94213	Ddx50	DEAD (Asp-Glu-Ala-Asp) box polypeptide 50
381091	H2-Eb2	histocompatibility 2, class II antigen E beta2
268420	Alkbh5	alkB, alkylation repair homolog 5 (E. coli)
670480	6720475J19Rik	RIKEN cDNA 6720475J19 gene
226245	9930023K05Rik	RIKEN cDNA 9930023K05 gene
331045	A530083I20Rik	RIKEN cDNA A530083I20 gene
12145	Blr1	Burkitt lymphoma receptor 1

Table S2.2. Genes significantly downregulated in *Aire*$^{+/+}$ vs. *Aire* $^{-/-}$ eTACs. Genes are labeled according to accession number, gene symbol, and gene name, and ranked in descending order by fold change of Aire-repression.

Table S2.2

Aire-repressed genes in eTACs

EntrezGeneID	Gene Symbo	Gene Name
71198	Otud1	OTU domain containing 1
320244	Ttll5	tubulin tyrosine ligase-like family, member 5
17276	Mela	Melanoma antigen
81535	Sgpp1	sphingosine-1-phosphate phosphatase 1
20307	Ccl8	chemokine (C-C motif) ligand 8
12262	C1qc	complement component 1, q subcomponent, C chain
74558	Gvin1	GTPase, very large interferon inducible 1
17533	Mrc1	mannose receptor, C type 1
230787	BC013712	cDNA sequence BC013712
58203	Zbp1	Z-DNA binding protein 1
229900	Gbp6	guanylate binding protein 6
20556	Slfn2	schlafen 2
76933	Ifi27	interferon, alpha-inducible protein 27
110454	Ly6a	lymphocyte antigen 6 complex, locus A
16145	Igtp	interferon gamma induced GTPase
66141	Ifitm3	interferon induced transmembrane protein 3
66988	Lap3	leucine aminopeptidase 3
76192	Abhd12	abhydrolase domain containing 12
244871	Zc3h12c	zinc finger CCCH type containing 12C
74774	1110015C02R	RIKEN cDNA 1110015C02 gene
99101	AI851523	expressed sequence AI851523
14727	Gp49a	glycoprotein 49 A
26891	Cops4	COP9 (constitutive photomorphogenic) homolog, subunit 4
12524	Cd86	CD86 antigen
20452	St8sia4	ST8 alpha-N-acetyl-neuraminide alpha-2,8-sialyltransferase 4
14619	Gjb2	gap junction membrane channel protein beta 2
93834	Peli2	pellino 2
21838	Thy1	thymus cell antigen 1, theta
107568	Wwp1	WW domain containing E3 ubiquitin protein ligase 1
20620	Plk2	polo-like kinase 2 (Drosophila)
216080	Ube2d1	ubiquitin-conjugating enzyme E2D 1, UBC4
15953	Ifi47	interferon gamma inducible protein 47
14131	Fcgr3	Fc receptor, IgG, low affinity III
20363	Sepp1	selenoprotein P, plasma, 1
20715	Serpina3g	serine (or cysteine) peptidase inhibitor, clade A, member 3G
80876	Ifitm2	interferon induced transmembrane protein 2
19211	Pten	phosphatase and tensin homolog
14360	Fyn	Fyn proto-oncogene
192176	Flna	filamin, alpha
665433	RP23-480B19	similar to histone 2a
71733	Susd2	sushi domain containing 2
15442	Hpse	heparanase
109136	Mmaa	methylmalonic aciduria (cobalamin deficiency) type A
17105	Lyzs	lysozyme
67809	1200015F23R	RIKEN cDNA 1200015F23 gene
667914	Igk-V21-12	immunoglobulin kappa chain variable 21 (V21)-12
106622	AI605517	expressed sequence AI605517
69189	1810033B17R	RIKEN cDNA 1810033B17 gene
60533	Cd274	CD274 antigen
66614	Gpatc4	G patch domain containing 4
17084	Ly86	lymphocyte antigen 86
18301	Fxyd5	FXYD domain-containing ion transport regulator 5
17766	Nudt1	nudix (nucleoside diphosphate linked moiety X)-type motif 1
67414	Mfn1	mitofusin 1
68612	Ube2c	ubiquitin-conjugating enzyme E2C
19181	Pmsc2	proteasome (prosome, macropain) 26S subunit, ATPase 2
16331	Inpp5d	inositol polyphosphate-5-phosphatase D
13032	Ctsc	Cathepsin C
17279	Melk	maternal embryonic leucine zipper kinase
15566	Htr7	5-hydroxytryptamine (serotonin) receptor 7
12266	C3	complement component 3

total number of Aire-regulated genes in eTACs and the fold change of expression of those genes were smaller than has been observed in mTECs, perhaps reflecting the lower and potentially transient expression of *Aire* in the periphery. Strikingly, there was little overlap between Aire-regulated genes in eTACs and those in mTECs (**Figure 2.3B**), suggesting that Aire in the periphery may regulate expression of a unique set of self-antigens. Despite these differences, however, we found a significant enhancement for TSAs among the positively *Aire*-regulated genes in eTACs (**Figure 2.3C**), several of which were confirmed by quantitative RT-PCR (**Figure 2.3D**). The list of genes regulated by Aire in eTACs also included a number of self-antigens whose human homologs have been described as autoantigens in human autoimmune diseases, including desmoglein 1a (pemphigus foliaceus; *(18)*) ladinin 1 (linear IgA dermatosis, *(19)*), and the NMDA receptor 2C (systemic lupus erythematosis, *(20)*). Like other professional APCs, eTACs also expressed a large number of antigen-processing and presentation genes, suggesting a likely role for T-cell interaction (**Figure 2.3E**). Comparison of global gene expression profiles between eTACs, mTECs, cTECs, thymic DCs and macrophages indicated that eTACs were most similar to DCs and mTECs (**Figure 2.3F**).

To directly test the ability of eTACs to promote tolerance by interacting with and deleting autoreactive T cells, adoptive co-transfer of CFSE-labeled congenic *8.3* and polyclonal CD8+ T cells was employed. Upon transfer into wildtype hosts, *8.3* CD8+ T cells proliferated only in the pancreatic lymph nodes, and persisted in all lymph nodes for up to two weeks (**Figure 2.4A**). When transferred into *Adig* hosts, however, the entire population of *8.3* T cells proliferated rapidly in all secondary lymphoid organs by three days (**Figure 2.4A**), and had nearly disappeared by two weeks (**Figure 2.4A, C**). To confirm that the absence of *8.3* T cells in transgenic recipients was due to cell death and not egress, these experiments were repeated in the presence of the S1P1 inhibitor FTY 720 (*(21)*, **Figure S2.5**). Further, to determine whether a radioresistant eTAC population was sufficient to directly mediate this deletion, irradiated wildtype and *Adig* mice were reconstituted with bone marrow deficient for *β2-microglobulin* ($\beta 2M^{-/-}$) so that only radioresistant cells were capable of interacting with CD8+ lymphocytes. Chimerism was confirmed both by blood typing and functionally by observing that *8.3* T cells failed to proliferate in the pancreatic lymph nodes of nontransgenic $\beta 2M^{-/-}$ reconstituted mice (**Figure 2.4B**). In contrast, *8.3* T cells continued to proliferate in all secondary lymphoid organs of *Adig* $\beta 2M^{-/-}$ reconstituted mice at 3 days, and all divided *8.3* T cells had been deleted by 14 days (**Figure 2.4B, C**). While *8.3* cell division was less robust at day 3 in $\beta 2M^{-/-}$ chimeric *Adig* mice when compared to unirradiated *Adig* mice, antigen-specific cell death at day 14 was even more dramatic in this setting (**Figure 2.4A vs. B**).

To clearly delineate whether eTACs can directly interact with T cells, two-photon microscopy of explanted lymph nodes was employed. GFP+ cells were observed uniquely in all examined lymph nodes of *Adig* mice (**Movie s1; movies can be viewed or downloaded online at www.sciencemag.org/cgi/content/full/sci;321/5890/843/DC1**), in a distribution that mirrored the localization of eTACs observed by immunofluorescent

Figure 2.4. eTACs directly interact with autoreactive lymphocytes and mediate deletional tolerance. (**a**) Flow cytometry of CFSE-labeled and adoptively cotransferred *8.3* CD8+ T cells (Thy1.1) and polyclonal CD8+ T cells (Thy 1.2). Cells were harvested at day 3 (left) and day 14 (right) post-transfer (**b**) Adoptive transfer of the same donor populations as (a) into lethally irradiated wildtype (top) and *Adig* (bottom) recipients reconstituted with $\beta 2M^{-/-}$ bone marrow. (**c**) Quantitation of antigen-specific deletion after adoptive transfer at day 14 in (a) and (b), showing the ratio of *8.3*:polyclonal CD8+ T cells in wildtype (black) and *Adig* (white) NOD recipients. Representative of at least three mice each. (**d-g**) Two-photon imaging of *8.3* and polyclonal CD8+ T cells in axillary lymph nodes 4 hours after adoptive transfer into *Adig* NOD recipients. (**d**) 10-minute displacement analysis of all *8.3* CD8+ T cell tracks (left) and polyclonal CD8+ T cell tracks (right). (**e**) Representative images of interaction between *8.3* CD8+ T cells (red), polyclonal CD8+ T cells (yellow) and eTACs (green) (**f**) Average T cell track speed (left), percent of time in which a T cell is stopped (middle), and percent of time in which a T cell is making contact with an eTAC (right) among polyclonal (Poly) and *8.3* (*8.3*) CD8 T cells. ** $P<0.001$. (**g**) Histogram displaying the duration of individual T cell-eTAC interaction times per contact for polyclonal (black bars) and *8.3* (white bars) CD8+ T cells.

Figure 2.4

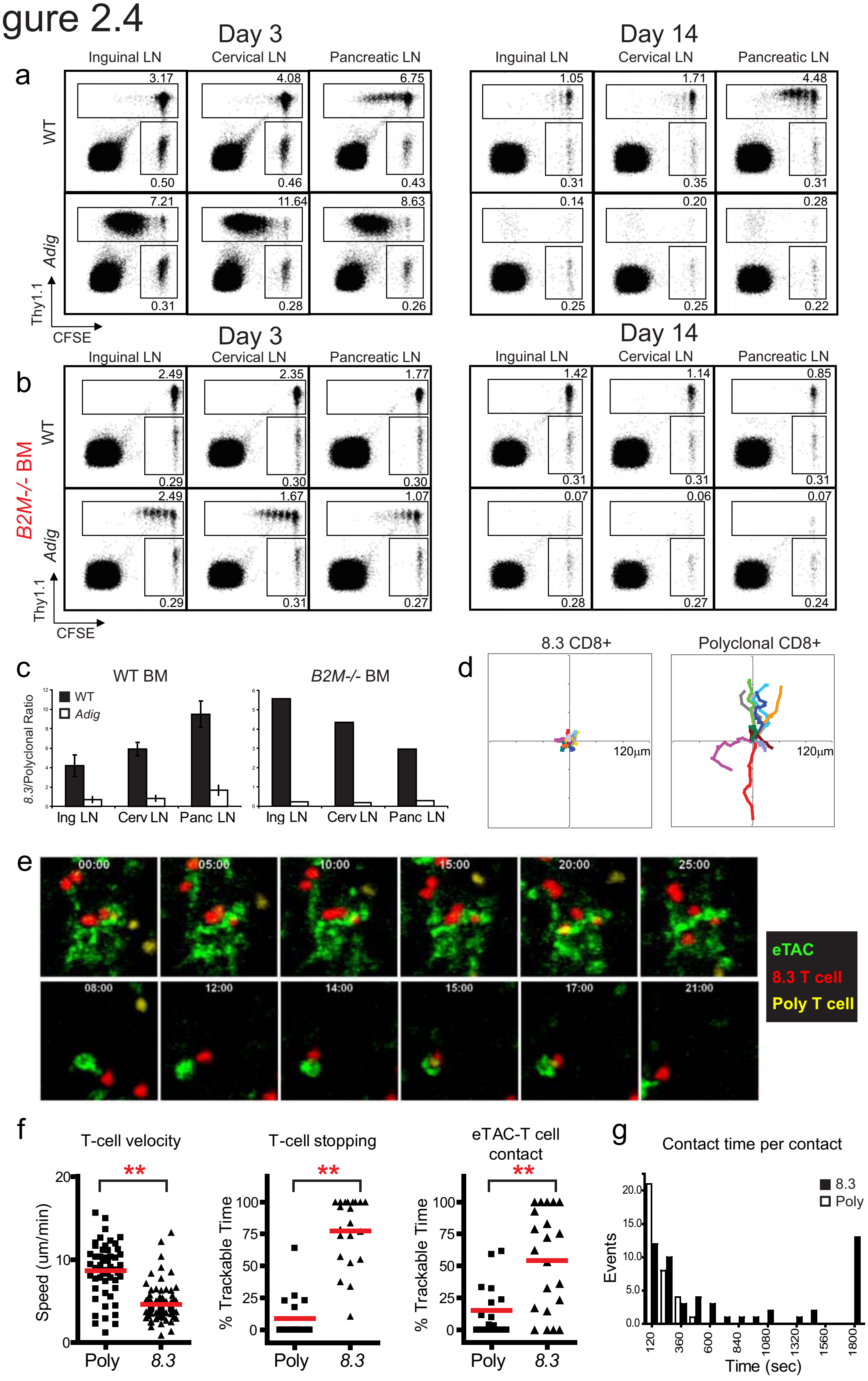
a
Day 3
Day 14
Inguinal LN
Cervical LN
Pancreatic LN
WT
Adig
Thy1.1
CFSE
3.17
0.50
4.08
0.46
6.75
0.43
1.05
0.31
1.71
0.35
4.48
0.31
7.21
0.31
11.64
0.28
8.63
0.26
0.14
0.25
0.20
0.25
0.28
0.22
b
B2M-/- BM
2.49
0.29
2.35
0.30
1.77
0.30
1.42
0.31
1.14
0.31
0.85
0.31
2.49
0.29
1.67
0.31
1.07
0.27
0.07
0.28
0.06
0.27
0.07
0.24
c
WT BM
B2M-/- BM
8.3/Polyclonal Ratio
WT
Adig
Ing LN
Cerv LN
Panc LN
d
8.3 CD8+
Polyclonal CD8+
120µm
e
00:00
05:00
10:00
15:00
20:00
25:00
08:00
12:00
14:00
15:00
17:00
21:00
eTAC
8.3 T cell
Poly T cell
f
T-cell velocity
Speed (um/min)
T-cell stopping
% Trackable Time
eTAC-T cell contact
**
Poly
8.3
g
Contact time per contact
Events
Time (sec)
8.3
Poly

Figure S2.5. The relative absence of 8.3 T cells after adoptive transfer into *Adig* mice is not due to egress (**a**) Representative flow cytometric analysis of CD4+, CD62+, CD69lo thymocytes stained with anti-S1P1 (red) or isotype (green) in wildtype (middle panel) or *Adig* (left and right panels) recipients treated with saline (left panel) or FTY 720 (middle and right panels) every 2 days for 14 days. (**b**) Representative CFSE and Thy1.1 levels of CFSE-labeled and adoptively cotransferred 8.3 CD8+ T cells (Thy1.1) and polyclonal CD8+ T cells (Thy 1.2) pre-gated on forward/side scatter and CD4- CD8+ status. Cells were harvested after 14 days in either wildtype (top panels) or *Adig* NOD mice (bottom panels) treated with FTY 720 during incubation. (**c**) Quantitation of antigen-specific deletion after adoptive transfer at day 14 in (b), showing the ratio of 8.3:Polyclonal CD8+ T cells in wildtype (black) and *Adig* (white) recipients; representative of at least four mice per group.

Figure S2.5

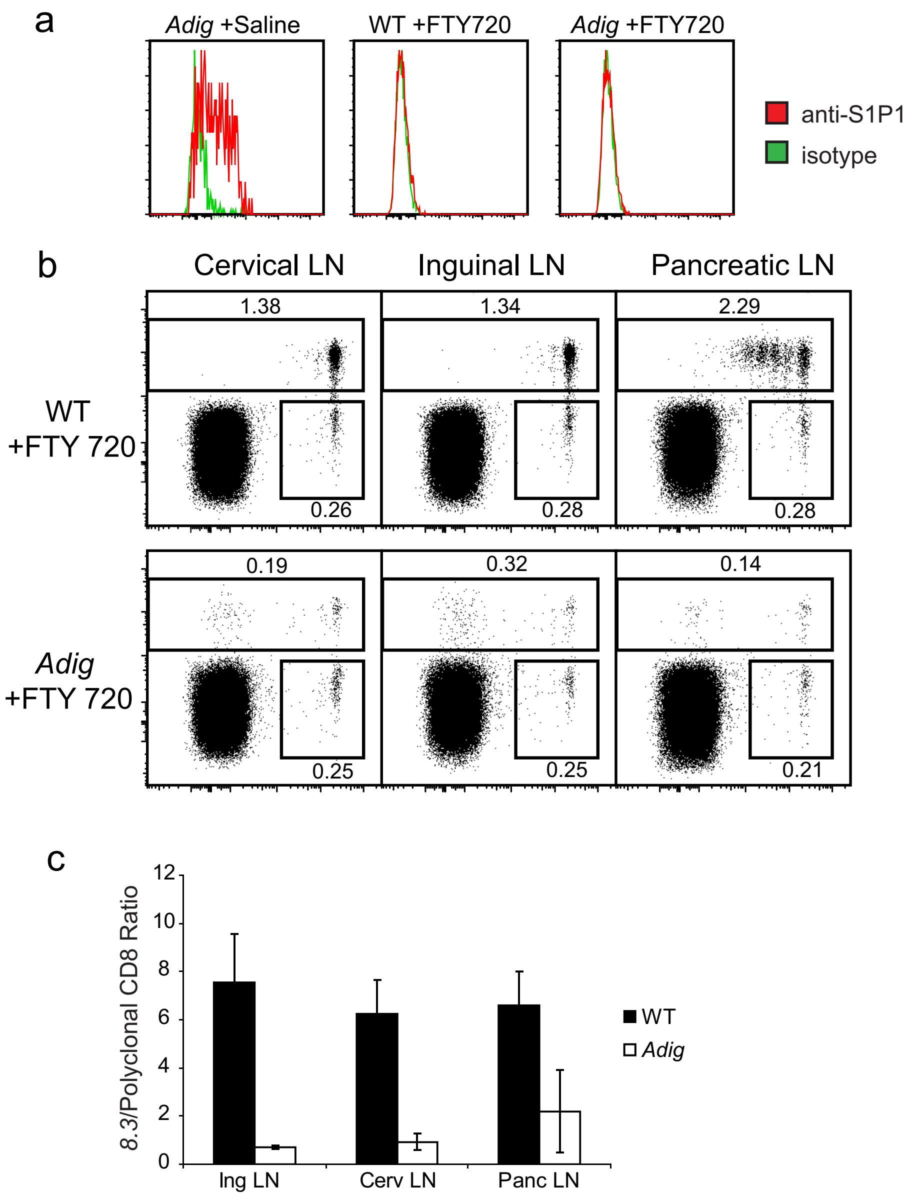
a
Adig +Saline
WT +FTY720
Adig +FTY720
🟥 anti-S1P1
🟩 isotype
b
Cervical LN
Inguinal LN
Pancreatic LN
WT
+FTY 720
1.38
0.26
1.34
0.28
2.29
0.28
Adig
+FTY 720
0.19
0.25
0.32
0.25
0.14
0.21
c
8.3/Polyclonal CD8 Ratio
12
10
8
6
4
2
0
Ing LN
Cerv LN
Panc LN
■ WT
□ *Adig*

staining (**Movie s2, Figure 2.2A**). Adoptive cotransfer of fluorophore-labeled *8.3* and polyclonal CD8+ T cells demonstrated sustained antigen-specific association between naïve *8.3* T cells and eTACs as early as four hours post-transfer (**Figure 2.4D, 2.4E, Movies s3-s4**). *8.3* T cells exhibited distinct reductions in speed and total displacement relative to polyclonal CD8+ T cells (**Figure 2.4D, F**), and *8.3* T cells spent significantly more time both stopped and in direct contact with eTACs (**Figure 2.4F**). Indeed, the upper limit of this interaction time is unknown, as many *8.3* T cells spent the entire 30-minute duration of the acquisition periods in continuous contact (**Figure 2.4G, Movie s5**). Some GFP+ cells in the lymph node appeared highly motile, but *8.3* T cells were able to maintain antigen-specific interactions despite this motility (**Figure 2.4E, Movie s6**). Together, these results suggested that eTACs can form early, stable, long-term contacts with naïve autoreactive T cells entering the lymph node, and that such interaction leads to rapid proliferation and deletion of these T cells.

Discussion

Here we have identified a novel population of extrathymic *Aire*-expressing cells (eTACs) that may play a significant and previously uncharacterized role in self-tolerance via the deletion of autoreactive T cells. Indeed eTACs share certain characteristics with mTECs, including being equipped to act as professional antigen-presenting cells and the Aire-regulated expression of unique tissue-specific antigens (TSAs). Interestingly, the set of Aire-regulated TSAs expressed in eTACs appears to have little overlap with thymic

Aire-regulated antigens, which may explain why previous efforts examining known thymic TSAs for expression in secondary lymphoid organs have been inconsistent or conflicting. The lack of overlap suggests that there may be a higher order of Aire-dependent transcriptional regulation of TSA expression, whether direct or indirect, that differs between the thymus and the periphery. Many important questions remain, including the developmental origin of eTACs, and their relationship with other possible radioresistant APC populations *(9)*. In this regard, the precise identification of eTACs will provide the framework for further exploring these issues. Further, it will be important to determine the physiologic relevance of this cell population in a non-transgenic setting, given the modest levels of TSA expression and and Aire-dependent gene upregulation in eTACs (approximately two-fold). However, it is notable that similar analyses of Aire-expressing thymic epithelial cells (mTECs) have demonstrated that TSAs are expressed at low levels in these cells *(2, 4)*, but even this low level of expression has proven critical for the maintenance of immune tolerance *(4, 22)*. Indeed, our findings suggest that eTACs may represent a "safety net" within the entire immunologic periphery which functions to screen out naïve autoreactive T cell clones that escape thymic negative selection. Finally, we speculate that eTACs may play an increasingly significant role with advancing age, as the thymus involutes and the burden of maintaining self-tolerance shifts to the periphery.

Supplementary movies and movie legends can be viewed online at: www.sciencemag.org/cgi/content/full/sci;321/5890/843/DC1

Materials and Methods

Transgene Construction, BAC Recombineering, and Purification

Aire-driven *Igrp-Gfp (Adig)* transgenic mice were generated by standard methods using a bacterial artificial chromosome (BAC) recombineering and transgenesis strategy. Briefly, we first generated a plasmid for BAC-targeted recombineering, JDLNL, which contained 5' and 3' *Aire* homology arms flanking the IGRP-GFP fusion protein sequence. The green fluorescent protein and SV40 polyadenylation sequence were cloned from the vector eGFP-N3 (Clontech) through polymerase chain reaction. The 5' and 3' *Aire* homology arms were cloned from murine genomic DNA. To stabilize transgene expression, a β-globin splice donor and acceptor cassette were placed in the first exon of the Aire gene just upstream of the ATG translation initiation site. The *Igrp-Gfp* fusion/SV40 sequence was inserted immediately downstream of this β-globin splice site. All inserted fragments were produced through polymerase chain reaction and cloned into the pcDNA vector via compatible restriction ends.

This targeting construct, JDLNL, was then inserted via standard recombineering *(23)* into a BAC clone from the Children's Hospital of Oakland Research Institute (CHORI) BACPAC Resource Center, clone 461e7 from the RPCI 23 Mouse BAC Library, which contained the *Aire* gene and approximately 90Kb of flanking sequence both upstream and downstream. The BAC identity was verified by PCR and restriction digestion, then purified and transfected via electroporation using standard techniques into the heat-inducible recombinase-competent and arabinose-inducible Cre-expressing bacterial strain EL350. The *loxP* site in the eBAC3.6 vector was first removed by targeted homologous recombination. Heat-induced recombination was achieved by culturing the bacteria at 42°C, rapidly cooling, then electroporating in the presence of linearized JDLNL plasmid. After selection and PCR-screening of recombinants, Cre expression was induced in positive clones by culturing in 0.1% arabinose for three hours at 30°C. Cre-recombinant clones were screened by replica-plating for acquisition of kanamycin sensitivity. Positive clones were then rescreened by Southern blot using KpnI and SpeI digests and a 600-bp probe downstream of *Aire* exon 3 generated by the primers 5'-TCTCGTCCTCAAGAGTGCC-3' and 5'-GTCATGTTGACGGATCCA-3'.

Highly purified BAC DNA was prepared for oocyte injection by high-speed centrifugation in a CsCl gradient. Bulk DNA was extracted from 2L of overnight bacterial culture at 32°C by alkaline lysis and isopropanol/ethanol precipitation. This bulk DNA was then resuspended in TE plus 1.05g/mL CsCl with .01% Ethidium Bromide and ultracentrifuged at 65,000 rpm for 18 hours without brake. After centrifugation, BAC DNA was clearly visible as a band distinct from bacterial genomic DNA. This DNA was gently extracted via 18-gauge needle aspiration, ethanol-precipitated, and resuspended in injection buffer (10mM Tris-HCL, 0.1 mM EDTA, pH 7.5). Resuspended BAC DNA was then injected into fertilized oocytes by the UCSF Mouse Transgenic Core with the assistance of J. Dietrich and N. Killeen.

Mice and Genotyping

Adig transgenic NOD and C57BL/6/d2 founder mice (two founders each) were generated as described above. Founders were bred into their respective backgrounds and offspring were screened for the presence of the IGRP-GFP transgene using the genotyping primers 5'-AAGTTCATCTGCACCACC-3' and 5'-TCCTTGAAGAAGATGGTGCG-3'. Of the initial four founders generated, the two NOD founders had slightly higher levels of transgene expression, and these two lines were propagated and used for all subsequent analysis. The *Adig* transgene was maintained in heterozygosity for all experiments. TCR-transgenic *8.3* NOD mice were acquired from J. Bluestone and Q. Tang and also maintained in heterozygosity, and were screened for the presence of the *8.3* TCR transgene by peripheral blood FACS using a clonotype-specific antibody against the Vβ8.1 chain of the TCR (BD Pharmingen). Clonotype-specific antibody staining allowed us to genotype animals which were *8.3/Adig* double-transgenic, as these animals retained high levels of Vβ8.1 usage despite the loss of tetramer-reactivity due to thymic negative selection of IGRP-reactive clones. Mice were genotyped for *Aire* status using the primers 5'-GTCCCTGAGGACAAGTTCCA-3' and 5'-TCTTTGAGGCCAGAGTTGCT-3'.

All mice were maintained in microisolator cages and treated in accordance with NIH and American Association of Laboratory Animal Care standards, and consistent with the animal care and use regulations of the University of California, San Francisco.

Flow Cytometry and Cell Sorting

All antibodies were purchased from BD Pharmingen, eBioscience, Invitrogen, or Southern Biotech with the exception of 2.4G2 and I-Ag7, which were purified and donated by J. Bluestone, and EpCAM, which was purified and biotinylated by K. Johannes. Stromal cells were prepared for FACS by mincing with surgical razor blades followed by mechanical disruption and enzymatic digestion in 0.125% Collagenase D (Roche) and 20ug/mL DNase I (Roche). Subsequently 10ug/ml Dispase I (Roche) was added to ensure complete digestion. Digested cells were then resuspended in PBS with 0.5% BSA and 2mM EDTA, and passed through a 70μm cell-strainer. Density-gradient centrifugation using a three-layer Percoll gradient (GE Healthcare) with specific gravities of 1.115, 1.065, and 1.0 was used to enrich for stromal cells, which reside in the light fraction. Cells isolated from the Percoll-light fraction, between the 1.065 and 1.0 layers, were then resuspended in FACS buffer and counted. Prior to antibody staining, cells were incubated with anti-Fc receptor blocking antibody clone 2.4G2 for ten minutes. Cells were then incubated with antibody cocktails for 20 minutes on ice, washed three times in PBS and re-filtered. To exclude dead cells, either 4',6-diamidino-2-phenylindole (DAPI) or Propidium Iodide (PI) was added prior to acquisition. Immunostained cells were analyzed by flow cytometry on an LSR II (BD Biosciences), and analyzed using FloJo data analysis software (Tree Star). To sort specific cell populations we followed the same preparation and staining protocol as above, but used a MoFlo fluorescent cell sorting machine (Dako) with the assistance of S. Jiang. We sorted cells directly into cold DMEM with 50% FCS.

Lymphocytes for flow cytometry were prepared by mashing thymi, lymph nodes, or spleens, filtering these cells through a 70μm cell-strainer, lysing red blood cells by two minutes' incubation in ACK buffer (spleen only; 0.15 M NH_4Cl, 10 mM $KHC0_3$, 0.1 mM Na_2EDTA), resuspending in anti-Fc receptor blocking antibody clone 2.4G2 for ten minutes, then incubating on ice with antibody cocktails for twenty minutes. For peptide/class I MHC tetramer staining, cells were incubated on ice with antibody cocktail along with either IGRP mimetope/class I MHC tetramer NRP-V7-PE (KYNKANVFL/K^d) or with irrelevant tetramer TUM-PE (KYQAVTTTL/K^d, NIAID

MHC Tetramer Core Facility) for one hour, then washed and analyzed by flow cytometry as described above.

Isolation of RNA, Microarray and Real-Time PCR

Specific subpopulations of stromal cells which had been purified by cell-sorting were stored on ice during the collection period and immediately lysed for RNA extraction upon completion of the sort. RNA was purified using the Absolutely RNA Microprep kit (Stratagene) and quantitated using a NanoDrop spectrophotometer (Thermo Fisher Scientific). For Microarray analysis, RNA was then processed by the Gladstone Institute Genomics Core. Briefly, RNA was first analyzed for quality and sample degradation using the Eukaryote Total RNA Pico Series II chip on a 2100 Bioanalyzer (Agilent). Because of small sample sizes, RNA samples were then amplified using the Ribo-SPIA process (NuGen Technologies). *In vitro* transcription was then performed to produce biotinylated cRNA, which was subsequently fragmented by partial hydrolysis in the presence of Mg++ and high temperature before hybridization onto GeneChip® Mouse Genome 430 2.0 arrays (Affymetrix). Array data was deposited into the Gene Expression Omnibus public database.

For real-time PCR, stromal cells were isolated from thymus, spleen, and pooled lymph nodes as described above. eTACs, mTECs, and DCs were sorted from nontransgenic *Aire*-wildtype and *Aire*-knockout mice between 3 and 6 weeks of age based on the following surface markers: eTACs and mTECs: PI-, CD45-, CD11c-, MHC II+, EpCAM+; bulk DCs: PI-, CD45+, CD11c+, MHC II+, EpCAM-. RNA was purified using the Absolutely RNA Microprep kit (Stratagene) and quantitated using a NanoDrop spectrophotometer (Thermo Fisher Scientific). After quantitation, RNA was reverse-transcribed into cDNA using oligo-dT (Invitrogen) and Sensiscript reverse transcriptase (Qiagen). Equivalent reactions without reverse transcriptase were run for each sample. To confirm the identity of the *Aire*-regulated genes in eTACs, we used TaqMan® Gene Expression Assays (Applied Biosystems) for gulonolactone-(L) oxidase (*Gulo*), ras-related associated with diabetes (*Rrad*), glutamate receptor, ionotropic, NMDA2C (*Grin2c*), ladinin (*Lad1*), and desmoglein 1 alpha (*Dsg1a*). Cyclophilin was used as an endogenous control, for which we employed the primers 5'-

CAGACGCCACTGTCGCTTT-3’ and 5’-TGTCTTTGGAACTTTGTCTGCAA-3’ and the FAM/BHQ probe 5’-CCCTTGGGCCGCGTCTCCTT-3’. *Aire* expression was quantitated using the knockout-distinguishing primers 5’-CAGCCGCCTGCATAGCAT-3’ and 5’-GGCTCCTCCAGTGCTTTTCTCT-3’ and the FAM/BHQ probe 5’-GGCTTCCCAAAAGATGTGGACCTAAA-3’. PCR reactions and data acquisition were performed with the 7500 Fast Real-Time PCR System (Applied Biosystems) run for 50 cycles, and data analysis was performed using Excel (Microsoft).

For real-time PCR analysis of *Aire*, *Igrp*, and insulin transcripts in the thymus and pancreas, whole pancreas and CD45-depleted thymus (Miltenyi AutoMACS-depletion) were lysed and RNA-extracted using the Absolutely RNA Microprep kit (Stratagene), then reverse-transcribed to cDNA as described above. Real-time PCR was run on thymic and pancreatic cDNA samples for *Aire* (primers/probe as above), *Igrp* (forward: 5’-GCAGTTTCCTACTACGTGTGAAACA-3’, reverse: 5’-ACGCACGATGAGCCCATT-3’, FAM/TAMRA probe: 5’-CCCAGGAAGTCCATCTGGCCACG-3’), and insulin (forward: 5’-CTTCAGACCTTGGCGTTGGA-3’, reverse: 5’-ATGCTGGTGCAGCACTGATC-3’, FAM/TAMRA probe: 5’-CCCGGCAGAAGCGTGGCATT-3’).

Microarray Data Analysis

Expression data was processed with Robust Multichip Analysis (RMA) normalization in GeneSpring (Agilent). Genes were then filtered for expression of greater than 200 in at least 50% of the samples. Significance analysis of microarrays (SAM) was used to identify genes differentially expressed in *Aire*-wildtype and *Aire*-knockout eTACs. 109 genes were induced and 61 genes were repressed in *Aire*-wildtype eTACs relative to *Aire*-knockout eTACs (FDR<0.15). Expression values for each gene were mean-centered across all of the arrays and unsupervised hierarchical clustering was carried out with the Cluster software and displayed with Treeview software *(24)*. The same analysis with the same parameters was performed to identify genes differentially expressed in *Aire*-wildtype and *Aire*-knockout mTECs from previously published expression profiles that were performed on the same array platform (GSE8563) *(25)*. 1343 genes were induced and 499 genes were repressed in *Aire*-wildtype mTECs relative to *Aire*-knockout mTECs (FDR<0.15).

Tissue-specific self-antigens (TSAs) were defined based on previously published expression data across 34 different mouse tissues (GSE1133) *(26)*. This expression data was processed with RMA normalization in GeneSpring. Genes with expression greater than 200 in one to five tissues were defined as TSAs. Each of the following was considered a single tissue: 1) all central nervous system tissues; 2) small and large intestine; and 3) all epidermal tissues. Tissue from embryos was excluded from the analysis. Additionally, genes in which tissue-specificity corresponded to the tissue from which the sample was taken (e.g. lymph node, thymus, spleen) were excluded from analysis.

Expression of antigen processing and presentation genes was determined for eTACs as well as mTECs, DCs, T cells, and B cells (GSE8563 and GSE6259) *(3, 27)*. The level of expression of each gene in each sample was normalized by median centering to the expression of all genes in each array, and unsupervised hierarchical clustering was carried out on the genes with Cluster software and displayed with Treeview software (***Error! Bookmark not defined.***).

The expression profiles of the eTACs were used to evaluate their similarity to other immune cells, specifically mTECs, cTECs, dendritic cells, and macrophages. Based on previously published expression profiles of mTECs, cTECs, dendritic cells, and macrophages (GSE2585) *(3)*, centroids were defined for each of these immune cells that distinguish each cell type using multi-class SAM analysis. Pearson correlations were calculated for each centroid with our eTACs expression profile as well as an independent mTECs expression profile (GSE8563, ***Error! Bookmark not defined.***).

Immunofluorescent Staining and Quantitation

All primary and secondary antibodies were purchased from AbCam, BD Pharmingen, Invitrogen, or eBioscience, with the exception of anti-gp38 and anti-S1P1, which were generous gifts from J. Cyster, and the anti-Aire antibodies 5C-11 and 5H-12, which were gifts of H. Scott. Organs were harvested from experimental animals and embedded in Tissue-Tek Optimal Cutting Temperature (OCT) media (Fisher), then frozen to -80 C for storage. 8μm frozen sections were cut using a CM3050S Cryostat (Leica) and allowed to dry for 30 minutes at room temperature. Sections were then fixed in -20 C acetone for 10 minutes and dried at room temperature for thirty minutes before storage at -80 C or immediate staining. Slides were washed three times in PBS and incubated in 10% secondary serum for thirty minutes at room temperature to block. Primary antibody cocktails diluted in 3% BSA in PBS were then added directly to blocking solution on the tissue section and incubated for one hour at room temperature. Slides were washed three times in PBS and then incubated in secondary antibody cocktail in 3% BSA in PBS for one hour. When used (for anti-Aire staining in the thymus and periphery), tertiary antibody solutions were similarly applied. Slides were mounted in Vectashild mounting medium (Vector Laboratories) and visualized on an Axioskop 2 Plus Widefield Scope (Leica) attached to a C4742-95 digital camera (Hamamatsu). Images were acquired using OpenLab software (Improvision), and analyzed, processed via linear contrast adjustment, and merged with Photoshop CS3 (Adobe).

For quantitation of Aire/GFP localization in the thymus and the periphery, frozen tissue sections from multiple independent founders were co-stained for GFP and Aire using two independent anti-Aire monoclonal antibodies (clones 5C11 and 5H12). Per-cell corrlation was then analyzed by independent observers for each condition (Aire antibody, founder) in duplicate, with each count totaling greater than 100 cells. The results were pooled to generate average values.

Bone Marrow Chimeras

Reciprocal bone marrow chimeras were generated using *Adig* and wildtype NOD mice as recipients. All recipient mice received 1300 rads during two irradiation cycles of 900 and 400 rads each, separated by a minimum of six hours. Between irradiation cycles, marrow was harvested from *β2-microglobulin* knockout (*β2M*$^{-/-}$) mice by removal and flushing of the long bones (femurs, tibia, humeri) and filtration of marrow suspension through a 70μm cell-strainer. Bone marrow cells were then depleted of T lymphocytes by incubation for 15 minutes on ice in the presence of anti-CD4 (clone GK1.5) and anti-CD8 (clone 3.155) antibodies, followed by the addition of rabbit complement in prewarmed RPMI and incubation for an additional hour at 37 degrees. Cells were then washed three times in PBS, counted, and resuspended in Hank's BSS media for injection. After the second (400 rad) irradiation of recipient mice, 10e7 donor-derived bone marrow cells were introduced into each recipient via tail vein injection. Uninjected controls were included in each experiment. Mice were allowed to reconstitute for 8 weeks, confirmed for chimerism in both the lymphocyte and DC populations by blood typing of class I MHC expression on B220+, and CD11c+ cells.

Purification, CFSE and CMTMR-labeling, and Adoptive Transfer of T cells

For adoptive transfer of naive *8.3* and polyclonal CD8+ T cells, the spleen and all major peripheral lymph nodes except pancreatic lymph nodes were harvested from nondiabetic donors, pooled by group, ACK-lysed and purified by negative selection using an AutoMACS (Miltenyi). Cells were incubated for fifteen minutes with a cocktail of biotinylated anti-CD19, anti-Ly6G, anti-MHC II, anti-CD24, anti-CD117, and anti-CD4 (Southern Biotech), washed and incubated for fifteen minutes with anti-biotin tetrameric antibody complex (StemCell Technologies). Magnetic colloid was then added (StemCell Technologies), and cells were incubated an additional fifteen minutes before being washed, recounted, and run through a single AutoMACS depletion cycle. Cells were subsequently washed, recounted, and samples set aside for FACS confirmation of purity.

When labeling for FACS, AutoMACS-purified cells were pooled in a ~5:1 ratio of *8.3* T cells:polycolonal CD8 T cells then labeled in 2.5μM CFSE (Invitrogen) at room temperature for 5 minutes. Labeling was quenched with an equal volume of FCS, cells were washed twice in DMEM and once in Hank's BSS, counted and injected at 5e6 cells/recipient via the tail vein. When labeling for two-photon imaging, cell populations were kept separate and labeled with either 2.5μM CFSE alone or 2.5μM CFSE and 20μM CMTMR for 30 minutes at 37 degrees, then quenched with an equal volume of FCS. Cells were washed twice in DMEM and once in Hank's BSS, then pooled in a 1:1 ratio of *8.3* T cells:polycolonal CD8 T cells and injected via the tail vein at 5e6 total cells/recipient. Reciprocal labeling experiments were performed for both cell populations.

After transfer, animals were followed for the indicated periods and analyzed as described. For egress-inhibition experiments, mice were treated every 48 hours with 1mg/kg FTY 720 (a gift of J. Cyster) in saline, beginning one day after adoptive transfer and continuing for the duration of the two-week incubation period.

Two-Photon Laser Scanning Microscopy Imaging and Analysis

A custom resonant-scanning instrument based on published designs *(28)* containing a four–photomultiplier tube (PMT) array operating at video rate was used for two-photon microscopy. Axillary lymph nodes were immobilized on coverslips with the efferent lymphatics facing away from the objective, and imaged through the capsule. Lymph nodes were maintained at 36 °C in RPMI medium perfused with 95% O_2/5% CO_2. Samples were excited with a 10-W MaiTai TiSaphire laser (SpectraPhysics) tuned to a wavelength of 910 nm, and emission wavelengths of 455-495 nm (for second-harmonic emission), 500–520 nm (for GFP and CFSE), 528-556 nm (for CFSE and autofluorescence) and 567–640 nm (for CMTMR) were collected. To improve detection of GFP+ cells, the 500-520 nm channel was collected using a high-gain PMT module (H7422P, Hamamatsu). A custom four-dimensional acquisition module in the VideoSavant digital video recording software (IO Industries) was used for image acquisition. For time-lapse image acquisition, each *xy* plane spanned 313μm x 261μm at a resolution of 0.653μm/pixel. 20-30 video-rate frames were averaged, giving effective collection times of approximately 0.5-1 second per plane. Images of up to 30 *xy* mμplanes with 3μm *Z*-spacing were acquired every 30 sec for 30 min.

Data was visualized and analyzed using Imaris 5.7.2 Software (Bitplane). CMTMR + CFSE double-labeled cells were identified by colocalization of signal in the 500-520nm and 567-640nm channels using Imaris software. Single-channel fluorescence from double-labeled cells and autofluorescence in the 500-520nm and 567-640nm channels were eliminated by linear unmixing using Imaris and MATLAB (Mathworks) software. Individual cells were identified and tracked by Imaris, and cell speed and displacement were calculated from tracks. Cell-cell interaction and stopping of tracked cells were manually scored. Statistical analysis of speeds, stopping times, and interaction times was done using Prism 4.0 (GraphPad Software) employing an unpaired t-test with Welch's correction and a two-tailed 95% confidence interval.

References

1. Smith KM, Olson DC, Hirose R, Hanahan D. Pancreatic gene expression in rare cells of thymic medulla: evidence for functional contribution to T cell tolerance. Int Immunol 1997;9:1355-65.
2. Derbinski J, Schulte A, Kyewski B, Klein L. Promiscuous gene expression in medullary thymic epithelial cells mirrors the peripheral self. Nat Immunol 2001;2:1032-9.
3. Derbinski J, Gabler J, Brors B, et al. Promiscuous gene expression in thymic epithelial cells is regulated at multiple levels. J Exp Med 2005;202:33-45.
4. Anderson MS, Venanzi ES, Klein L, et al. Projection of an immunological self shadow within the thymus by the aire protein. Science 2002;298:1395-401.
5. Liston A, Lesage S, Wilson J, Peltonen L, Goodnow CC. Aire regulates negative selection of organ-specific T cells. Nat Immunol 2003;4:350-4.
6. Ramsey C, Winqvist O, Puhakka L, et al. Aire deficient mice develop multiple features of APECED phenotype and show altered immune response. Hum Mol Genet 2002;11:397-409.
7. Nagamine K, Peterson P, Scott HS, et al. Positional cloning of the APECED gene. Nat Genet 1997;17:393-8.
8. An autoimmune disease, APECED, caused by mutations in a novel gene featuring two PHD-type zinc-finger domains. Nat Genet 1997;17:399-403.
9. Lee JW, Epardaud M, Sun J, et al. Peripheral antigen display by lymph node stroma promotes T cell tolerance to intestinal self. Nat Immunol 2007;8:181-90.
10. Halonen M, Pelto-Huikko M, Eskelin P, Peltonen L, Ulmanen I, Kolmer M. Subcellular location and expression pattern of autoimmune regulator (Aire), the mouse orthologue for human gene defective in autoimmune polyendocrinopathy candidiasis ectodermal dystrophy (APECED). J Histochem Cytochem 2001;49:197-208.
11. Hubert FX, Kinkel SA, Webster KE, et al. A specific anti-Aire antibody reveals aire expression is restricted to medullary thymic epithelial cells and not expressed in periphery. J Immunol 2008;180:3824-32.

12. Yu W, Misulovin Z, Suh H, et al. Coordinate regulation of RAG1 and RAG2 by cell type-specific DNA elements 5' of RAG2. Science 1999;285:1080-4.

13. Nagata M, Santamaria P, Kawamura T, Utsugi T, Yoon JW. Evidence for the role of CD8+ cytotoxic T cells in the destruction of pancreatic beta-cells in nonobese diabetic mice. J Immunol 1994;152:2042-50.

14. Han B, Serra P, Yamanouchi J, et al. Developmental control of CD8 T cell-avidity maturation in autoimmune diabetes. J Clin Invest 2005;115:1879-87.

15. Lieberman SM, Evans AM, Han B, et al. Identification of the beta cell antigen targeted by a prevalent population of pathogenic CD8+ T cells in autoimmune diabetes. Proc Natl Acad Sci U S A 2003;100:8384-8.

16. Jarchum I, Nichol L, Trucco M, Santamaria P, DiLorenzo TP. Identification of novel IGRP epitopes targeted in type 1 diabetes patients. Clin Immunol 2008;127:359-65.

17. Gray D, Abramson J, Benoist C, Mathis D. Proliferative arrest and rapid turnover of thymic epithelial cells expressing Aire. J Exp Med 2007;204:2521-8.

18. Lin MS, Fu CL, Aoki V, et al. Desmoglein-1-specific T lymphocytes from patients with endemic pemphigus foliaceus (fogo selvagem). J Clin Invest 2000;105:207-13.

19. Marinkovich MP, Taylor TB, Keene DR, Burgeson RE, Zone JJ. LAD-1, the linear IgA bullous dermatosis autoantigen, is a novel 120-kDa anchoring filament protein synthesized by epidermal cells. J Invest Dermatol 1996;106:734-8.

20. Kowal C, Degiorgio LA, Lee JY, et al. Human lupus autoantibodies against NMDA receptors mediate cognitive impairment. Proc Natl Acad Sci U S A 2006;103:19854-9.

21. Matloubian M, Lo CG, Cinamon G, et al. Lymphocyte egress from thymus and peripheral lymphoid organs is dependent on S1P receptor 1. Nature 2004;427:355-60.

22. DeVoss J, Hou Y, Johannes K, et al. Spontaneous autoimmunity prevented by thymic expression of a single self-antigen. J Exp Med 2006;203:2727-35.

23. Lee EC, Yu D, Martinez de Velasco J, et al. A highly efficient Escherichia coli-based chromosome engineering system adapted for recombinogenic targeting and subcloning of BAC DNA. Genomics 2001;73:56-65.

24. Eisen MB, Spellman PT, Brown PO, Botstein D. Cluster analysis and display of genome-wide expression patterns. Proc Natl Acad Sci U S A 1998;95:14863-8.

25. Venanzi ES, Melamed R, Mathis D, Benoist C. The variable immunological self: genetic variation and nongenetic noise in Aire-regulated transcription. Proc Natl Acad Sci U S A 2008;105:15860-5.

26. Su AI, Wiltshire T, Batalov S, et al. A gene atlas of the mouse and human protein-encoding transcriptomes. Proc Natl Acad Sci U S A 2004;101:6062-7.

27. Dudziak D, Kamphorst AO, Heidkamp GF, et al. Differential antigen processing by dendritic cell subsets in vivo. Science 2007;315:107-11.

28. Sanderson MJ, Parker I. Video-rate confocal microscopy. Methods Enzymol 2003;360:447-81.

Chapter III

Self-Antigen Expression in eTACs Prevents Autoimmunity

Introduction

Clonal diversity within the adaptive immune system, while endowing organisms with the ability to respond to a broad range of potential pathogens, presents a substantial risk for autoimmunity. Numerous complementary mechanisms have evolved to curtail such deleterious outcomes, and to establish and maintain appropriate tolerance to self. Thymic selection is an essential component of this process, and relies in part on the display of a diverse set of self-antigens by medullary thymic epithelial cells (mTECs) *(1, 2)*.

Much self-antigen expression in mTECs in mice and humans is dependent on the activity of the autoimmune regulator (*Aire*) gene. *AIRE* was first identified in humans by positional cloning as the defective gene in the monogenic, autosomal recessive disease Autoimmune Polyglandular Syndrome Type I *(3, 4)* (APS-1). Like APS-1 patients, *Aire*-knockout mice develop severe, pleiotropic, multi-organ autoimmunity*(5, 6)*. Recent work has demonstrated that thymic *Aire* expression promotes the transcription of a host of tissue-specific antigens (TSAs) like insulin *(5)*, inter-photoreceptor retinoid binding protein *(7)* (IRBP), and vomeromodulin *(8)* (VM), and that such thymic TSA expression is essential to the prevention of autoimmunity.

In addition to its role in the thymus, growing evidence now suggests that expression of both *Aire* and a diverse set of TSAs may also occur in the secondary lymphoid organs. *Aire* expression has been detected at the transcript level in the secondary lymphoid organs by a number of groups *(5, 9-11)*, and more recently, radioresistant populations in these tissues have been shown to express putative TSAs including intestinal fatty acid binding protein *(10)*, glucagon *(12)*, and the melanocyte antigen tyrosinase *(13)*. It has also been suggested that the levels of TSA expression in the pancreatic lymph nodes correlate chronologically with disease progression in non-obese diabetic (NOD) mice *(12)*.

Recently, using a transcriptional *Aire*-reporter system, we identified a discrete population of extrathymic *Aire*-expressing cells in the secondary lymphoid organs *(11)*. Like mTECs, eTACs are a radioresistant MHC class II+ population expressing a host of TSAs, but surprisingly the genes regulated by *Aire* in this population appear to be distinct from those regulated by *Aire* in the thymus *(11)*. These findings, consistent with other reports showing cell type-specific effects of *Aire* expression *(14)*, suggest that such extrathymic *Aire*-expressing cells might enforce tolerance by eliminating autoreactive T cells that evade thymic selection. Although evidence is thus accumulating that expression of both *Aire* and diverse TSAs occurs in the secondary lymphoid organs, the ability of self-antigen expression in these populations to directly prevent autoimmunity remains unknown. Furthermore, the high levels of MHC class II expression on eTACs suggest that, like mTECs, these cells may interact directly with CD4+ T cells, and that such interaction could have functional consequences for immune tolerance. Studies to date, however, have shown only interactions between CD8+ T cells and these radioresistant cells of the secondary lymphoid organs *(10, 11, 13)*.

Here we describe protection from autoimmune diabetes by self-antigen expression in extrathymic *Aire*-expressing cells (eTACs) using two independent models. First, using a novel transgenic system in which the *Aire* promoter drives expression of a mimetope peptide recognized by the islet-specific CD4+ T cell clone BDC2.5, we show that eTACs can directly interact with CD4+ T cells, and that such self-antigen expression in eTACs leads to functional inactivation of cognate CD4+ T cells and protection from autoimmune diabetes. We demonstrate that eTAC-CD4 interactions also lead to an enrichment of FoxP3+ regulatory T cells, but that tolerance induction does not depend on such regulatory T cell populations. Rather, eTAC interaction induces a functional inactivation of CD4+ effectors that is stable when transferred serially into immunodeficient secondary hosts. Subsequently, using a system in which the *Aire* promoter drives expression of the pancreatic antigen islet-specific glucose-6-phosphatase related protein (IGRP), we show that IGRP expression in eTACs leads to protection from autoimmune diabetes mediated by the IGRP-specific CD8+ T cell clone 8.3. We demonstrate that this protection can be mediated by a radioresistant cell population, and, as argued previously, that such eTAC-CD8+ interactions induce tolerance through deletion of CD8+ effectors. Together these results identify self-antigen expression in eTACs as a robust potential mechanism for the physiologic and therapeutic prevention of autoimmunity.

Results

Transgenic *Aire*-driven BDC peptide is expressed in mTECs and eTACs

Growing evidence now suggests that both *Aire* and TSA expression are hallmarks of radioresistant populations in the secondary lymphoid organs *(9-13)*. Given the high levels of MHC class II expression on eTACs *(11)*, and prevalence and significance of CD4+ T cells among peripheral lymphocytes, we hypothesized that eTACs might also have the ability to interact directly with such populations, and that such interactions might promote immunologic self-tolerance. To investigate this, we used an established murine diabetes model, the BDC2.5 TCR-transgenic mouse, and a BDC2.5 mimetope antigen, the p31 peptide. BDC2.5 T cells recognize a pancreatic antigen, chromogranin A (ChrA)*(15)*, and can adoptively transfer diabetes into secondary hosts *(16, 17)*. Prior to the recent identification of ChrA as the cognate antigen, mimetope agonist peptides had been identified by library screening which induced activation of BDC2.5 T cells *in vitro* *(17, 18)*, and bound BDC2.5 T cells in the context of an I-Ag7 tetramer *(19)*.

To drive expression of one such BDC2.5 agonist peptide, 1040-31 (referred to as p31) in mTECs and eTACs, we used a bacterial artificial chromosome (BAC) transgenic construct to express the murine Invariant Chain (Ii; CD74) under transcriptional control of the *Aire* promoter, replacing the CLIP peptide sequence with the sequence coding for p31 (**Fig. 3.1a**). Similar strategies of CLIP peptide replacement have been used previously to target peptide antigens into APC populations *(20)*. The bicistronic BAC construct also included a 3' internal ribosomal entry site (IRES)- enhanced green fluorescent protein (EGFP) cassette to identify the *Aire*-expressing populations and to monitor the specificity of transgene expression. We termed this mouse *Aire*-driven BDC-

Figure 3.1. The *Adbig* transgene recapitulates *Aire* expression in mTECs and eTACs. (**a**) Schematic of *Aire*-driven BDC peptide Invariant Chain-GFP construct targeting the bacterial artificial chromosome (BAC) containing the murine *Aire* locus. (**b**) Representative flow cytometric analysis and gating from wildtype and *Adbig* NOD thymus, spleen, and lymph node stroma analyzed for CD45, DAPI, MHC II, and GFP. (**c**) Immunofluorescent staining of *Adbig* thymus, spleen, and lymph node with anti-GFP (green; all panels), B220 (red; spleen and lymph node left panels), cytokeratin 5 (red; thymus left panel) and anti-AIRE (red, right panels) co-staining of thymus, spleen. (**d**) Flow cytometric analysis of DAPI-negative, CD45-low, GFP+ populations from the thymus (T), spleen (S), and lymph node (L) of *Adig* (blue) and *Adbig* (red) mice for the indicated markers or stained with isoptype control (black).

Figure 3.1

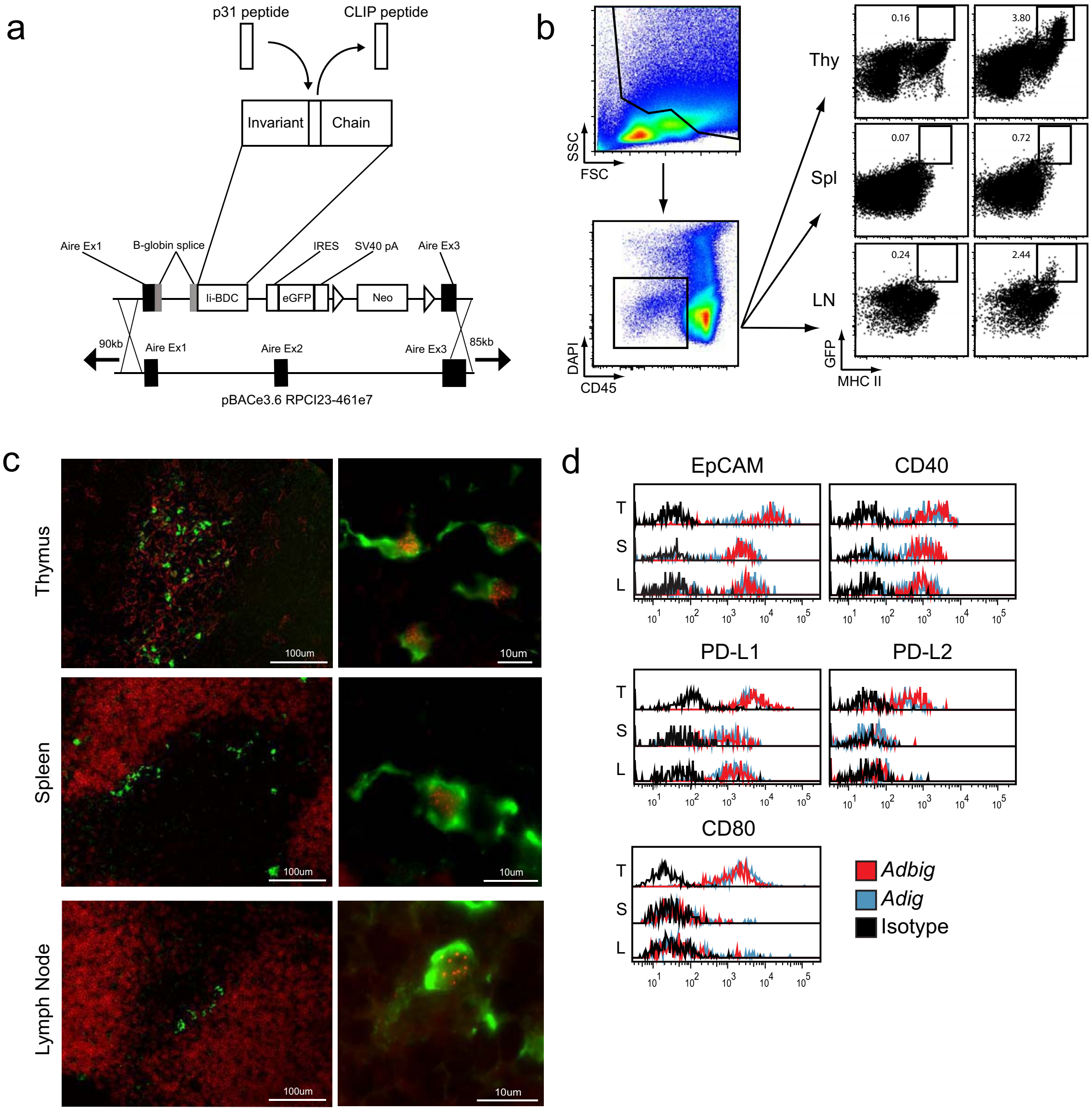
a
p31 peptide
CLIP peptide
Invariant
Chain
Aire Ex1
B-globin splice
Ii-BDC
eGFP
IRES
SV40 pA
Neo
Aire Ex3
90kb
Aire Ex1
Aire Ex2
Aire Ex3
85kb
pBACe3.6 RPCI23-461e7
b
SSC
FSC
DAPI
CD45
WT
Adbig
Thy
0.16
3.80
Spl
0.07
0.72
LN
0.24
2.44
GFP
MHC II
c
Thymus
Spleen
Lymph Node
100um
10um
100um
10um
100um
10um
d
EpCAM
CD40
PD-L1
PD-L2
CD80
T
S
L
10^1
10^2
10^3
10^4
10^5
🟥 *Adbig*
🟦 *Adig*
⬛ Isotype

Invariant Chain GFP (*Adbig*). As in other *Aire* reporter lines*(11)*, we detected MHC II-high, CD45-low, GFP-positive cells in both the thymus and secondary lymphoid organs of *Adbig* mice (**Fig. 3.1b**). In the thymus, GFP expression was restricted to the medulla, and expressed in cells containing Aire protein in nuclear speckles (**Fig. 3.1c**). In the secondary lymphoid organs, GFP expression was restricted to cells localized to the T cell-B cell boundary regions, and nuclear Aire protein was also detected within this population (**Fig. 3.1c**). Additionally, sorted mTECs and eTACs from *Adbig* mice were significantly enriched for *Aire* transcript (**Fig. S3.1**). To determine whether GFP+ cells in the primary and secondary lymphoid organs represented the same eTAC populations previously described using *Aire*-driven IGRP-GFP (*Adig*) mice *(11)*, we compared surface marker expression of GFP+ cells from the thymus, spleen, and lymph nodes of *Adig* and *Adbig* mice. We found that mTECs and eTACs from both *Aire*-reporter lines showed similar expression of all surface markers examined (**Fig. 3.1d**). Notably, eTACs expressed high levels of the epithelial cell marker EpCAM, as well as CD40 and PD-L1, but unlike mTECs, eTACs did not express CD80 or PD-L2. Together, these results confirm that the *Adbig* transgene faithfully recapitulates endogenous *Aire* expression in mTECs and eTACs, and that eTACs represent a unique *Aire*-expressing population in the secondary lymphoid organs.

BDC mimetope expression in eTACs induces functional inactivation and regulatory cell generation in BDC2.5 T cells

Figure S3.1. GFP+ mTECs and eTACs from *Adbig* mice are significantly enriched for *Aire* transcript. Real-time PCR analysis of cDNA isolated from eTACs (DAPI-, CD45-, MHCII+, CD11c-, GFP+) and peripheral DCs (PDC; DAPI-, CD45+, MHCII+, CD11c+) from the spleen and lymph nodes and mTECs (DAPI-, CD45-, MHCII+, CD11c-, GFP+) and thymic DCs (TDC; DAPI-, CD45+, MHCII+, CD11c+) from the thymus of *Adbig* mice. Values represent *Aire* transcript normalized to actin endogenous control signal, and are set relative to mTEC *Aire* signal.

Figure S3.1

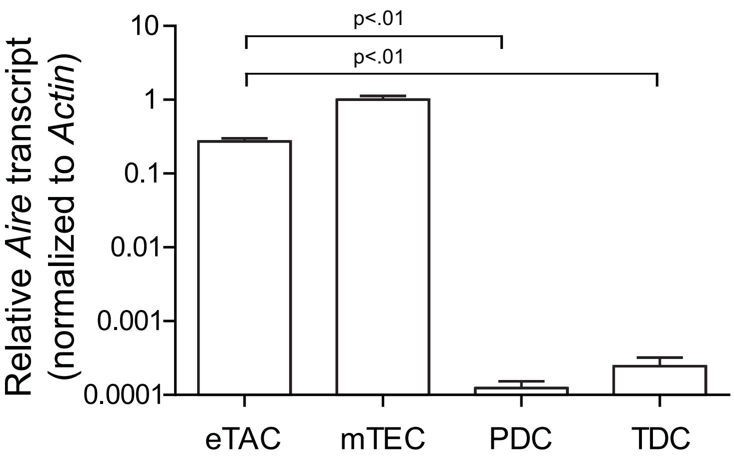

p<.01
p<.01
10
1
0.1
0.01
0.001
0.0001
Relative *Aire* transcript (normalized to *Actin*)
eTAC
mTEC
PDC
TDC

To test whether eTACs can present antigen directly to CD4+ T cells, we employed an adoptive cotransfer system using CFSE-labeled Thy1.1+ BDC2.5 CD4+ T cells and Thy1.2+ polyclonal CD4+ T cells. Three days post-adoptive transfer, wildtype recipients induced proliferation of BDC2.5 T cells only in the pancreatic lymph nodes, while *Adbig* recipients, in contrast, induced robust proliferation of BDC2.5 T cells in all secondary lymphoid organs examined (**Fig. 3.2a**). Surprisingly, many proliferating BDC2.5 T cells in *Adbig* hosts also appeared to downregulate CD90, a phenomenon not observed in BDC2.5 T cells proliferating in the pancreatic lymph nodes of wildtype hosts. While proliferating BDC2.5 T cells in *Adbig* recipients underwent contraction by two weeks post-transfer, significant residual populations remained which had completely diluted CFSE (**Fig. 3.2a**). Residual BDC2.5 T cells in *Adbig* mice appeared to collect most prominently in the spleen relative to Thy1.2+ polyclonal T cells, though some preferential enrichment in the pancreatic lymph nodes was also observed (**Fig. 3.2b**).

Previously we had described eTACs as a radioresistant population *(11)*. To determine whether the proliferation of BDC2.5 T cells in the secondary lymphoid organs was due to direct interaction with eTACs or a result of antigen transfer to other professional APC populations, we lethally irradiated and reconstituted wildtype and *Adbig* NOD mice with MHC class II-deficient bone marrow prior to adoptive transfer. Reconstitution of the hematopoietic compartment was confirmed by lack of class II expression on B cells and DCs (**Fig. S3.2**) and by the failure of BDC2.5 T cells to proliferate in the pancreatic lymph nodes of wildtype MHC class II-deficient chimeric

Figure 3.2. eTACs directly interact with CD4+ T cells and induce functional T-cell unresponsiveness. (**a**) Flow cytometric analysis of CD4+ lymphocyte populations in wildtype (top) and *Adbig* (bottom) hosts at 3 (left) and 14 days (right) post adoptive co-transfer of CFSE-labeled Thy1.1+ BDC2.5 T cells and Thy1.2+ polyclonal T cells. (**b**) Quantitation of the total residual populations in (a) of Thy1.1+ BDC2.5 T cells (black) and polyclonal CD4+ T cells (white) at day 14 post-adoptive transfer. (**c**) Flow cytometric analysis of CD4+ lymphocyte populations in wildtype (top) and *Adbig* (bottom) bone-marrow chimeric hosts reconstituted with MHC II-knockout bone marrow at three (left) and fourteen days (right) post-adoptive co-transfer of CFSE-labeled Thy1.1+ BDC2.5 T cells and Thy1.2+ polyclonal T cells. (**d**) Flow cytometric analysis of I-Ag7-p31 tetramer avidity among residual Thy1.1+ BDC2.5 T cells at day 14 post-adoptive transfer into wildtype (blue) or *Adbig* (red) hosts compared with mock I-Ag7-CLIP tetramer (black) (**e**) FoxP3 staining of CD4+ Thy1.1+ BDC2.5 T cells 14 days after adoptive transfer into wildtype or *Adbig* hosts. (**f**) Quantitation of (e) showing percentage of Thy1.1+ CD4+ cells that are FoxP3+ (left) and total number of FoxP3+ cells (right) in wildtype (white) or *Adbig* (black) recipients. (**g**) Schematic illustration of p31/CFA immunization protocol after adoptive transfer. (**h**) IFN-γ production among CD4+ Thy1.1+ BDC2.5 T cells isolated from mice indicated in (g); bar graph shows quantitation of pooled data with N=4 for each group.

Figure 3.2

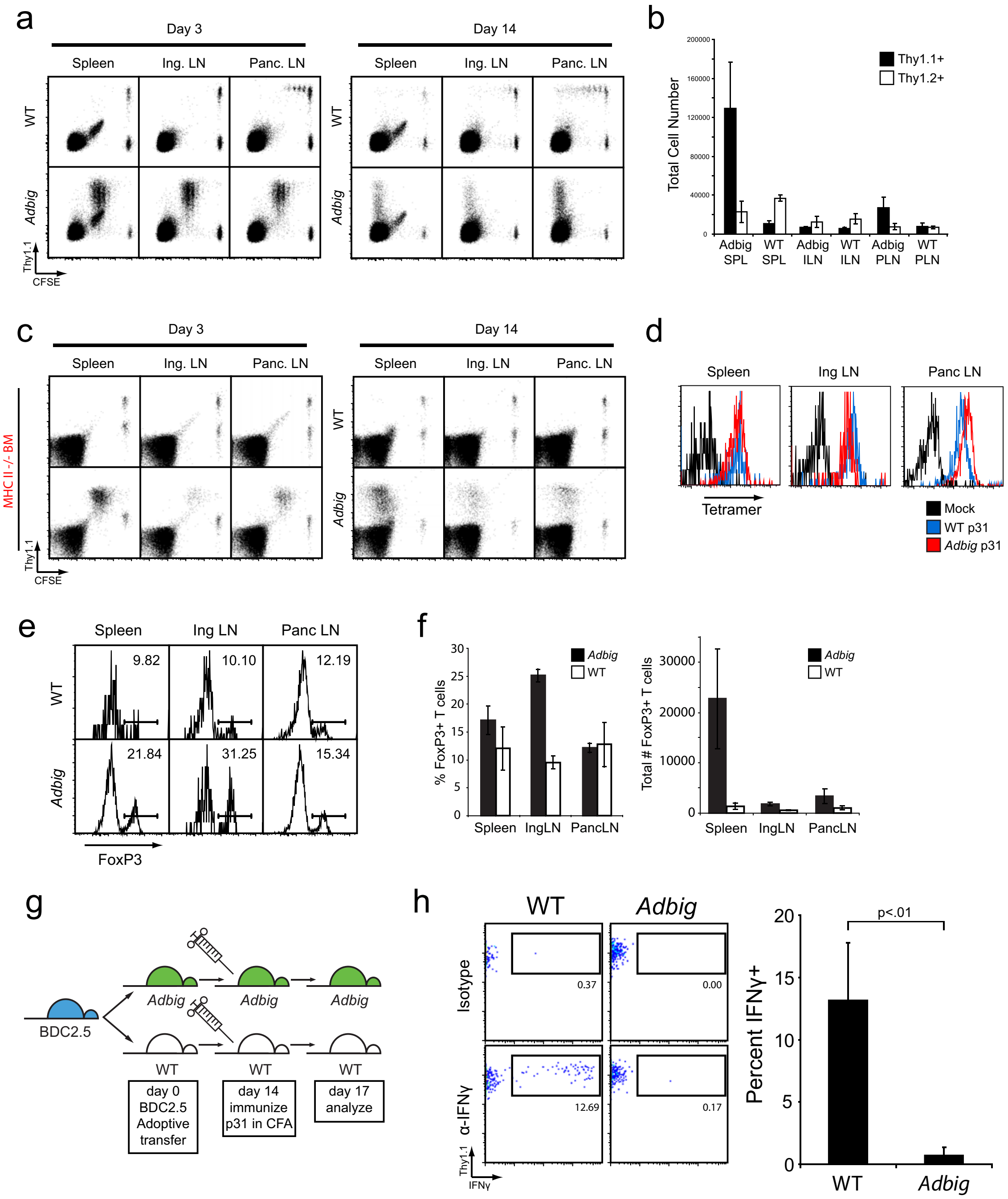

a
Day 3
Day 14
Spleen
Ing. LN
Panc. LN
WT
Adbig
Thy1.1
CFSE
b
Thy1.1+
Thy1.2+
Total Cell Number
200000
160000
120000
80000
40000
0
Adbig SPL
WT SPL
Adbig ILN
WT ILN
Adbig PLN
WT PLN
c
MHC II -/- BM
d
Spleen
Ing LN
Panc LN
Tetramer
Mock
WT p31
Adbig p31
e
9.82
10.10
12.19
21.84
31.25
15.34
FoxP3
f
% FoxP3+ T cells
Total # FoxP3+ T cells
30
25
20
15
10
5
0
30000
20000
10000
Spleen
IngLN
PancLN
g
BDC2.5
day 0 BDC2.5 Adoptive transfer
day 14 immunize p31 in CFA
day 17 analyze
h
Isotype
α-IFNγ
IFNγ
0.37
0.00
12.69
0.17
Percent IFNγ+
p<.01

Figure S3.2. Efficiency of reconstitution in wildtype and *Adbig* NOD mice lethally irradiated and reconstituted with MHC II-/- bone marrow. Representative flow cytometric analysis of MHC II staining among B220+ B cells (left) or CD11c+ DCs (right) from the secondary lymphoid organs of *Adbig* NOD (black), MHC II-/- NOD (blue), or MHC II-/- bone-marrow chimeric *Adbig* NOD mice (red).

Figure S3.2

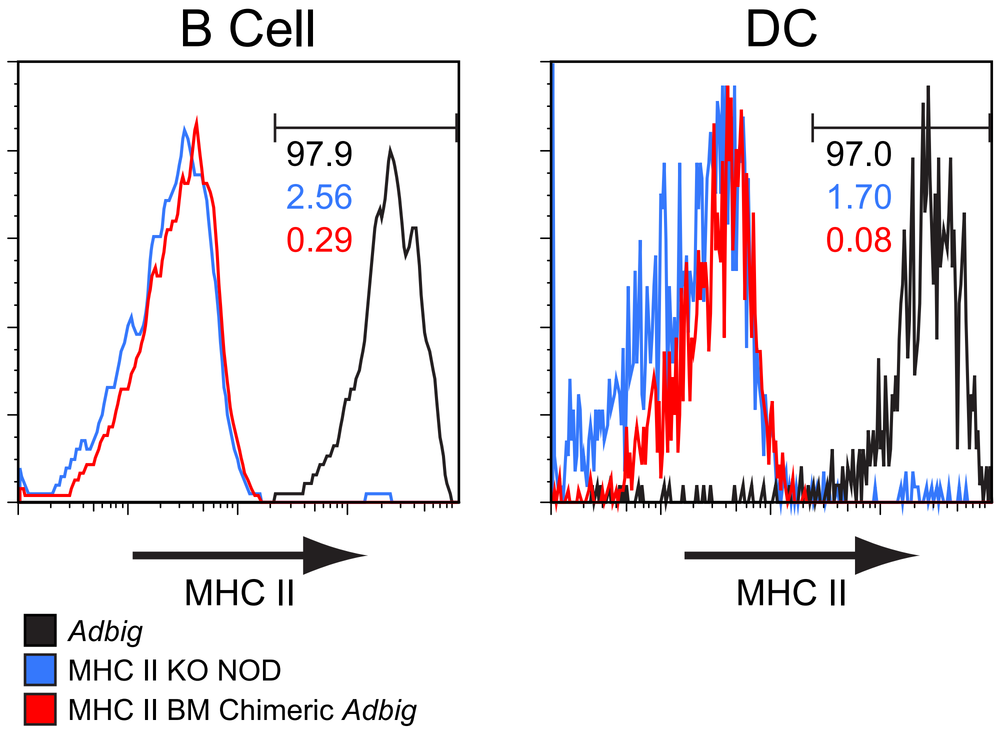
B Cell
97.9
2.56
0.29
MHC II
DC
97.0
1.70
0.08
MHC II
Adbig
MHC II KO NOD
MHC II BM Chimeric Adbig

recipients (**Fig. 3.2c**). Despite this absence of MHC class II expression on hematopoietic cells, bone-marrow chimeric *Adbig* recipients continued to induce robust proliferation of BDC2.5 T cells in all secondary lymphoid organs (**Fig. 3.2c**). As in non-chimeric recipients, a residual population of BDC2.5 T cells remained at two weeks post-transfer which had completely diluted CFSE. Thus, a radioresistant population of eTACs in the secondary lymphoid organs is able to interact directly with CD4+ T cells. However in contrast to interactions between eTACs and CD8+ T cells—which lead to proliferation followed by deletion of antigen-specific CD8+ T cells *(11)*—interactions between BDC mimetope-expressing eTACs and BDC2.5 CD4+ T cells lead to the persistence of residual populations of antigen-specific CD4+ T cells.

We then attempted to characterize the phenotype and function of these residual populations of BDC2.5 T cells in *Adbig* hosts. Despite prolonged interaction with antigen-bearing eTACs, residual BDC2.5 T cells retained significant avidity for I-Ag7-p31 tetramer (**Fig. 3.2d**), suggesting that the surviving T cells in this context had not lost their antigen-specificity or undergone T-cell receptor (TCR) downregulation. These residual BDC2.5 T cells, however, were significantly enriched for FoxP3+ regulatory T cells (**Fig. 3.2e**) despite pre-transfer CD25 depletion. This enrichment was observed in non-antigen draining lymph nodes and in the spleen (**Fig. 3.2e, f**), suggesting that in the absence of interaction with antigen-draining DCs in the pancreatic lymph node, eTAC interaction may favor the preferential expansion, retention, or survival of regulatory cells over effectors.

To directly test the functional ability of these residual BDC2.5 T cells to respond to antigen, *Adbig* and wildtype NOD adoptive transfer recipients were immunized at day 14 post-transfer with p31 peptide in complete Freund's adjuvant (CFA), and donor cytokine production was measured three days post-immunization (**Fig. 3.2g**). Whereas BDC2.5 T cells isolated from wildtype hosts retained the ability to produce interferon gamma in response to peptide challenge, BDC2.5 T cells isolated from *Adbig* mice remained largely unresponsive, suggesting that this population may be rendered functionally inactive in *Adbig* hosts (**Fig. 3.2h**). Thus, it appears that eTAC interaction induces both functional inactivation of effectors and selective enrichment for FoxP3+ regulatory T cell populations.

BDC mimetope expression in eTACs prevents autoimmune diabetes mediated by BDC2.5 T cells

To determine whether the observed interaction between BDC2.5 T cells and *Adbig* eTACs had functional relevance for the progression of autoimmune disease, we tested whether cognate antigen expression in eTACs could directly impact BDC2.5-mediated autoimmune diabetes. Purified populations of naïve, CD25-depleted BDC2.5 T cells rapidly and effectively transfer diabetes into NOD severe combined immunodeficiency (SCID) recipients (**Fig. 3.3a**). Strikingly, *Adbig* SCID recipients were completely protected from such adoptive transfer of diabetes and remained normoglycemic (**Fig. 3.3a**). This protection occurred despite a massive proliferation of BDC2.5 T cells in

Figure 3.3. Cognate antigen expression in eTACs prevents BDC2.5-mediated insulitis and autoimmune diabetes. (**a**) Blood sugar values (mg/dl) among wildtype SCID and *Adbig* SCID adoptive transfer recipients of CD25-depleted, CD4-enriched Thy1.1+ BDC2.5 T cells. (**b**) Flow cytometric analysis of peripheral blood from wildtype and *Adbig* SCID adoptive transfer recipients from (a) at indicated timepoints. (**c**) Hematoxylin and eosin-stained pancreatic islet histology of wildtype and *Adbig* SCID adoptive transfer recipients at day 10 post-transfer.

Figure 3.3

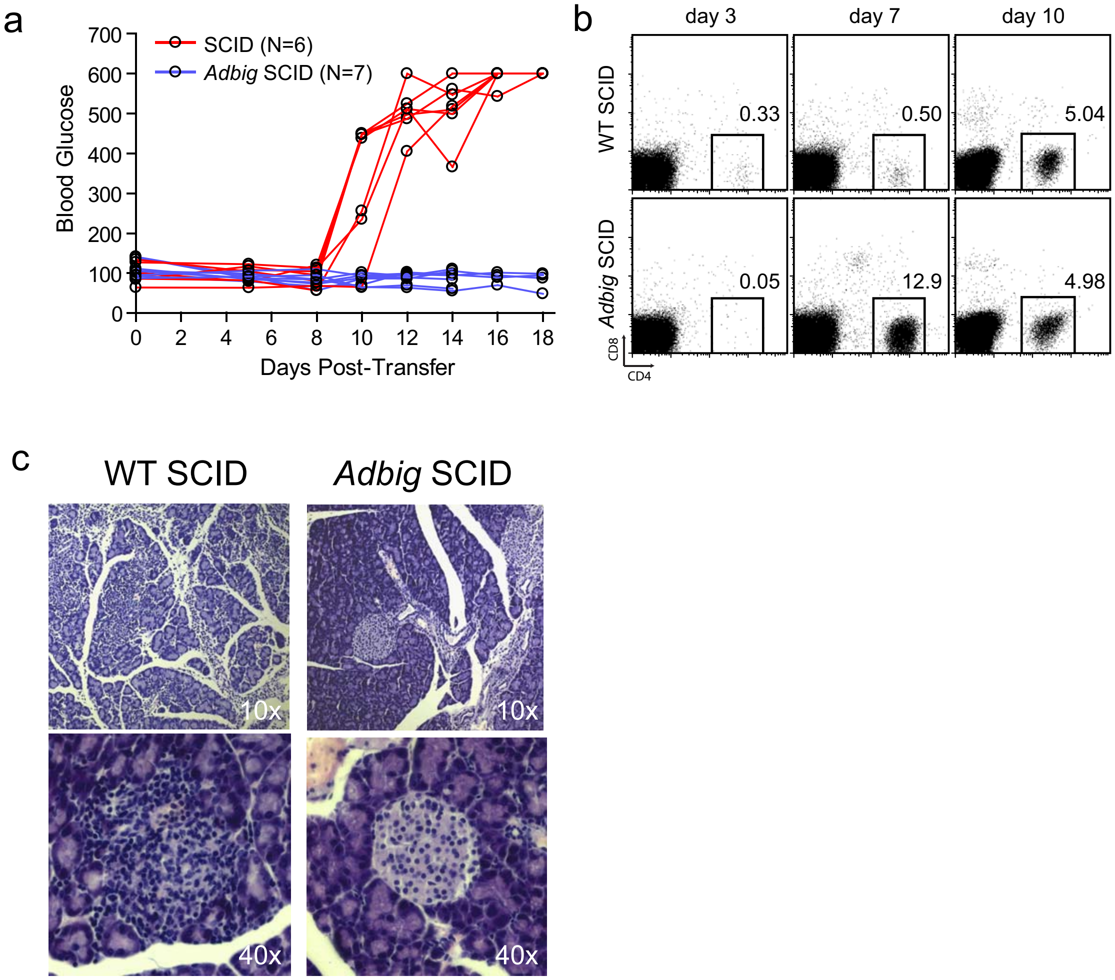
a
700
600
500
400
300
200
100
0
Blood Glucose
0
2
4
6
8
10
12
14
16
18
Days Post-Transfer
SCID (N=6)
Adbig SCID (N=7)
b
day 3
day 7
day 10
WT SCID
Adbig SCID
0.33
0.50
5.04
0.05
12.9
4.98
CD8
CD4
c
WT SCID
Adbig SCID
10x
10x
40x
40x

Adbig SCID hosts, which could be seen to mobilize into the peripheral blood (**Fig. 3.3b**). In spite of the robust proliferation of BDC2.5 T cells in *Adbig* SCID recipients and their mobilization into the peripheral blood, the pancreatic islets of *Adbig* SCID mice were completely devoid of lymphocytic infiltrates or peri-insulitis (**Fig. 3.3c**), suggesting that proliferating BDC2.5 T cells in *Adbig* SCID recipients were unable to reach target organs and died or remained functionally sequestered in the blood and secondary lymphoid organs. Together, these data suggest that antigen specific eTAC-CD4 interactions lead to rapid proliferation and subsequent inactivation of adoptively transferred CD4+ T cell populations, and can result in protection from both insulitis and autoimmune diabetes.

eTAC interaction induces functional inactivation of naive BDC2.5 T cells in a regulatory T cell-independent fashion

To determine the relative contributions of functional inactivation versus regulatory T cell induction in establishing this tolerance, and to define whether the disease protection in *Adbig* SCID recipients represented a stable T cell phenotype or required continuous exposure to antigen-expressing eTACs, we next employed a serial co-transfer system. Ten days after adoptive transfer of CD25-depleted Thy1.1+ BDC2.5 T cells into wildtype and *Adbig* SCID hosts, lymphocytes were harvested, purified, and re-transferred into new wildtype lymphopenic recipients either alone or mixed 1:1 with freshly isolated naïve, CD25-depleted BDC2.5 T cells (**Fig. 3.4a**). BDC2.5 lymphocytes transferred

Figure 3.4. eTAC-induced self-tolerance in BDC2.5 T cells is cell-intrinsic and does not require the presence of regulatory T cell populations. (**a**) Schematic illustration of BDC2.5 serial adoptive transfer strategy. CD25-depleted, CD4-enriched BDC2.5 T cells were transferred into wildtype SCID and *Adbig* SCID mice; at day 10, lymphocytes were re-harvested, purified, and serially transferred into wildtype SCID secondary hosts alone or in 1:1 mixture with fresh, CD25-depleted, CD4-enriched BDC2.5 T cells. (**b**) Diabetes incidence after adoptive transfer among serial recipient NOD SCID groups indicated in (a). (**c**) Blood sugar values (mg/dl) among DT-treated wildtype SCID and *Adbig* SCID hosts after adoptive transfer of CD4-enriched, DT-treated BDC2.5 FoxP3-DTR T cells. Asterisks indicate premature deaths. (**d**) Hematoxylin and eosin-stained pancreatic islet histology of wildtype SCID and *Adbig* SCID recipients in (c) day 20 post-transfer.

Figure 3.4

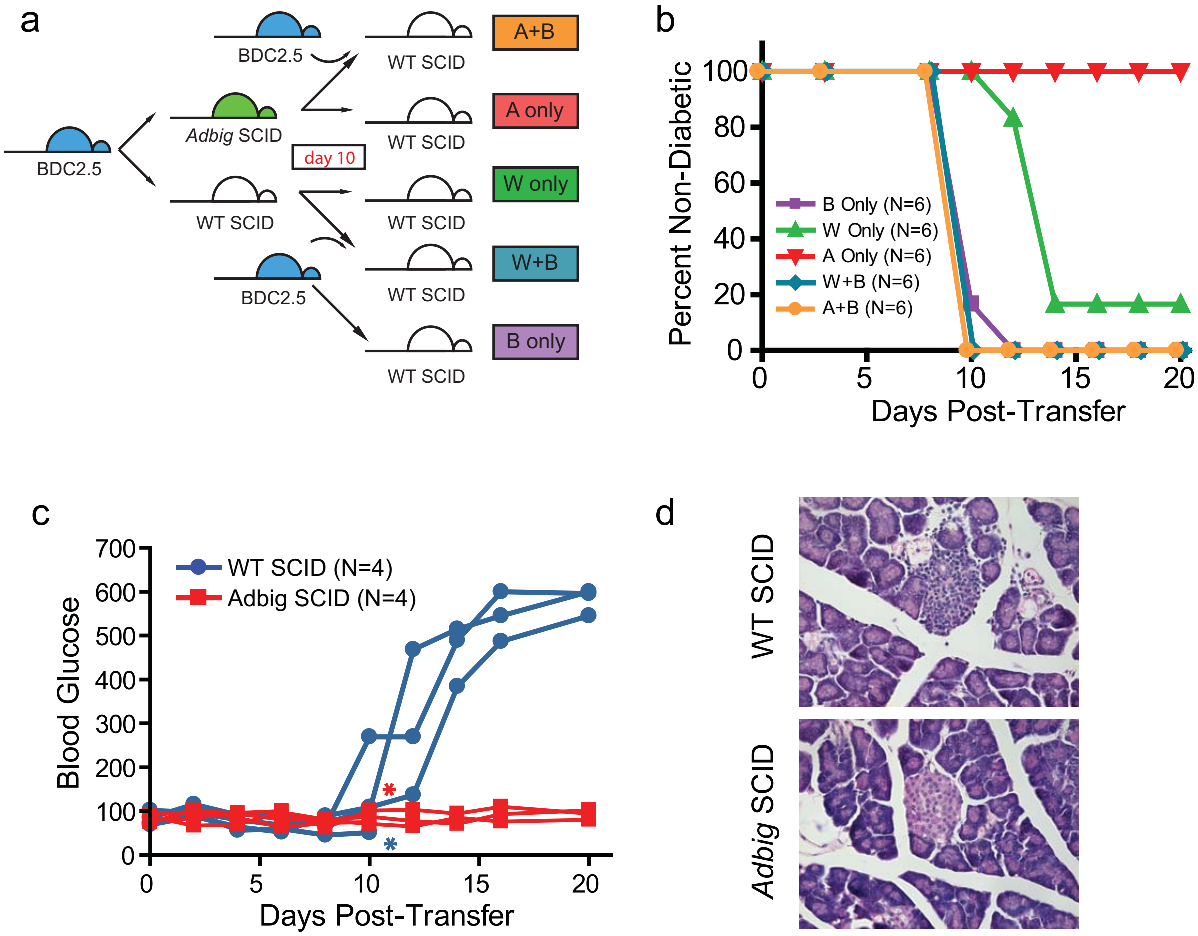
a
BDC2.5
BDC2.5
Adbig SCID
WT SCID
BDC2.5
day 10
WT SCID
WT SCID
WT SCID
WT SCID
WT SCID
A+B
A only
W only
W+B
B only
b
Percent Non-Diabetic
0
20
40
60
80
100
0
5
10
15
20
Days Post-Transfer
B Only (N=6)
W Only (N=6)
A Only (N=6)
W+B (N=6)
A+B (N=6)
c
Blood Glucose
0
100
200
300
400
500
600
700
0
5
10
15
20
Days Post-Transfer
WT SCID (N=4)
Adbig SCID (N=4)
*
*
d
WT SCID
Adbig SCID

from wildtype SCID mice ("W only") again induced diabetes in secondary SCID hosts, while lymphocytes from *Adbig* SCID mice ("A only") failed to induce diabetes despite the absence of continued exposure to cognate antigen-loaded eTACs (**Fig. 3.4b**). This suggests that the observed functional inactivation of effector T cells is a stable phenotype, and does not require continuous eTAC interaction. Conversely, BDC2.5 T cells harvested from either wildtype or *Adbig* SCID hosts did not appear to have acquired "dominant" tolerance, as serial co-transfer of purified CD4+ lymphocytes mixed 1:1 with freshly isolated naïve BDC2.5 T cells failed to suppress or delay disease onset (**Fig. 3.4b**). Together, these data suggest that functional inactivation of effectors in *cis*, and not dominant tolerance in *trans,* may account for the disease protection observed in this model.

To confirm that functional inactivation of effector T cells alone is sufficient to explain eTAC-induced CD4+ T cell tolerance, we crossed BDC2.5 TCR-transgenic mice with NOD FoxP3-diphtheria toxin receptor (DTR) transgenic mice, which selectively deplete FoxP3+ cells upon exposure to diphtheria toxin *(21)* (**Fig. S3.3**). Adoptive transfer of BDC2.5+ FoxP3-DTR+ T cells into wildtype or *Adbig* SCID mice treated continuously with diphtheria toxin revealed that while wildtype SCID hosts progressed rapidly to diabetes after adoptive transfer, *Adbig* SCID recipients remained disease-free (**Fig. 3.4c**). Furthermore, the islets of such *Adbig* SCID hosts remained devoid of T-cell infiltrates, suggesting that the inability of eTAC-experienced BDC2.5 T

Figure S3.3. Effeciency of depletion of FoxP3+ regulatory T cells in FoxP3-DTR BDC2.5 mice. Flow cytometric analysis of FoxP3 staining among CD4+ T cells from wildtype and FoxP3-DTR mice treated with a single dose of PBS or DT (50ug/kg), one day post-treatment.

Figure S3.3

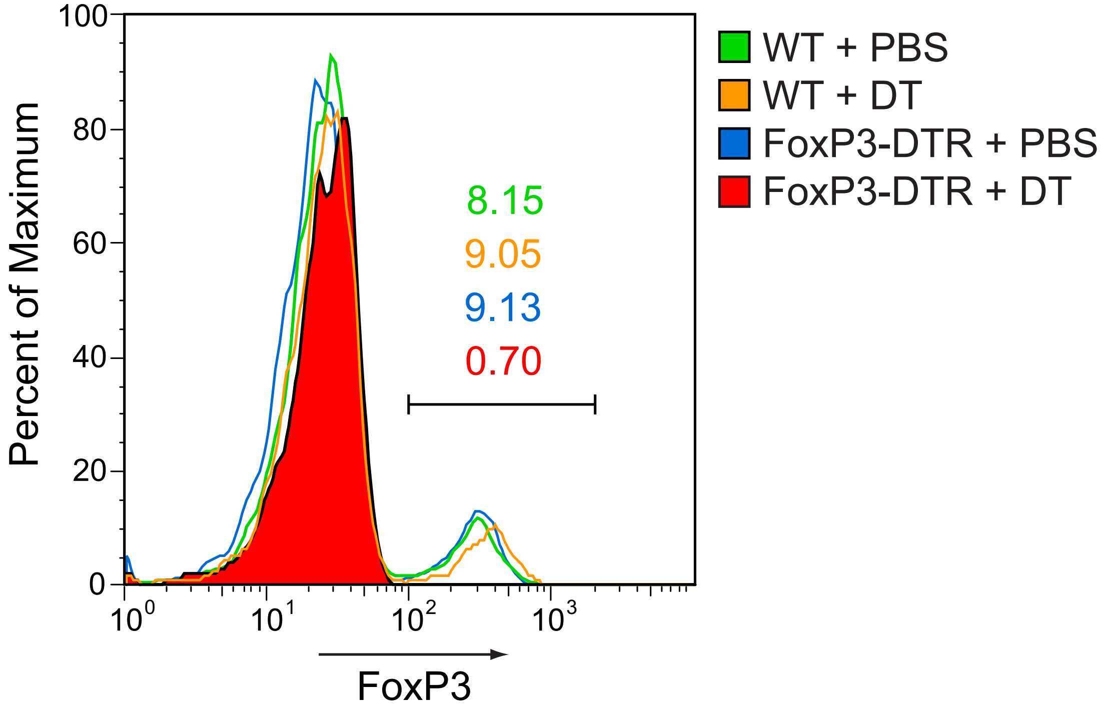
100
80
60
40
20
0
Percent of Maximum
10^0
10^1
10^2
10^3
FoxP3
8.15
9.05
9.13
0.70
🟩 WT + PBS
🟧 WT + DT
🟦 FoxP3-DTR + PBS
🟥 FoxP3-DTR + DT

cells to reach the target organ was not dependent on regulatory T cell populations (**Fig. 3.4d**).

Peripheral CD4+ tolerance induced by eTACs is not altered by CD40/TLR stimulus or PD-L1 blockade

While a number of antigen-presenting cell populations have been demonstrated to induce peripheral T-cell tolerance, many of these interactions can be abrogated or converted from tolerogenic to immunogenic upon stimulation of cell-surface receptors such as CD40, toll-like receptors (TLRs), or blockade of PD-1/PD-L1 interactions *(22-26)*. To determine whether eTAC-mediated tolerance could also be interrupted by such perturbations, we first treated *Adbig* mice with anti-CD40/polyI:C and observed whether such stimulus could induce a maturation similar to that observed among DC populations. While anti-CD40/PolyI:C treatment induced activation and upregulation of CD80 on CD11c+ dendritic cells, eTACs failed to upregulate CD80 in response to treatment (**Fig. 3.5a**) despite the presence of high levels of surface CD40. Likewise, anti-CD40/polyI:C pretreatment of *Adbig* SCID mice failed to impact eTAC-mediated T cell tolerance, and anti-CD40/PolyI:C-treated *Adbig* SCID mice remained completely protected from adoptive diabetes transfer mediated by BDC2.5 T cells (**Fig. 3.5b**). This suggests that eTACs may be resistant to maturation in the context of inflammatory stimuli that induce other APC populations to convert from tolerance to immunogenicity.

Figure 3.5. eTAC-mediated tolerance induction in BDC2.5 T cells is not abrogated by CD40/TLR stimulus or PD-L1 blockade. (**a**) Representative flow cytometric analysis of CD80 staining in DAPI-, CD45+, CD11c+ dendritic cells and DAPI-, CD45-, MHCII+, GFP+ eTACs in response to anti-CD40/PolyI:C stimulus; quantitation of MFI shifts shown at right. (**b**) Blood sugar values (mg/dl) among anti-CD40/PolyI:C treated wildtype SCID and *Adbig* SCID hosts after adoptive transfer of 200,000 CD25-depleted, CD4-enriched, BDC2.5 T cells. (**c**) Blood sugar values (mg/dl) among anti-PD-L1 treated wildtype SCID and *Adbig* SCID hosts after adoptive transfer of 200,000 CD25-depleted, CD4-enriched, BDC2.5 T cells. (**d**) Hematoxylin and eosin-stained pancreatic islet histology of wildtype SCID and *Adbig* SCID recipients in (c) day 14 post-transfer.

Figure 3.5

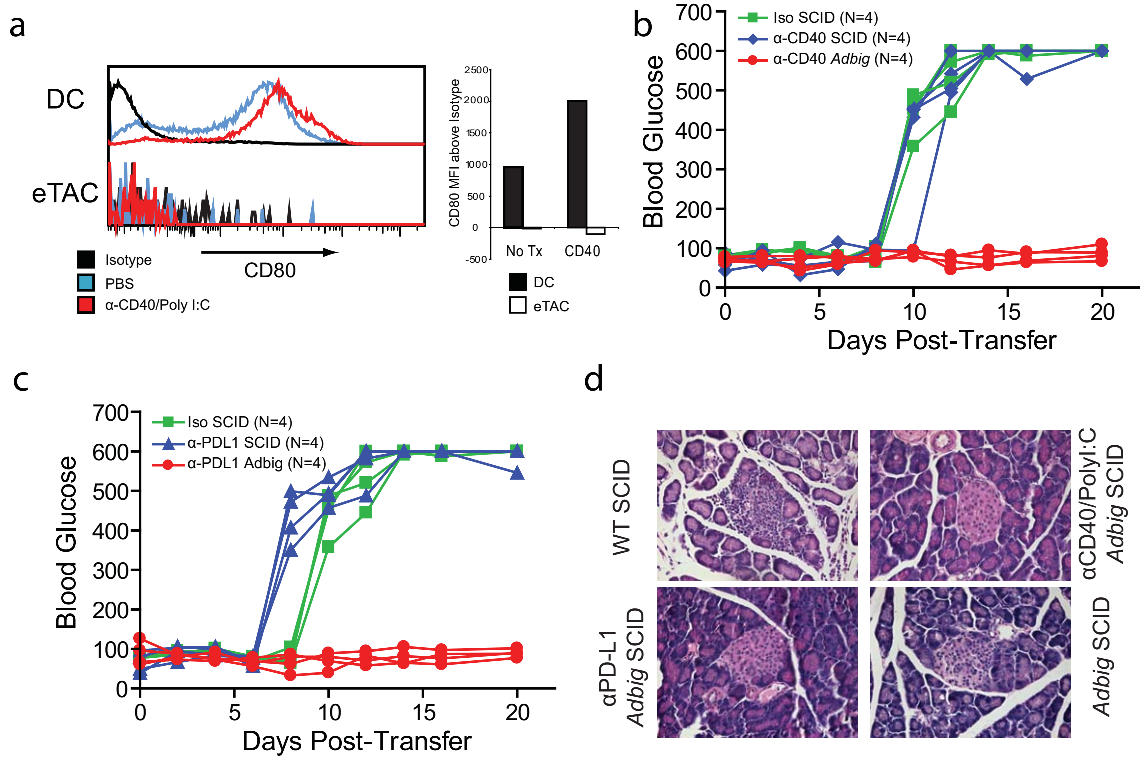
a
DC
eTAC
CD80
Isotype
PBS
α-CD40/Poly I:C
CD80 MFI above Isotype
2500
2000
1500
1000
500
0
-500
No Tx
CD40
DC
eTAC
b
Iso SCID (N=4)
α-CD40 SCID (N=4)
α-CD40 Adbig (N=4)
Blood Glucose
700
600
500
400
300
200
100
0
0
5
10
15
20
Days Post-Transfer
c
Iso SCID (N=4)
α-PDL1 SCID (N=4)
α-PDL1 Adbig (N=4)
Blood Glucose
Days Post-Transfer
d
WT SCID
αCD40/PolyI:C Adbig SCID
αPD-L1 Adbig SCID
Adbig SCID

PD-1/PD-L1 interactions have also been shown to be essential in the maintenance of peripheral tolerance in many experimental systems and notably play a key role in preventing autoimmune diabetes *(25-27)*. To determine whether such interactions also regulate eTAC-mediated tolerance, we treated wildtype and *Adbig* SCID mice with anti-PD-L1 before and during adoptive transfer. Despite the efficacy of this regimen in breaking islet self-tolerance in wildtype NOD mice (**Fig. S3.4**), anti-PD-L1-treated *Adbig* SCID mice remained entirely resistant to BDC2.5-induced diabetes (**Fig. 3.5c**). This suggests that PD-L1 is not required for eTAC-mediated tolerance, and furthermore that eTAC-experienced CD4+ T cells do not require PD-1/PD-L1 interaction on the target tissue to prevent autoimmunity. Consistent with this, the pancreata of both anti-CD40/Poly I:C- and anti-PD-L1-treated *Adbig* SCID mice remained free of peri-islet infiltrates, suggesting that despite these perturbations, eTAC-CD4 interactions prevented autoreactive effector T cells from reaching their target organ altogether (**Fig. 3.5d**). These results demonstrate that CD4+ T cell inactivation induced by eTACs is resistant to perturbations affecting many other peripheral tolerance mechanisms; such resistance may be important if eTACs do in fact serve as self-antigen expressing APCs at sites of lymphocyte priming in the secondary lymphoid organs.

eTAC-mediated tolerance is unique from that induced by other tolerogenic APC populations

Figure S3.4. Anti-PD-L1 treatment regimen induces rapid diabetes onset in wildtype NOD mice. Blood sugar levels among wildtype NOD mice receiving 200ug/mouse anti-PD-L1 (red) or isotype (blue) beginning at day 0.

Figure S3.4

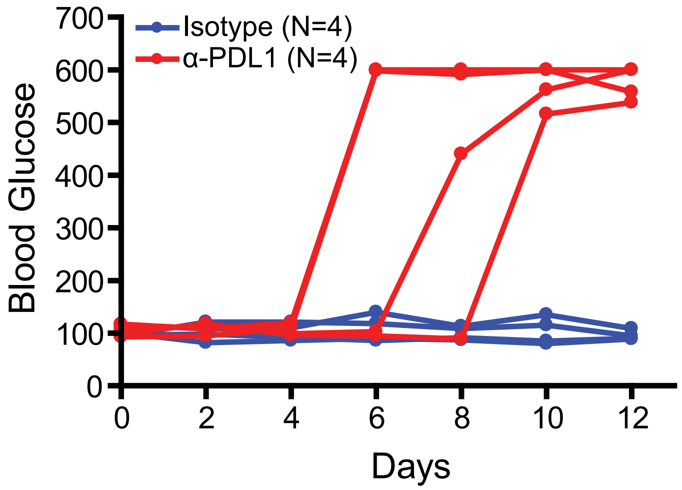
Isotype (N=4)
α-PDL1 (N=4)
Blood Glucose
700
600
500
400
300
200
100
0
0
2
4
6
8
10
12
Days

Despite these results, it remained unclear whether such CD4+ T-cell tolerance reflected a unique property of eTAC-CD4+ interactions, or if the same outcome would be observed when naïve CD4+ T cells encountered cognate antigen on other APC populations. To directly compare the outcome of BDC2.5-eTAC encounter to interaction with another putative tolerogenic APC population, we employed an antibody-mediated system to target a BDC mimetope peptide to DEC205+ dendritic cells (DCs). DEC205+ DCs can promote tolerogenic interactions and functional inactivation of naïve effectors if given without proinflammatory signals, and antibody-mediated targeting of peptide antigens to DEC205+ DC populations has previously been shown to induce interaction with cognate CD4+ and CD8+ T cells, resulting in functional T-cell unresponsiveness via anergy or deletion *(22, 23, 28)*. Importantly, targeting of self antigen to these DCs has not been shown to induce functional tolerance of CD4+ T cells in the context of ongoing autoimmunity. To this end, we employed a fusion antibody containing anti-DEC205 coupled to the BDC mimetope peptide 1040-55 *(17)*, which has a similar EC_{50} to 1040-p31 *(17)*, and which we termed αDEC1040.

As in *Adbig* recipients, pre-treatment of wildtype NOD mice with αDEC1040 before adoptive transfer of BDC2.5 T cells induced rapid antigen-specific BDC2.5 proliferation in all secondary lymphoid organs, while PBS-treated mice induced proliferation only in the pancreatic lymph node (**Fig. 3.6a**). Although BDC2.5 proliferation appeared slightly more rapid in *Adbig* mice than in αDEC1040-treated mice, both induced robust proliferation in all secondary lymphoid organs and >95% of

Figure 3.6. αDEC1040 treatment induces proliferation but not tolerance of BDC2.5 T cells. (**a**) CFSE dilution among CD4+ Thy1.1+ BDC2.5 T cells transferred into wildtype NOD mice treated with PBS (green) or αDEC1040 (blue), or into *Adbig* mice (red). (**b**) IFN-γ production among CD4+ Thy1.1+ BDC2.5 T cells isolated from indicated mice, quantitated in bar graph on right showing lymph nodes (white) and spleen (black). (**c**) Flow cytometric analysis of peripheral blood from NOD SCID mice treated with PBS or αDEC1040, or *Adbig* SCID mice, following adoptive transfer of BDC2.5 T cells. (**d**) Blood sugar values (mg/dl) among NOD SCID mice treated with PBS (green) or αDEC1040 (blue) or *Adbig* SCID mice (red) following adoptive transfer of BDC2.5 T cells.

Figure 3.6

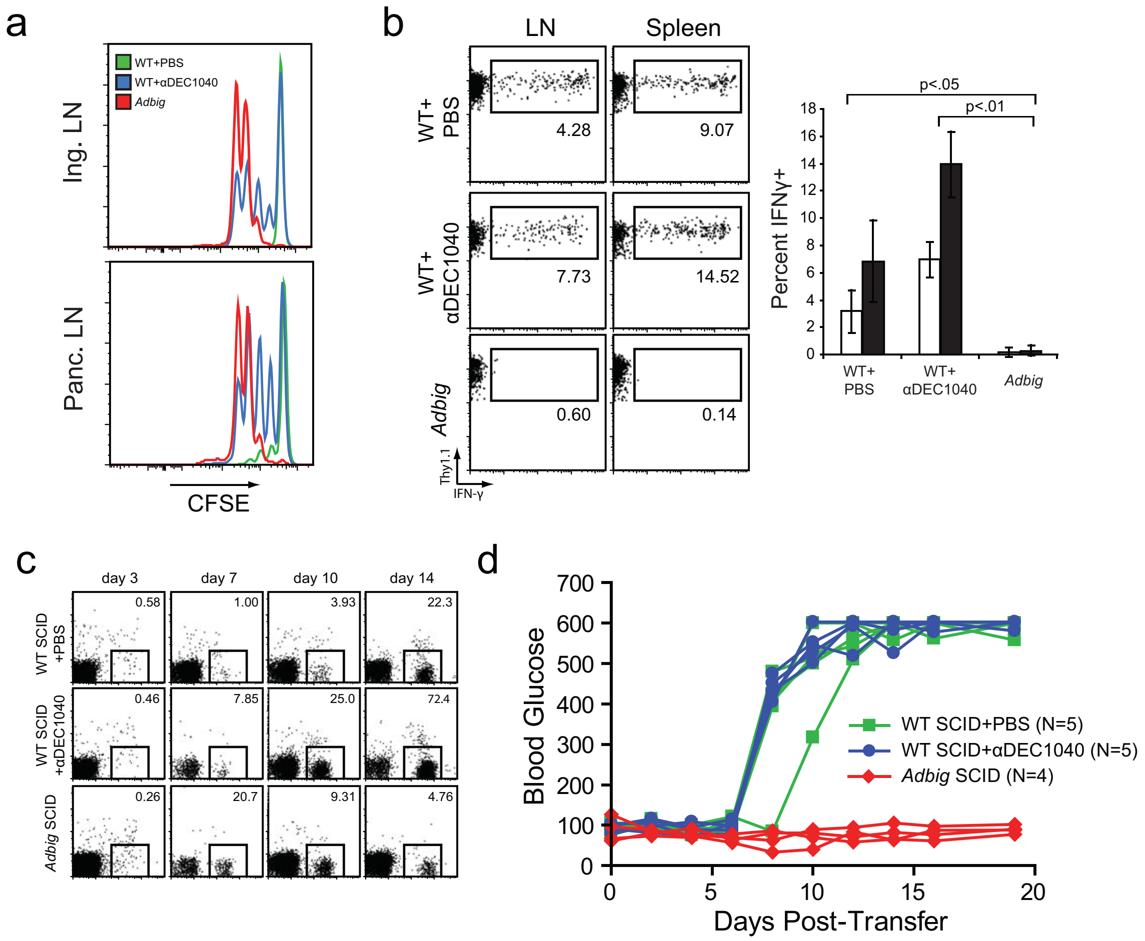
a
WT+PBS
WT+αDEC1040
Adbig
Ing. LN
Panc. LN
CFSE
b
LN
Spleen
WT+ PBS
4.28
9.07
WT+ αDEC1040
7.73
14.52
Adbig
0.60
0.14
Thy1.1
IFN-γ
p<.05
p<.01
Percent IFNγ+
18
16
14
12
10
8
6
4
2
0
WT+ PBS
WT+ αDEC1040
Adbig
c
day 3
day 7
day 10
day 14
WT SCID +PBS
0.58
1.00
3.93
22.3
WT SCID +αDEC1040
0.46
7.85
25.0
72.4
Adbig SCID
0.26
20.7
9.31
4.76
d
Blood Glucose
700
600
500
400
300
200
100
0
WT SCID+PBS (N=5)
WT SCID+αDEC1040 (N=5)
Adbig SCID (N=4)
0
5
10
15
20
Days Post-Transfer

cells eventually divided in both protocols when later time points were measured (data not shown). This suggested that the BDC mimetope antigen was being correctly processed and presented after administration of αDEC1040, and that adoptively transferred BDC2.5 T cells were able to effectively interact with these populations. However despite this rapid proliferation in both *Adbig* and αDEC1040-treated mice, we observed a marked difference in the functional outcomes for interacting BDC2.5 T cells. While BDC2.5 T cells in *Adbig* mice again failed to produce interferon gamma in response to secondary immunization, residual BDC2.5 T cells in αDEC1040-treated mice produced high levels if interferon similar to or greater than those observed in PBS-treated wildtype hosts (**Fig. 3.6b**).

We also tested whether such BDC2.5 interaction with DEC205+ DCs would have a similar protective effect on adoptive transfer of diabetes. We found, however, that despite robust proliferation in both *Adbig* and αDEC1040 SCID mice, continuous treatment with αDEC1040 did not induce a subsequent contraction of T cells after the initial proliferation (**Fig. 3.6c**). Furthermore, αDEC1040 treatment did not prevent or delay adoptive transfer of disease mediated by BDC2.5 T cells, while *Adbig* SCID mice remained completely protected from diabetes (**Fig. 3.6d**). Together these results suggest that eTACs may serve as more than simply a reservoir for self-antigen, as BDC2.5 cognate antigen presented in the context of a distinct but putatively non-immunogenic APC population is unable to induce tolerance or prevent disease in this autoimmune setting.

Expression of IGRP in eTACs prevents CD8+ T cell-mediated autoimmune diabetes

We previously described eTACs in the secondary lymphoid organs using the transgenic *Aire*-driven IGRP-GFP (*Adig*) mouse, which expresses a fusion protein of islet-specific glucose 6-phosphatase related protein (IGRP) conjugated to GFP under the control of the *Aire* promoter *(11)*. eTACs in *Adig* mice also express detectable nuclear Aire protein (**Fig. 3.7a**), and adoptive transfer of naïve IGRP-specific CD8+ T cells from TCR-transgenic *8.3* mice into *Adig* recipients leads to rapid proliferation and subsequent deletion of *8.3* T cells in all secondary lymphoid organs *(11)*. But whether such eTAC-CD8 interactions also result in immunologic tolerance, and specifically whether this leads to protection from autoimmune diabetes, is not known. While purified naïve 8.3 T cells alone do not adoptively transfer disease even into SCID recipients (data not shown), mice expressing the 8.3 TCR transgene itself do spontaneously develop accelerated diabetes *(29)*.

To directly test whether IGRP expression in eTACs is sufficient to prevent 8.3-mediated diabetes in the absence of thymic negative selection, we developed a system in which a permissive thymic environment for 8.3 development was generated in *Adig* mice by thymectomy and simultaneous thymic transplantation, followed by lethal irradiation and reconstitution with 8.3+ Thy1.1+ TCR-transgenic bone marrow (**Fig. 3.7b**). FACS analysis six weeks after bone-marrow transplant revealed complete reconstitution of hosts (**Fig. S3.5**) and a lack of thymic negative selection in both groups, with equivalent

Figure 3.7. IGRP expression in eTACs leads to peripheral deletion of 8.3 T cells and prevention of CD8-mediated diabetes. (**a**) Immunofluorescent staining of eTACs from *Adig* NOD lymph nodes stained for GFP (green) and AIRE (red) and counterstained with DAPI (blue). (**b**) Schematic illustration of *Adig*/8.3 thymectomy/thymic transplant/bone-marrow chimera strategy. (**c**) Representative flow cytometric analysis of thymocytes and lymphocytes from experimental mice described in (b). CD4/CD8 plots are pregated on FSC/SSC. Tetramer histograms are pre-gated on FSC/SSC and CD4-CD8+, and represent total cell number on Y axis for wildtype mock tetramer (green), wildtype NRP-V7 mimetope tetramer (blue), and *Adig* NRP-V7 tetramer (red). Insets show *Adig* populations alone as a percent of maximum. (**d**) Quantitation of total cell numbers in (c) for organs indicated, ±SD; 3 mice per group. NS, not significant (**e**) Diabetes incidence curves for cohorts of wildtype and *Adig* mice described in (b), shown as weeks post BM-reconstitution.

Figure 3.7

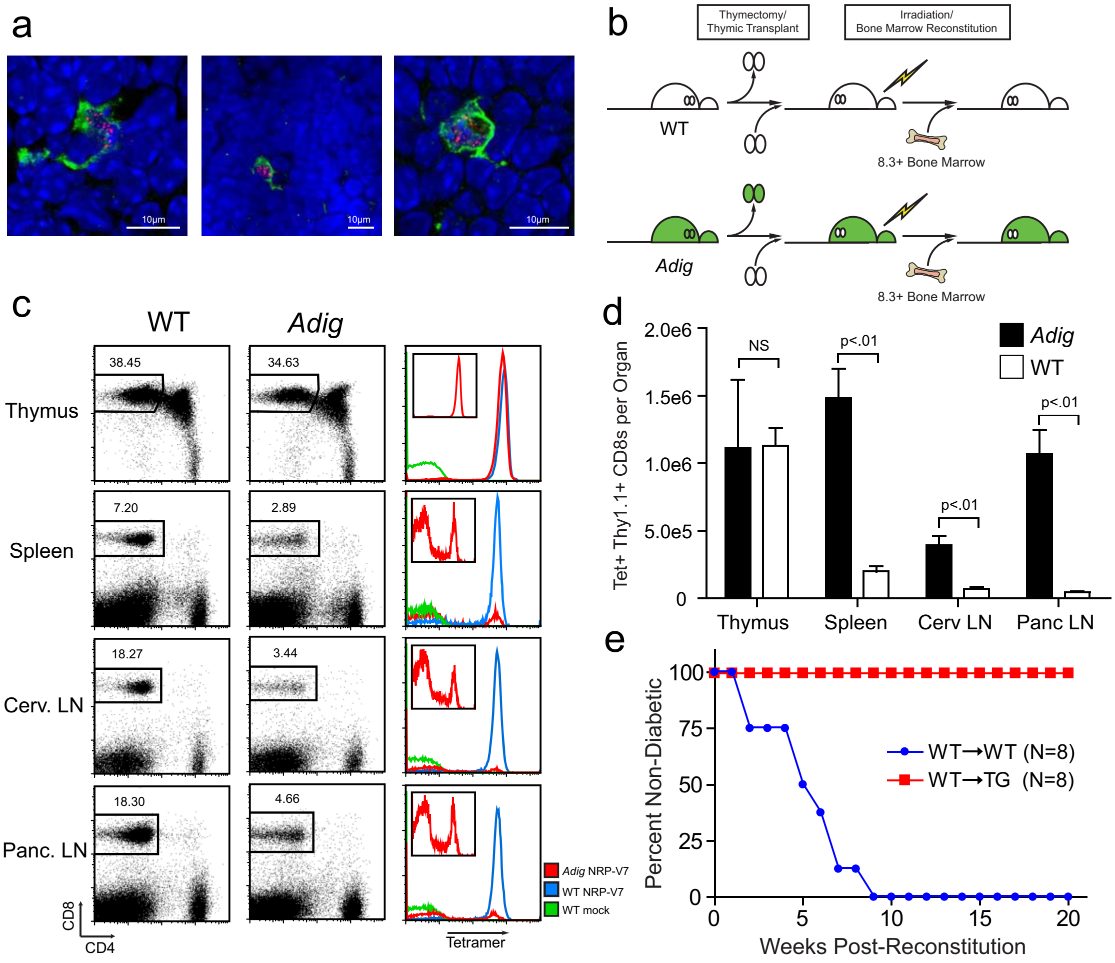
a
10μm
10μm
10μm
b
Thymectomy/
Thymic Transplant
Irradiation/
Bone Marrow Reconstitution
WT
8.3+ Bone Marrow
Adig
8.3+ Bone Marrow
c
WT
Adig
Thymus
38.45
34.63
Spleen
7.20
2.89
Cerv. LN
18.27
3.44
Panc. LN
18.30
4.66
CD8
CD4
Tetramer
Adig NRP-V7
WT NRP-V7
WT mock
d
Tet+ Thy1.1+ CD8s per Organ
2.0e6
1.5e6
1.0e6
5.0e5
0
NS
p<.01
p<.01
p<.01
Adig
WT
Thymus
Spleen
Cerv LN
Panc LN
e
Percent Non-Diabetic
100
75
50
25
0
WT→WT (N=8)
WT→TG (N=8)
0
5
10
15
20
Weeks Post-Reconstitution

Figure S3.5. Efficiency of reconstitution in *Adig* mice lethally irradiated and reconstituted with Thy1.1+ *8.3* bone marrow. Representative flow cytometric analysis of MHC II staining among CD8+ thymocytes from wildtype NOD (black), Thy1.1+ 8.3 bone-marrow chimeric wildtype NOD (blue), and Thy1.1+ 8.3 bone marrow chimeric *Adbig* NOD mice (red).

Figure S3.5

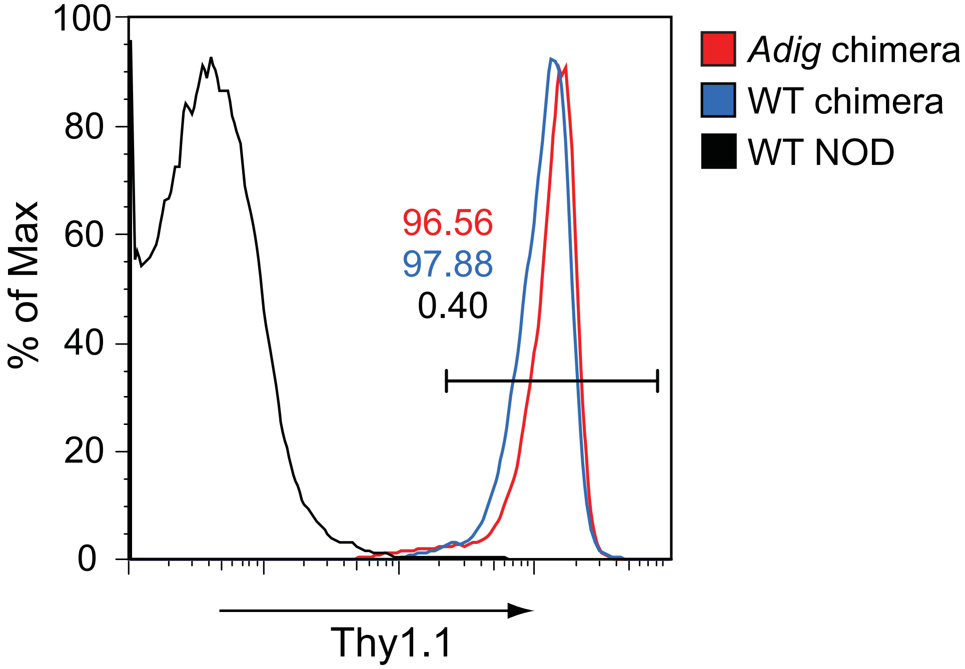
100
80
60
40
20
0
% of Max
96.56
97.88
0.40
Thy1.1
🟥 *Adig* chimera
🟦 WT chimera
⬛ WT NOD

numbers of total Thy1.1+ CD8 single-positive thymocytes, and similar tetramer-reactivity (**Fig. 3.7c, d**). This suggests that transgenic IGRP antigen was not being trafficked back to the transplanted thymus, creating differential thymic selection environments. In the secondary lymphoid organs, by contrast, the number of CD8+ T cells was dramatically reduced in *Adig* recipients, and the tetramer-reactivity of those remaining CD8+ Thy1.1+ T cells was markedly decreased (**Fig. 3.7c, d**). Thus, after egress from a permissive thymic selection environment, high-affinity 8.3 CD8+ T cells in *Adig* recipients appeared to undergo deletion upon eTAC encounter, leaving predominantly low IGRP-affinity CD8+ T cells in these mice (**Fig. 3.7d**). Importantly, whereas wildtype recipients of transplanted thymi and 8.3 bone marrow progressed gradually to completely penetrant autoimmune diabetes, *Adig* recipients were entirely protected from such disease (**Fig. 3.7e**). Together, these results suggest that self-antigen expression in eTACs can induce deletional tolerance of endogenously arising CD8+ T cells, and that eTAC interactions with autoreactive CD4+ and CD8+ T cell populations are sufficient to prevent anti-islet autoimmunity.

Discussion

The recent description of *Aire*-expressing cells and ectopic TSA transcription in the secondary lymphoid organs *(10, 11, 13, 30)* has raised the question of whether self-antigen expression in these populations can directly prevent autoimmune disease. Here, using transgenic systems in both the CD4+ and CD8+ T cell contexts, we describe a role for extrathymic *Aire*-expressing cells in preventing autoimmune diabetes. The *Aire*-driven peripheral expression of pancreas-specific antigens recognized by either the islet-specific CD4+ T cell clone BDC2.5 or the IGRP-specific CD8+ T cell clone 8.3 induces a robust T-cell tolerance in both populations, and protects such transgenic mice from cognate T cell-mediated diabetes. Of note, this tolerance occurs even in the setting of lymphopenia, which is often thought to provoke autoimmunity in the context of antigen encounter ***(31-33)***. These results demonstrate that self-antigen expression in eTACs is sufficient to prevent autoimmunity mediated by diverse antigen-specific T cells, and provide evidence for a novel mechanism contributing to the maintenance of peripheral tolerance.

Previous descriptions of putatively tolerogenic radioresistant populations in the secondary lymphoid organs have focused on interactions with CD8+ T cells ***(10, 11, 13)***, but given the ubiquity of class I MHC expression on all nucleated cells, it was not clear to us whether the observed deletion of cognate CD8+ T cells in these systems represented a unique feature of these populations or was merely a byproduct of self-antigen expression in any cell population lacking appropriate inflammatory or costimulatory signals. Based on the high levels of class II MHC expressed on eTACs ***(11)***, and the significance of CD4+ T cell populations in autoimmune disease ***(34, 35)***, we chose to investigate whether eTACs might play a unique role in peripheral tolerance induction by interacting with both CD4+ and CD8+ T cells. Indeed BDC2.5 T cells adoptively transferred into *Adbig* mice proliferate in all secondary lymphoid organs, and this interaction is preserved even in the absence of class II MHC expression on hematopoietic cells. In such bone-marrow MHC II-deficient chimeric animals, while BDC2.5 interaction with endogenous DCs draining antigen from the pancreatic lymph node is completely abrogated, BDC2.5-eTAC interactions are sustained in all secondary lymphoid organs of *Adbig* mice. This suggests that eTACs can directly interact with CD4+ T cells, a novel role for a radioresistant population in the secondary lymphoid organs. It is important to note that the nature of the *Adbig* transgenic system facilitates loading of the BDC2.5 mimetope peptide directly into the class II MHC pathway through the modified Invariant chain, and may differ from the pathway normally used by eTACs to cell-autonomously process and present antigen. It will therefore be important in future studies to determine if eTACs can similarly process and present their own tissue-specific antigens via class II MHC in such a cell-autonomous fashion. Along these lines there is recent evidence that autophagy plays a role in antigen processing and presentation in mTECs *(36)*, and it will be of interest to determine whether the same is true in eTACs.

Interestingly, whereas eTAC-CD8 interaction induces T-cell deletion, interaction of BDC2.5 CD4+ T cells with eTACs results in the persistence of a residual population consisting of functionally inactive effectors and *FoxP3+* regulatory T cells. While both functional inactivation of effectors and enrichment of regulatory T cells may play a role in eTAC-mediated CD4+ tolerance, it appears that functional inactivation alone is sufficient to prevent autoimmunity. The evidence for this is twofold. First, BDC2.5 FoxP3-DTR+ T cells continuously depleted of regulatory T cells remain unable to transfer disease into *Adbig* SCID recipients. Second, eTAC-experienced BDC2.5 T cells are unable to transfer disease serially in *cis* into secondary lymphopenic hosts, but also cannot suppress adoptive transfer of disease by other naïve BDC2.5 T cells in *trans*. Together these results support the idea that the primary mechanism of eTAC-mediated disease prevention in this model is recessive—a functional inactivation of effectors as opposed to a preferential enrichment of regulatory T cells.

Our results also suggest that eTACs have a unique tolerogenic capacity, and serve as more than simply an antigen reservoir in the periphery. In support of this, targeting of a BDC mimetope peptide to another putative tolerogenic APC population, DEC205+ DCs, induces proliferation of adoptively transferred BDC2.5 T cells similar to that seen in *Adbig* recipients, but does not prevent such transferred BDC2.5 T cells from producing effector cytokines in response to secondary peptide immunization. Nor does targeting the BDC mimetope peptide to DEC205+ DCs protect or delay SCID mice from adoptively transferred diabetes. One possible difference between delivery of antigen via αDEC1040 and *Adbig* mice may be the dose and length of antigen exposure, which could affect tolerance induction. But given the established role for immature DEC205+ DCs in tolerance induction *(22, 23, 28)*, it is unclear precisely why BDC2.5 T cells fail to become tolerant after such interaction. However, evidence suggests that DCs in NOD mice may have defects in tolerance induction *(37)*, and unlike eTACs, DCs do respond to inflammatory environmental changes, and may lose the ability to induce CD4+ tolerance in NOD mice. Although tolerance of islet-specific CD8+ T cells via DEC205+ DCs has been observed in NOD mice, induction of tolerance for CD4+ T cells appears to be more sensitive to the genetic and environmental changes that occur in autoimmune NOD mice.

The unique nature of eTAC-mediated tolerance leads us to speculate whether diabetes protection in this setting may act via a novel mechanism, as it appears insensitive to the perturbations that mitigate many forms of peripheral tolerance. For example, it is striking that self-antigen expression in eTACs induces robust tolerance even in lymphopenic SCID mice, while many similar systems of peripheral antigen display switch from tolerogenic to immunogenic in the context of lymphopenia *(31-33)*. Likewise, while T cell tolerance established by "immature" DC populations is commonly abrogated by maturation signals such as CD40 and TLR stimulus *(22, 23)*, these same signals do not appear to induce maturation of eTACs, nor do such stimuli interfere with the observed disease protection in *Adbig* SCID mice. Finally, PD-1/PD-L1 interactions have been shown to play an essential role in peripheral tolerance induction in numerous settings *(24-27)*, but appear to have no effect on eTAC-mediated CD4+ T cell tolerance. Together these findings suggest that self-antigen expression in eTACs induces a remarkably robust T-cell tolerance that is highly resistant to conversion from tolerance to immunogenicity. If indeed eTACs serve as a source of diverse self-antigen in the secondary lymphoid tissues, such resistance to immunogenicity may be important in preventing cross-priming of self-reactive T cells. Further defining the mechanism of this tolerance will be of significant future interest, but it is interesting to note that despite the massive proliferation of BDC2.5 T cells in *Adbig* SCID mice, and the mobilization of these cells into the peripheral blood, the pancreata remain completely free of infiltrate and the majority of the residual T cells are found in the spleen. This suggests that perhaps eTAC interaction interferes with trans-endothelial migration of activated CD4+ T cells into target tissue, leading to their sequestration within the secondary lymphoid system and peripheral blood. The lack of the classical costimulatory molecules CD80 and CD86 on eTACs *(11)* also suggests that the observed aberrant activation of CD4+ T cells may result from the absence of appropriate second signals delivered by eTACs.

Together these results suggest that pancreatic self-antigen expression in extrathymic *Aire*-expressing cells can mediate robust peripheral self-tolerance and provide protection from autoimmune diabetes, but also raise many important questions. For example, it will be important to determine whether endogenous antigens expressed in eTACs can mediate a similar protection from disease, and naturally whether Aire plays a role in this process. Though Aire has been suggested to induce the expression of a novel array of self-antigens in eTACs, a physiologic role for such endogenously Aire-regulated antigens outside the thymus has yet to be defined. Similarly, it will be of significant interest to determine what role eTACs play in normal homeostasis, and whether their absence leads to a predisposition toward autoimmunity. As we come to better understand the role of this population in immune tolerance, it will also be important to define the fundamental biology of these cells, both their origin and their relationship to other characterized APC populations. The recent report that populations of *Aire*-expressing cells reside in human secondary lymphoid organs *(30)* makes this inquiry all the more relevant for understanding human immunologic tolerance, and for therapeutic intervention in autoimmunity.

Methods

Transgene construction, BAC recombineering, and purification

Aire-driven BDC2.5 peptide Invariant Chain GFP *(Adbig)* transgenic mice were generated by standard cloning methods using a bacterial artificial chromosome (BAC) recombineering and transgenesis strategy. Briefly, the 1040-31 (p31) peptide (YVRPLWVRME*(17)*) coding sequence was introduced in place of the CLIP sequence of the Invariant Chain using overlapping bi-directional PCR from the pTIM vector (a gift of H. Van Santen) with the forward/reverse primer pairs 5’-AGAATTCCTAGAGGCTAGAGCC-3’/ 5’-tcgtacgtaCACAGGTTTGGCAGATTTC-3’ (product 1) and 5’-acgtacgaccactatgggtacgaatggaaCGTCCAATGtccatggat-3’/ 5’-ggcgtgaactggaagatct-3’ (product 2). These two PCR products were sub-cloned into pCR-Blunt II TOPO vectors (Invitrogen), sequenced, and digested with EcoR1 and BsiW1 (product one) or BglII and BsiW1 (product two), and ligated sequentially into pLitmus28i (New England Biolabs) to generate a complete p31-containing fragment. This EcoR1/BglII fragment was then inserted into the pTIM vector via EcoR1 partial and BglII complete digest, generating the pBDCTIM vector. The complete Ii-BDC construct was amplified from pBDCTIM by PCR using the primers 5’-cgcGGATCCTTAATTAAatggatgaccaacgcgac-3’/5’-cgcGGATCCtcacagggtgacttgaccc-3’, and this product was subcloned into the pCR-Blunt II TOPO vector for sequencing. This Ii-BDC fragment was inserted into the BamH1 site of pIRES2-EGFP (Clontech), generating the pIi-BDC-IRES2-EGFP vector.

The Ii-BDC-IRES-EGFP fragment was then extracted by PacI/NotI digest and ligated into pAireFNF, a BAC-targeting plasmid containing 5’ and 3’ homology arms to the mouse *Aire* gene. pAireFNF itself was generated from JDFNF, an *Aire* BAC-targeting expression construct previously described*(11)*. To generate pAireFNF, the multiple cloning site from the vector pLitmus 38i (New England Biolabs) was amplified with the primers 5'-GGTTAATTAACTTCTCTGCAGGATATCTG-3'/5'-GGCCTGCAGGGCCTTGACTAGAGGGTC-3', subcloned into pCR-BluntII-TOPO, sequenced, and ligated by NotI partial/HindIII complete digest into JDFNF. Ligation of the Ii-BDC-IRES-EGFP fragment into pAireFNF generated the construct pAireFNF-Ii-BDC.

This targeting construct, pAireFNF-Ii-BDC, was then inserted via standard recombineering*(38)* into a BAC clone from the Children's Hospital of Oakland Research Institute (CHORI) BACPAC Resource Center, clone 461e7 from the RPCI 23 Mouse BAC Library, which contained the *Aire* gene and approximately 90Kb of flanking sequence both upstream and downstream. The BAC identity was previously verified by PCR and restriction digestion, then purified and transfected via electroporation using standard techniques into the heat-inducible recombinase-competent and arabinose-inducible Flpe-expressing bacterial strain SW105. The *loxP* site in the eBAC3.6 vector was first removed by targeted homologous recombination. Heat-induced recombination was achieved by culturing the bacteria at 42°C, rapidly cooling, then electroporating in the presence of linearized pAireFNF-BDC-Ii plasmid. After selection and PCR-screening of recombinants, *Flpe* expression was induced in positive clones by culturing in 0.1% arabinose for three hours at 30°C. Flpe-recombinant clones were screened by replica-plating for acquisition of kanamycin sensitivity. Positive clones were then rescreened by Southern blot using SpeI digest and a 600-bp probe downstream of *Aire* exon 3 generated by the primers 5'-TCTCGTCCTCAAGAGTGCC-3' and 5'-GTCATGTTGACGGATCCA-3'.

Highly purified Ii-BDC-Aire BAC DNA was carefully prepared for fertilized oocyte injection by column purification using a modified Midiprep kit protocol (Qiagen). 100ml of clonal liquid culture was pelleted, gently alkaline-lysed, protein-precipitated, and centrifuged. Supernatant was applied to equilibrated Midiprep columns, washed according to manufacturer's instructions, and eluted with prewarmed 65-degree Buffer QF (Qiagen). BAC DNA was precipitated and pelleted in an ultracentrifuge (Sorvall). Pellets were washed, centrifuged, and allowed to air-dry, then gently resuspended in injection buffer (10mM Tris-HCL, 0.1 mM EDTA, pH 7.5), and evaluated for integrity by KpnI digestion and gel electrophoresis. Resuspended BAC DNA was injected into fertilized NOD oocytes by the UCSF Mouse Transgenic Core with the assistance of H. Lu and N. Killeen.

Mice and genotyping

Adbig transgenic NOD mice were screened by real-time PCR using the primers 5'-CTGCTGCCCGACAACCA-3' and 5'-TGTGATCGCGCTTCTCGTT-3' and the probe Cy5-TACCTGAGCACCCAGTCCGCCCT-BHQ along with an endogenous control reaction for CD86 using the primers 5'-CTTGATAGTGTGAATGCCAAGTACCT-3' and 5'-TGATCTGAACATTGTGAAGTCGTAGA-3' and the probe FAM-CCGCACGAGCTTTGACAGGAACAACT-TAMRA. This same reaction was used to genotype *Adig* mice, as it detects genomic GFP present in both transgenes. Both *Adig* and *Adbig* transgenes were maintained in heterozygosity for all experiments.

TCR-transgenic BDC2.5 NOD mice and TCR-transgenic *8.3* NOD mice were acquired from J. Bluestone and Q. Tang and crossed onto CD90.1 congenic NOD strains. Both TCR transgenes were maintained in heterozygosity, and were FACS-genotyped by usage of the Vβ4 (BDC2.5) or Vβ8.1 (8.3) clonotype specific antibodies (BD Pharmingen) among peripheral blood CD4s (BDC2.5) or CD8s (8.3). FoxP3-DTR NOD mice were acquired from D. Mathis and C. Benoist and the Center on Immunological Tolerance in Type-1 Diabetes at Jackson Laboratories. NOD MHC II-knockout mice were obtained from Jackson Laboratories (stock# 004256).

All mice were maintained in microisolator cages and treated in accordance with NIH and American Association of Laboratory Animal Care standards, and consistent with the animal care and use regulations of the University of California, San Francisco.

Flow cytometry and cell sorting

All FACS antibodies were purchased from BD Pharmingen, eBioscience, Invitrogen, or Southern Biotech with the exception of anti-CD32/16 (clone 2.4G2), which was purified by the UCSF hybridoma core, and anti-EpCAM (clone G8.8), which was purified and biotinylated by K. Johannes. Stromal cells were prepared for FACS as described*(11)*. Lymphocytes for flow cytometry were prepared by mashing thymi, lymph nodes, or spleens, filtering these cells through a 70μm cell-strainer, lysing red blood cells by incubation in ACK buffer (spleen only; 0.15 M NH_4Cl, 10 mM $KHC0_3$, 0.1 mM Na_2EDTA), counting by trypan blue exclusion, resuspending in anti-Fc receptor blocking antibody clone 2.4G2 in FACS buffer for ten minutes, then incubating on ice with antibody cocktails for twenty minutes. For peptide/class I MHC tetramer staining, cells were incubated on ice with antibody cocktail along with either IGRP mimetope/class I MHC tetramer NRP-V7-PE (KYNKANVFL/K^d) or with mock tetramer TUM-PE (KYQAVTTTL/K^d, NIAID MHC Tetramer Core Facility) for one hour, then washed and analyzed by flow cytometry. For peptide/class II MHC tetramer staining, cells were incubated on ice with antibody cocktail with either BDC2.5 mimetope/class II MHC tetramer p31-PE (RTRPLWVRME/I-Ag7) or with irrelevant tetramer CLIP-PE (PVSKMRMATPLLMQA/I-Ag7, NIAID MHC Tetramer Core Facility) for one hour, then washed and analyzed by flow cytometry as described. For intracellular FoxP3 staining, lymphocytes were first stained for cell-surface markers, then fixed and permeabilized according to the instructions of the FoxP3 staining buffer set (eBioscience) and incubated for 30 minutes with anti-FoxP3 (eBioscience), washed in permeabilization buffer and then FACS buffer, and analyzed by FACS.

Isolation of RNA and real-time PCR

For real-time PCR, stromal cells were isolated from thymus, spleen, and pooled lymph nodes as described above. eTACs, mTECs, and DCs were sorted from nontransgenic *Adbig* mice based on the following surface markers: eTACs and mTECs: PI-, CD45-, CD11c-, MHC II+, GFP+; DCs: PI-, CD45+, CD11c+, MHC II+. RNA was purified using the Absolutely RNA Microprep kit (Stratagene) and quantitated using a NanoDrop spectrophotometer (Thermo Fisher Scientific). After quantitation, RNA was reverse-transcribed into cDNA using oligo-dT (Invitrogen) and Superscript III reverse transcriptase (Qiagen). Equivalent reactions without reverse transcriptase (-RT) were run for each sample. *Aire* transcript levels were assessed by real-time PCR using the Exon2-3 amplifying primers 5’-CAGCCGCCTGCATAGCA-3’ and 5’-CTTTCCGGGACTGGTTTAGGT-3’ and probe FAM-CCTGGACGGCTTCCCAAAAGATGTG-BHQ. Sample quantities were normalized to Actin signal, detected using SYBR green master mix (Applied Biosystems) and the primers 5’-ACGGCCAGGTCATCACTATTG-3’ and 5’-AGGATTCCATACCCAAGAAGGAA-3’. Real-time PCR reactions were run on a 7500 Fast Real-Time PCR System (Applied Biosystems).

Statistical Analysis

Statistical analysis of data was performed with Excel 2003 (Microsoft) and Prism 4.0 (GraphPad). Statistical comparisons were made using a Student’s two-tailed T-test, and results with $p<0.05$ were considered statistically significant.

Histology, immunofluorescent staining and quantitation

All primary and secondary antibodies for histology were purchased from AbCam, BD Pharmingen, Invitrogen, Jackson, or eBioscience, with the exception of the anti-AIRE antibodies 5C-11 and 5H-12, which were gifts of H. Scott. For *Adig* mice, organs were harvested from experimental animals and embedded in Tissue-Tek Optimal Cutting Temperature (OCT) media (Fisher), then processed as described*(11)*. Slides were mounted in Vectashield mounting medium (Vector Laboratories) and visualized with an SP2-AOBS Confocal Microscope (Leica). Images were acquired using Leica Confocal Software (Leica).

For *Adbig* mice, fixation conditions were modified to properly fix cytoplasmic GFP. Organs were harvested from experimental animals and directly fixed in a 1.5% paraformaldehyde (Fisher) solution at 4°C for 3 hours. Tissues were then transferred to a 30% sucrose solution and left at 4°C for 3 hours prior to embedding in OCT. Sections were cut as before, and GFP was then labeled using a Tyramide Signal Amplification kit (Perkin Elmer) according to the manufacturer’s protocol. Following GFP signal amplification, additional markers were labeled using the standard immunostaining procedure described above. Slides were mounted in Vectashield mounting medium (Vector Laboratories) and visualized on an Axioskop 2 Plus Widefield Scope (Leica) attached to a C4742-95 digital camera (Hamamatsu). Images were acquired using AxioVision 4.6 (Zeiss) and analyzed, processed via linear contrast adjustment, and merged with Photoshop CS3 (Adobe).

For hematoxylin and eosin staining of pancreatic sections, tissues were fixed overnight in formalin at 4°C, then dehydrated in 30% ethanol for 30 minutes and stored in 70% ethanol prior to embedding in paraffin. 10-micron sections were cut, stained with hematoxylin and eosin as described (REF) and visualized with an AxioImager Brightfield microscope (Zeiss) using AxioVision 4.6 (Zeiss) acquisition software. All microscopy image merging, contrast-adjustment, or formatting was applied equivalently to control and experimental images using Photoshop CS3 (Adobe).

Purification, CFSE-labeling, and adoptive transfer/serial transfer of T cells

For adoptive transfer of naïve, CD25-depleted, CD4-enriched T cells, the spleen and all major peripheral lymph nodes except pancreatic were harvested from nondiabetic donors, pooled by group, ACK-lysed and counted. Cells were then CD25-depleted by addition of anti-CD25 hybridoma 7D4 supernatant, incubated for 25 minutes on ice, then incubated with rabbit complement in DMEM for 50 minutes in 37-degree rotator. Cells were washed, counted, and resuspended in Robosep buffer (StemCell Technologies) with 5% rat serum before CD4 enrichment using Mouse CD4+ Negative Selection Kit in the Robosep 20000 (StemCell Technologies) with the 1-Quadrant High Recovery protocol. Aliquots at each step were used to confirm depletion or purification. Cells were counted, and for disease transfer were resuspended in Hank's Buffered Salt Solution (HBSS) without Phenol Red at 1e6 cells/ml, then 200ul was injected IV per recipient by tail vein. For CFSE labeling prior to adoptive transfer, purified cells were pooled in a ~1:1 ratio of BDC2.5 T cells:polycolonal CD4+ T cells then labeled in 2.5μM CFSE (Invitrogen) at room temperature for 5 minutes. Labeling was quenched with an equal volume of FCS, cells were washed twice in DMEM and once in HBSS, counted and injected at 1-2e6 cells/recipient via the tail vein. For adoptive transfer of diabetes into SCID and Adbig SCID recipients, the same protocol was followed but purified BDC2.5 T cells were not CFSE-labeled or mixed with polyclonal cells, simply resuspended to 1e6 cells/ml and injected at 200uL per mouse via tail vein.

Serial co-transfer of T cells was performed at day 10 post-primary transfer. Non-pancreatic lymph nodes and spleen were harvested from SCID and *Adbig* SCID primary recipients, pooled, ACK-lysed, and counted. These cells were counted and purified for

CD4+ T cells as described above. Simultaneously, naïve BDC2.5 T cells were harvested from unmanipulated BDC2.5 mice and purified by CD25-depletion and CD4-enrichment as described above. Purified serially transferred CD4+ T cells were injected alone or mixed 1:1 with naïve BDC2.5 T cells and injected at 200,000 cells/recipient into secondary immunodeficient hosts, which were followed for diabetes as described below.

Treatment and analysis of adoptive transfer recipients

Indicated recipient SCID and *Adbig* SCID mice were treated with 200ug/mouse of anti-PD-L1 (clone 9G2; Bio-Express), a 1:1 mixture of anti-CD40 (clone FGK4.5; UCSF Hybridoma Core) and poly I:C (Sigma), or isotype rat IgG (Bio-Express). Mice were injected intraperitoneally one day before and one day after adoptive transfer (for anti-CD40/PolyI:C) or one day before and continuously every other day after (for anti-PD-L1 and isotype). Disease transfer SCID and *Adbig* SCID mice receiving *FoxP3-DTR*+ BDC2.5 T cells were treated with 50ug/kg diphtheria toxin (DT) in PBS injected intraperitoneally the day of adoptive transfer and at day 2 post-transfer, then every three days over the course of observation. Recipient mice were monitored for diabetes onset at the indicated timepoints by serial analysis of blood glucose using an Ascensia Elite XL blood glucometer (Bayer). For incidence curves mice were considered diabetic after two successive blood glucose readings >350mg/dl. For αDEC1040 experiments, wildtype NOD mice were injected with 400ng of αDEC1040 or an equivalent volume of PBS one day prior to transfer of 1e6 BDC2.5 T cells, and were analyzed for CFSE dilution 40 hours post-transfer. NOD SCID mice were treated with 100ng αDEC1040 or PBS one day prior to adoptive transfer of BDC2.5 T cells, and then re-treated with 100ng every three days throughout the course of observation.

For peptide/CFA immunization experiments at day 14 post-adoptive transfer, mice were injected subcutaneously with p31 peptide emulsified in Complete Freund's Adjuvant (CFA), made from Incomplete Freund's Adjuvant (Sigma) with 4mg/ml H37RA tuberculosis (DIFCO). Acetylated p31 peptide (Genscript) was added to CFA to a final concentration of 500ug/ml. The p31/CFA solution was emulsified by sonication, and injected subcutaneously at 100ul/mouse. Three days post-immunization, lymphocytes and spleen were harvested, ACK-lysed, and plated at 5e6 cells/well in 1ml complete DMEM + 10% FCS plus 0.5uM p31 peptide. After four hours of incubation at 37 degrees in 5% CO_2, 1.33uL GolgiStop (BD Biosciences) was added and cells incubated an additional six hours. Cells were then washed, stained with CD4/CD90.1 antibodies, then fixed in 4% PFA, permeabilized with permeabilization buffer (eBioscience) and stained intracellularly for interferon gamma or isotype.

Generation of αDEC-1040 reagent

Hybrid antibodies were prepared similarly to Hawiger, et al.*(28)* Plasmid containing the anti-DEC-205 V region heavy-chain linked to the 1040-55 peptide (RVRPLWVRME*(17)*) were transfected into 293T cells together with a second plasmid containing the kappa chain recognizing DEC-205. 293T cells were maintained in high glucose DMEM containing L-glutamine and 110 mg/L sodium pyruvate, 10% Low IgG FBS, 100U/mL penicillin, 100μg/mL streptomycin, and 50μg/mL gentamicin (all from Gibco except gentamicin from Quality Biologicals). Four to six days after transfection supernatants were harvested and antibody was purified over Protein G-sepharose columns (GE Healthcare). Antibodies were dialyzed overnight to PBS and examined for LPS contamination by LAL assay (Lonza) and for purity by SDS-PAGE and GelCode Blue staining (Pierce). LPS levels below 0.1 EU/mL were considered endotoxin-free. Antibody concentration was determined by spectrophotometric analysis.

Thymectomy and thymic transplantation

One week prior to thymectomy/thymic transplant, donor thymi were harvested from 2-3 day-old wildtype NOD pups and incubated in 12-well Costar transwell plates (Corning) in complete DMEM + 10% FCS and 1.35mM 2-deoxyguanosine (Sigma). One day before transplant, media was changed to complete DMEM + 10% FCS without 2-DG.

Thymectomy and thymic transplantation was performed on 4-6 week-old wildtype or *Adig* NOD mice as previously described*(7, 39)*. Briefly, mice were anesthetized with Ketamine (80mg/kg) and Xylazine (10mg/kg), and thymectomy was performed by surgical accession of the superior mediastinum followed by vacuum aspiration of the thymic lobes. Completeness of thymectomy was confirmed before wound closure and again at the time of autopsy. Immediately after thymectomy, transplantation of thymi was performed under the kidney capsule by surgical accession of the peritoneum, incision of the kidney capsule with a 25-gauge needle, and mechanical implantation of both thymic lobes to a subcapsular site distal to the incision with sterile 0.51mm silastic laboratory tubing (Dow Corning). Capsule incisions were cauterized with a portable Bovie electrocautery (Aaron Medical) before wound closure. Transplants were evaluated at the time of autopsy for growth and by thymocyte flow cytometry for CD4 and CD8 expression supporting normal T-cell development. Skin staples were removed within two weeks of surgery, and all experimental mice were monitored and treated continuously with post-operative analgesia consistent with IACUC procedures.

References

1. Kyewski B, Klein L. A central role for central tolerance. Annu Rev Immunol 2006;24:571-606.
2. Derbinski J, Schulte A, Kyewski B, Klein L. Promiscuous gene expression in medullary thymic epithelial cells mirrors the peripheral self. Nat Immunol 2001;2:1032-9.
3. Nagamine K, Peterson P, Scott HS, et al. Positional cloning of the APECED gene. Nat Genet 1997;17:393-8.
4. An autoimmune disease, APECED, caused by mutations in a novel gene featuring two PHD-type zinc-finger domains. Nat Genet 1997;17:399-403.
5. Anderson MS, Venanzi ES, Klein L, et al. Projection of an immunological self shadow within the thymus by the aire protein. Science 2002;298:1395-401.
6. Jiang W, Anderson MS, Bronson R, Mathis D, Benoist C. Modifier loci condition autoimmunity provoked by Aire deficiency. J Exp Med 2005;202:805-15.
7. DeVoss J, Hou Y, Johannes K, et al. Spontaneous autoimmunity prevented by thymic expression of a single self-antigen. J Exp Med 2006;203:2727-35.
8. Shum AK, DeVoss J, Tan CL, et al. Identification of an Autoantigen Demonstrates a Link Between Interstitial Lung Disease and a Defect in Central Tolerance. Science Translational Medicine 2009;1:9ra20-9ra.
9. Heino M, Peterson P, Sillanpaa N, et al. RNA and protein expression of the murine autoimmune regulator gene (Aire) in normal, RelB-deficient and in NOD mouse. Eur J Immunol 2000;30:1884-93.

10. Lee JW, Epardaud M, Sun J, et al. Peripheral antigen display by lymph node stroma promotes T cell tolerance to intestinal self. Nat Immunol 2007;8:181-90.

11. Gardner JM, Devoss JJ, Friedman RS, et al. Deletional tolerance mediated by extrathymic Aire-expressing cells. Science 2008;321:843-7.

12. Yip L, Su L, Sheng D, et al. Deaf1 isoforms control the expression of genes encoding peripheral tissue antigens in the pancreatic lymph nodes during type 1 diabetes. Nat Immunol 2009;10:1026-33.

13. Nichols LA, Chen Y, Colella TA, Bennett CL, Clausen BE, Engelhard VH. Deletional self-tolerance to a melanocyte/melanoma antigen derived from tyrosinase is mediated by a radio-resistant cell in peripheral and mesenteric lymph nodes. J Immunol 2007;179:993-1003.

14. Guerau-de-Arellano M, Mathis D, Benoist C. Transcriptional impact of Aire varies with cell type. Proc Natl Acad Sci U S A 2008;105:14011-6.

15. Stadinski BD, Delong T, Reisdorph N, et al. Chromogranin A is an autoantigen in type 1 diabetes. Nat Immunol;11:225-31.

16. Haskins K, McDuffie M. Acceleration of diabetes in young NOD mice with a CD4+ islet-specific T cell clone. Science 1990;249:1433-6.

17. Judkowski V, Pinilla C, Schroder K, Tucker L, Sarvetnick N, Wilson DB. Identification of MHC class II-restricted peptide ligands, including a glutamic acid decarboxylase 65 sequence, that stimulate diabetogenic T cells from transgenic BDC2.5 nonobese diabetic mice. J Immunol 2001;166:908-17.

18. Yoshida K, Martin T, Yamamoto K, et al. Evidence for shared recognition of a peptide ligand by a diverse panel of non-obese diabetic mice-derived, islet-specific, diabetogenic T cell clones. Int Immunol 2002;14:1439-47.

19. You S, Chen C, Lee WH, et al. Detection and characterization of T cells specific for BDC2.5 T cell-stimulating peptides. J Immunol 2003;170:4011-20.

20. van Santen HM, Benoist C, Mathis D. Number of T reg cells that differentiate does not increase upon encounter of agonist ligand on thymic epithelial cells. J Exp Med 2004;200:1221-30.

21. Feuerer M, Shen Y, Littman DR, Benoist C, Mathis D. How punctual ablation of regulatory T cells unleashes an autoimmune lesion within the pancreatic islets. Immunity 2009;31:654-64.

22. Bonifaz L, Bonnyay D, Mahnke K, Rivera M, Nussenzweig MC, Steinman RM. Efficient targeting of protein antigen to the dendritic cell receptor DEC-205 in the

steady state leads to antigen presentation on major histocompatibility complex class I products and peripheral CD8+ T cell tolerance. J Exp Med 2002;196:1627-38.

23. Mukhopadhaya A, Hanafusa T, Jarchum I, et al. Selective delivery of beta cell antigen to dendritic cells in vivo leads to deletion and tolerance of autoreactive CD8+ T cells in NOD mice. Proc Natl Acad Sci U S A 2008;105:6374-9.

24. Latchman YE, Liang SC, Wu Y, et al. PD-L1-deficient mice show that PD-L1 on T cells, antigen-presenting cells, and host tissues negatively regulates T cells. Proc Natl Acad Sci U S A 2004;101:10691-6.

25. Fife BT, Guleria I, Gubbels Bupp M, et al. Insulin-induced remission in new-onset NOD mice is maintained by the PD-1-PD-L1 pathway. J Exp Med 2006;203:2737-47.

26. Reynoso ED, Elpek KG, Francisco L, et al. Intestinal tolerance is converted to autoimmune enteritis upon PD-1 ligand blockade. J Immunol 2009;182:2102-12.

27. Keir ME, Liang SC, Guleria I, et al. Tissue expression of PD-L1 mediates peripheral T cell tolerance. J Exp Med 2006;203:883-95.

28. Hawiger D, Inaba K, Dorsett Y, et al. Dendritic cells induce peripheral T cell unresponsiveness under steady state conditions in vivo. J Exp Med 2001;194:769-79.

29. Verdaguer J, Schmidt D, Amrani A, Anderson B, Averill N, Santamaria P. Spontaneous autoimmune diabetes in monoclonal T cell nonobese diabetic mice. J Exp Med 1997;186:1663-76.

30. Poliani PL, Kisand K, Marrella V, et al. Human Peripheral Lymphoid Tissues Contain Autoimmune Regulator-Expressing Dendritic Cells. Am J Pathol.

31. Lohr J, Knoechel B, Kahn EC, Abbas AK. Role of B7 in T cell tolerance. J Immunol 2004;173:5028-35.

32. Knoechel B, Lohr J, Kahn E, Bluestone JA, Abbas AK. Sequential development of interleukin 2-dependent effector and regulatory T cells in response to endogenous systemic antigen. J Exp Med 2005;202:1375-86.

33. King C, Ilic A, Koelsch K, Sarvetnick N. Homeostatic expansion of T cells during immune insufficiency generates autoimmunity. Cell 2004;117:265-77.

34. Shizuru JA, Taylor-Edwards C, Banks BA, Gregory AK, Fathman CG. Immunotherapy of the nonobese diabetic mouse: treatment with an antibody to T-helper lymphocytes. Science 1988;240:659-62.

35. Devoss JJ, Shum AK, Johannes KP, et al. Effector mechanisms of the autoimmune syndrome in the murine model of autoimmune polyglandular syndrome type 1. J Immunol 2008;181:4072-9.

36. Nedjic J, Aichinger M, Emmerich J, Mizushima N, Klein L. Autophagy in thymic epithelium shapes the T-cell repertoire and is essential for tolerance. Nature 2008;455:396-400.
37. Hamilton-Williams EE, Martinez X, Clark J, et al. Expression of diabetes-associated genes by dendritic cells and CD4 T cells drives the loss of tolerance in nonobese diabetic mice. J Immunol 2009;183:1533-41.
38. Lee EC, Yu D, Martinez de Velasco J, et al. A highly efficient Escherichia coli-based chromosome engineering system adapted for recombinogenic targeting and subcloning of BAC DNA. Genomics 2001;73:56-65.
39. Reeves JP, Reeves PA, Chin LT. Survival surgery: removal of the spleen or thymus. Curr Protoc Immunol 2001;Chapter 1:Unit 1 10.

Chapter IV

The *AireDTR* Mouse and Autoimmunity

Introduction

The previous chapters have described the identification of eTACs, have demonstrated that Aire regulates a unique set of self-antigens in this population, and that such interactions promote immune self-tolerance. While these results indicate that eTACs are sources of TSA expression in the periphery, and that self-antigen expression in eTACs is sufficient to induce immune self-tolerance, they do not strictly identify a role for eTACs in the normal maintenance of tolerance. Likewise, in the thymus, despite the well-establish role of Aire established by knockout mice, the precise role of *Aire*-expressing mTECs remains uncertain. To directly study the contribution of eTACs and Aire-expressing mTECs to the maintenance of immune tolerance, we have generated a novel transgenic mouse in which we can specifically and temporally delete *Aire*-expressing cells. This chapter will describe the development and preliminary findings related to this mouse model, and discuss ongoing and proposed experiments for this system.

Cell-type specific deletion of defined populations has been used in diverse settings from immunology to developmental biology to study the contribution of specific cells to normal homeostasis. One common approach to achieve such deletion exploits the human heparin-binding EGF-like growth factor (*HBEGF*) gene, also known as the diphtheria toxin receptor (DTR), which binds with high affinity to diphtheria toxin (DT), a translational inhibitor. While the mouse shares a homologous *Hbgef* gene, the tissue-selectivity of this approach is conferred because murine *Hbgef* has 10^3-10^5-fold lower affinity for diphtheria toxin (DT) than its human counterpart (reviewed in *(1)*). Thus, mice can systemically tolerate significantly higher dosage of DT than humans, allowing for relatively low nonspecific toxicity in non DTR-expressing mouse cells.

Expression of the human *HBGEF* gene under control of a cell-type specific promoter in mice thus confers upon that population a high sensitivity to diphtheria toxin, and this approach has been used to successfully deplete a diverse range of cells including FoxP3+ regulatory T cells *(2)*, CD11b+ monocytes and macrophages *(3)*, and CD11c+ or Langerlin+ DCs *(4, 5)*, among many others. Cell death after DT internalization is generally believed to occur via apoptosis, purportedly reducing the risk that such death itself will cause inflammation and contribute to immune perturbation *(3)*. However cell-death related artifacts are certainly to be considered when interpreting any data related to such systems. Further, this approach has additional limitations that should be noted, most prominently: (1) DT itself is immunogenic, and thus mice continuously exposed to DT will gradually generate an anti-DT antibody response, which can potentially limit the effective treatment window; and (2) despite the lower affinity for the mouse *Hbgef* gene, DT retains significant nonspecific toxicity at higher doses, particularly in young mice. Despite these potential limitations, DTR-transgenic mice have been essential in dissecting the role of diverse cell populations of the immune system, and we hope an *AireDTR* mouse will provide significant insight into the role of mTECs and eTACs.

Results

The *AireDTR* Mouse Faithfully Recapitulates Aire Expression in mTECs and eTACs

In order to express the diphtheria toxin receptor specifically in mTECs and eTACs, we used a bacterial artificial chromosome (BAC)-targeting approach similar to those described previously *(6)* in the generation of the *Adig (7)* and *Adbig* (Chapter III) mouse strains. Employing a homologous recombineering strategy, we inserted the DTR-EGFP cassette in place of exons 1-3 of the mouse *Aire* gene in a BAC containing ~90 kilobases of flanking DNA in either direction, and injected this construct (**Fig. 4.1a**) into fertilized oocytes. We generated NOD founders which we termed *AireDTR* mice. As in previous *Aire*-driven transgenic lines, we used GFP to evaluate the pattern of transgene expression. Immunofluorescent staining demonstrated that in the thymus, GFP expression was largely restricted to cytokeratin 5-positive cells of the medulla, and colocalized with Aire protein (**Fig. 4.1b**). In the secondary lymphoid organs, GFP expression was restricted to populations residing at T-B boundary regions in the interfolicular ridges of lymph nodes (**Fig. 4.1b**) and at similar T-B boundaries between the PALS and the B-cell follicle in the spleen (data not shown). This pattern of expression in the thymus and secondary lymphoid organs is consistent with that observed in both the *Adig* and *Adbig* reporter mouse lines. Similarly, FACS analysis of the thymus and secondary lymphoid organs revealed populations of class II MHC+, GFP+ cells unique to transgenic animals, though expression in both organs was noticeably lower than seen in other *Aire*-reporter strains (**Fig. 4.1c**). This lower expression is perhaps not surprising given that other strains using the same DTR-EGFP construct have also shown very low GFP expression by FACS *(4)*.

Figure 4.1. The *AireDTR* transgene is expressed in mTECs and eTACs. (**a**) Schematic illustration of homologous recombineering to target the DTR-EGFP construct into the first three exons of a BAC containing the mouse *Aire* gene. (**b**) Immunofluorescent staining of thymus and lymph node frozen sections from *AireDTR* mice using the antibodies indicated. (**c**) Flow cytometric analysis of Percoll-light stromal fractions from wildtype and *AireDTR* thymus and lymph nodes pre-gated for FSC/SSC, CD45-low, and DAPI-negative status.

Figure 4.1

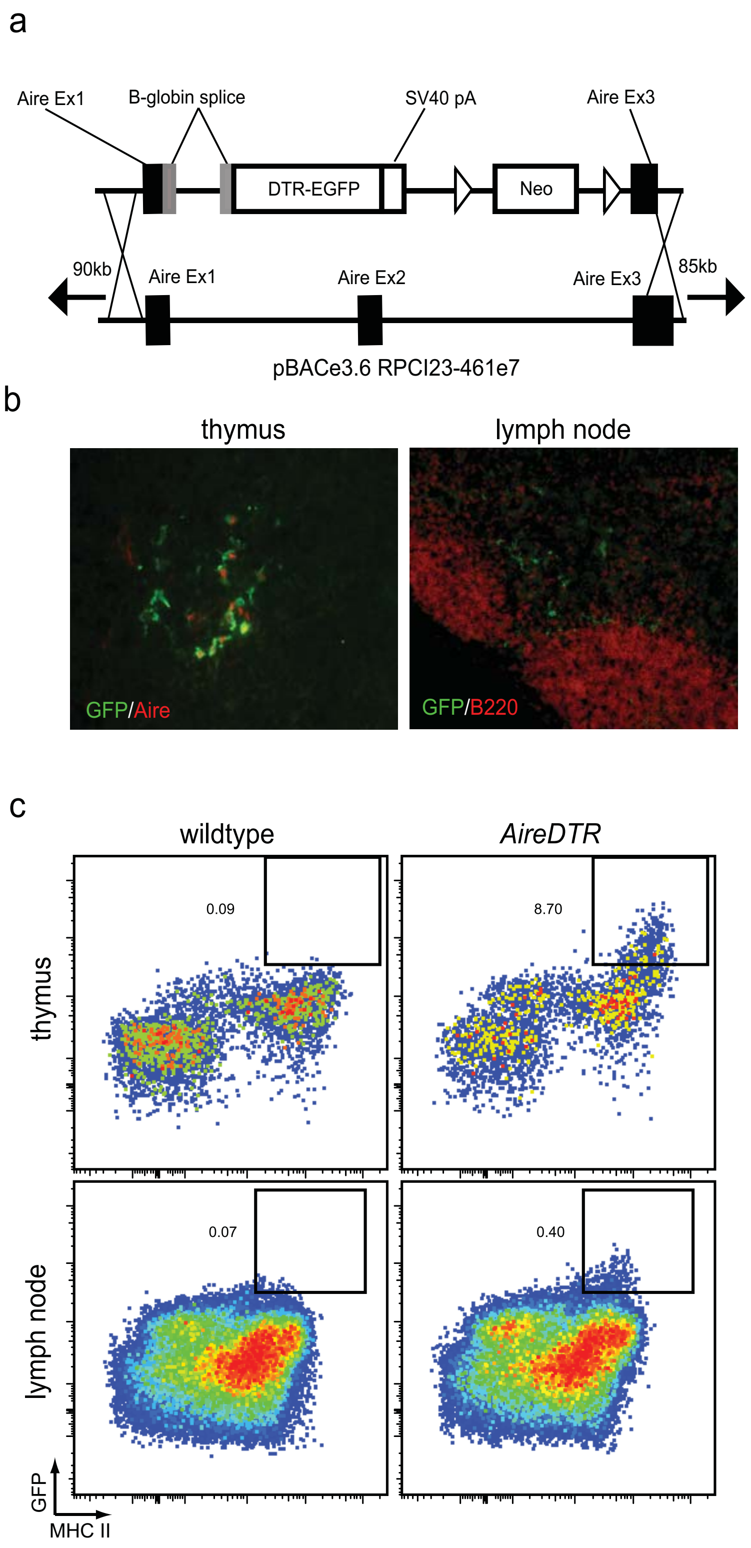
a
Aire Ex1
B-globin splice
SV40 pA
Aire Ex3
DTR-EGFP
Neo
90kb
Aire Ex1
Aire Ex2
Aire Ex3
85kb
pBACe3.6 RPCI23-461e7
b
thymus
lymph node
GFP/Aire
GFP/B220
c
wildtype
AireDTR
thymus
lymph node
0.09
8.70
0.07
0.40
GFP
MHC II

Together these results suggest that the DTR-EGFP transgene is being faithfully expressed in mTECs and eTACs in the *AireDTR* mouse.

Diphtheria Toxin Administration Rapidly and Effectively Depletes mTECs and eTACs

We next tested the ability of the *AireDTR* transgene to deplete mTECs and eTACs upon DT exposure. Wildtype, *Adbig*, and *AireDTR* mice were treated for two consecutive days with 50ug/kg DT injected intraperitoneally and then harvested on day three. In the thymus, FACS analysis revealed an essentially complete depletion of MHCII+, GFP+ mTECs in *AireDTR* mice, while *Adbig* mice were unaffected (**Fig. 4.2a**). Importantly, in such analysis we could distinguish between completely GFP+-depleted *AireDTR* mice and mis-genotyped mice both by immunofluorescent nuclear Aire staining (**Fig. 4.2c**) and by the frequency of MHCII-high, CD45-low cells in the thymus by FACS, which are uniquely depleted in DT-treated *AireDTR* mice (**Fig. 4.2b**). In the secondary lymphoid organs, an equally complete and transgene-specific depletion was observed among MHCII+ GFP+ eTACs (**Fig. 4.2c**).

Immunofluorescent staining of frozen sections with an anti-GFP antibody also revealed a complete absence of transgene signal after DT treatment in both the thymus and secondary lymphoid organs (**Fig. 4.2d**). The complete absence of anti-GFP reactivity in DT-treated *AireDTR* mice also suggests that fragmentary GFP may not be disseminated broadly in this mouse distinct from functional DTR, as treatment ablates all reactivity to the polyclonal GFP antibody (although fragmentary GFP may also be

Figure 4.2. DT administration induces effective depletion of *AireDTR* transgene-expressing cells in the thymus and secondary lymphoid organs. (**a**) Flow cytometric analysis of Percoll-light stromal fractions from thymi treated for two days as indicated, pre-gated for FSC/SSC, CD45-low, and DAPI-negative status. (**b**) Flow cytometric analysis of Percoll-light stromal fractions in (a) pre-gated just for FSC/SSC and DAPI-negative status. (**c**) Flow cytometric analysis of the same mice as (a) showing lymph nodes. (**d**) Immunofluorescent staining of thymus and lymph node frozen sections from *AireDTR* mice treated for two days as indicated; stained for GFP (green) and Aire (red; thymus only).

Figure 4.2

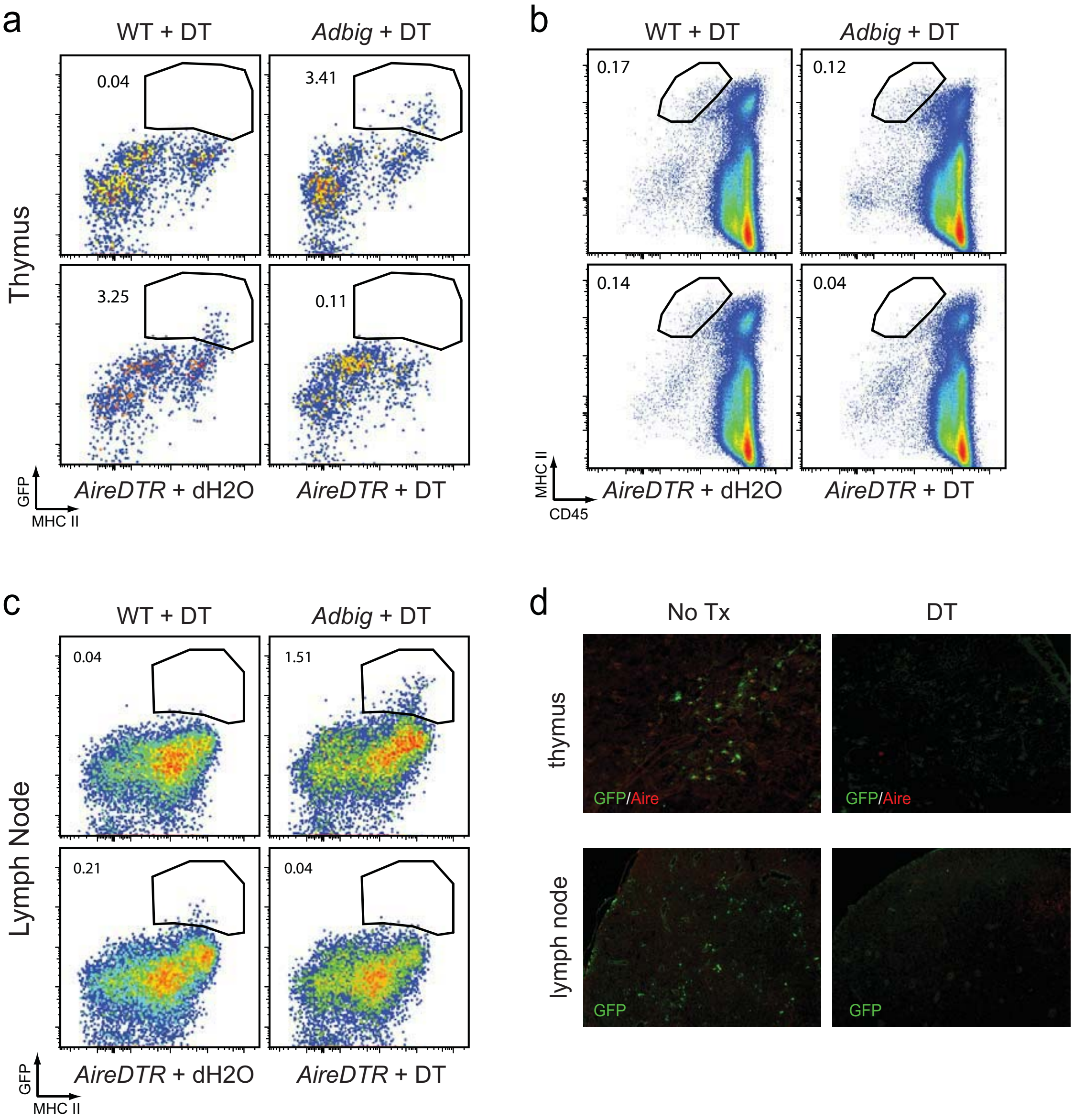
a
WT + DT
Adbig + DT
0.04
3.41
3.25
0.11
Thymus
GFP
MHC II
AireDTR + dH2O
AireDTR + DT
b
WT + DT
Adbig + DT
0.17
0.12
0.14
0.04
MHC II
CD45
AireDTR + dH2O
AireDTR + DT
c
WT + DT
Adbig + DT
0.04
1.51
0.21
0.04
Lymph Node
GFP
MHC II
AireDTR + dH2O
AireDTR + DT
d
No Tx
DT
thymus
GFP/Aire
GFP/Aire
lymph node
GFP
GFP

present but simply lost during staining). Finally, immunofluorescent anti-Aire staining in the thymus indicated that in addition to a complete absence of GFP in DT-treated *AireDTR* mice, we were also largely unable to detect Aire protein after two days of treatment (**Fig. 4.2d**), suggesting that the transgene is inducing depletion of essentially all endogenous *Aire*-expressing cells. Thus, the *AireDTR* construct appears to be faithfully expressed in mTECs and eTACs, and exposure to DT rapidly and completely depletes both cell populations.

Pharmacokinetics of DT administration

Validation of both transgene expression and efficacy of deletion in the *AireDTR* mouse suggested that the mouse might provide an appropriate tool for further studies of *Aire*-expressing cells. Before proceeding to longitudinal depletion experiments, dose-response titrations, mTEC and eTAC regeneration kinetics, and serum anti-DT antibody resistance kinetics were evaluated.

First, dose-response experiments were conducted to define the minimum dose required to achieve complete depletion of *Aire*-expressing mTECs and eTACs. Complete depletion in the thymus proved to require a higher dose than similar depletion in the periphery (data not shown), and therefore complete depletion in the thymus was used as the minimum standard for dose-response experiments. Treatment of *AireDTR* mice with a range of concentrations indicated clearly that an intermediate dose (25ug/kg) achieved maximal depletion (**Fig. 4.3a**), and that higher doses of 50 or 100ug/kg did not confer

Figure 4.3. Kinetics of DT depletion and recovery. (**a**) Flow cytometric analysis of *AireDTR* thymi treated with the indicated doses of DT (ug/kg) for two consecutive days prior to analysis; pre-gated on FSC/SSC, CD45-low, and DAPI-negative. Numbers next to the gate indicate cell number in the gate. Graph shows number of GFP+ cells relative to an untreated *AireDTR* mouse as a function of DT dose. (**b**) Number of GFP+ cells in the thymus, spleen, and lymph nodes of *AireDTR* mice as a function of time (days) after ending two days of depletion with 50ug/kg DT, displayed relative to the number observed in an untreated *AireDTR* mouse. (**c**) Immunofluorescent staining of *AireDTR* thymi treated continuously every other day for indicated times with 50ug/kg DT for cytokeratin 8 (K8; red) and GFP (green).

Figure 4.3

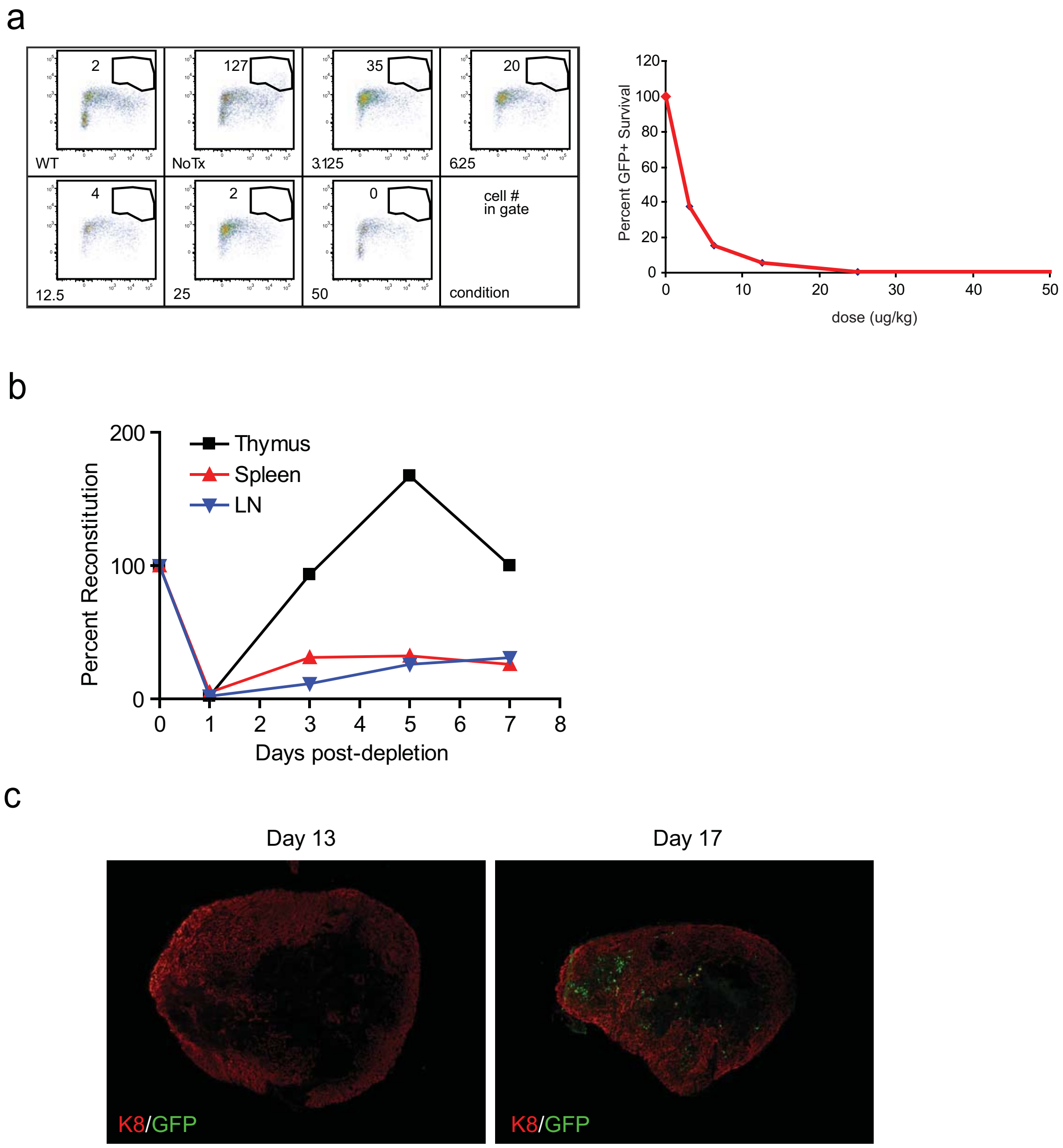
a
2
WT
127
NoTx
35
3.125
20
6.25
4
12.5
2
25
0
50
cell #
in gate
condition
Percent GFP+ Survival
120
100
80
60
40
20
0
0
10
20
30
40
50
dose (ug/kg)
b
Thymus
Spleen
LN
Percent Reconstitution
200
100
0
0
1
2
3
4
5
6
7
8
Days post-depletion
c
Day 13
Day 17
K8/GFP
K8/GFP

any additional benefit. Thus, for future experiments and for longitudinal disease studies, we believe 25ug/kg is an appropriate dose for complete depletion of mTECs and eTACs in the *AireDTR* mouse.

The kinetics of mTEC and eTAC regeneration after complete depletion were also studied to determine the required frequency of dosing. Mice were dosed for two consecutive days and then analyzed consecutively by FACS for GFP-expressing mTECs and eTACs. Surprisingly, mTEC recovery in the thymus was extremely rapid, with restoration of near-normal numbers of GFP+ cells by day three post-depletion, and an "overshoot" excess of cells at day five that normalized by day seven (**Fig. 4.3b**). These results are generally consistent with, though slightly more rapid than, the recovery seen in cyclophosphamide-induced Aire+ mTEC depletion *(8)*. In the spleen and lymph nodes, eTAC recovery was much more gradual, and even by seven days post-depletion we observed only partial restoration of GFP signal (**Fig. 4.3b**). These results indicate that frequent dosing may be required to achieve continuous depletion of mTECs, while eTACs ablation might be maintained by more widely spaced dose intervals. Furthermore, they suggest that *Aire*-expressing mTECs repopulate the thymus more quickly than eTACs do in the periphery. It will be of interest to determine whether this difference reflects simply the higher levels of *Aire* (and thus transgene) expression in mTECs, or perhaps suggests something about either the rate of division and differentiation, or even the anatomic location, of the progenitor cells for each population.

Finally, serial treatment of *AireDTR* mice was undertaken to determine the maximum treatment duration before the development of functional anti-DT blocking serum antibodies. Because of the rapid recovery of GFP+ mTECs, we used immunofluorescent thymic GFP signal as a readout for loss of DT efficacy. Mice were treated continuously at 50ug/kg on alternating days, and thymic GFP expression remained completely undetectable for up to thirteen days. However by day 17, we observed the re-emergence of some GFP+ cells in cytokeratin(K8)-negative regions (**Fig. 4.3c**), suggesting that the effective treatment window for complete ablation in adult mice at this dosage may be approximately two weeks. The calculation of this effective window should likely be repeated, however, in part because lower dosing (25ug/kg) may alter the development of resistance. Furthermore, there is some controversy over the degree to which serum anti-DT antibodies are reported to interfere with DT function *(9)*. Together these results indicate that complete ablation of *Aire*-expressing cells in *AireDTR* mice requires frequent dosing at 25ug/kg, which can effectively deplete these populations for a window of approximately two weeks. To extend this effective window in future experiments we may also consider using IgH-knockout mouse strains or bone marrow or antibody-mediated B cell depletion.

Unique thymic structural phenotype observed after prolonged depletion of Aire+ mTEC

In addition to the expected loss of GFP+ *Aire*-expressing mTECs, the continuous DT-treatment of *AireDTR* mice led to an unexpected thymic structural phenotype.

Cytokeratin 5 (K5) and cytokeratin 8 (K8) normally demarcate medullary and cortical thymic epithelial regions, respectively (**Fig. 4.4a**), and we therefore used these markers while monitoring re-emergence of GFP expression in DT-treated thymi to ensure that we were indeed examining medullary regions in each section. While K5/GFP staining in *AireDTR* thymi DT-treated for just one day showed an essentially normal thymic architecture with an absence of GFP+ cells, *AireDTR* thymi treated for nine days had a distinctly altered cytokeratin distribution, with a nearly complete absence of cytokeratin 5-positive cells (or any cytokeratin-positive cells) in the putative medullary regions (**Fig. 4.4a**). These large medullary "holes," essentially devoid of epithelium, were nevertheless filled with thymocytes, and indeed remained enriched for CD11c+ DCs, suggesting that they retained some medullary characteristics (**Fig. 4.4b**). Indeed those few K5-expressing cells remaining after prolonged DT treatment appeared to cluster in subcapsular regions at the outer edge of the medulla, an atypical site for K5 expression.

FACS analysis confirmed that prolonged treatment of *AireDTR* mice for nine days led to significant depletion of UEA-1+ Ly51-negative cells, general markers of medullary epithelium (**Fig. 4.4c**). Together these results suggest that prolonged treatment of *AireDTR* mice with diphtheria toxin leads to the near-complete absence of thymic medullary epithelium. Given that *Aire* is only thought to be expressed in ~30-40% of mTECs *(7, 10, 11)*, and furthermore only in terminally differentiated, putatively postmitotic mTECs *(10)*, it was a surprise to observe such complete medullary epithelial depletion after a modest period of DT treatment. This absence of medullary epithelium

Figure 4.4. Continuous depletion of *Aire*-expressing cells in the thymus induces complete loss of medullary epithelium and architecture. (**a**) Immunofluorescent staining of thymi from indicated mice for cytokeratin 5 (K5; red) and cytokeratin 8 (K8; green). (**b**) Immunofluorescent staining of thymi from indicated mice for K5 (red, top panels), K8 (green, top panels) and of serial sections for CD11c (red, bottom panels) and CD4 (blue, bottom panels). (**c**) Representative flow cytometric analysis of indicated thymi, pre-gated as FSC/SSC, CD45-low, and DAPI-negative, and stained for the epithelial antigen EpCAM and with a medullary epithelilum-specific agglutinin UEA-1. Numbers indicate percent of parent.

Figure 4.4

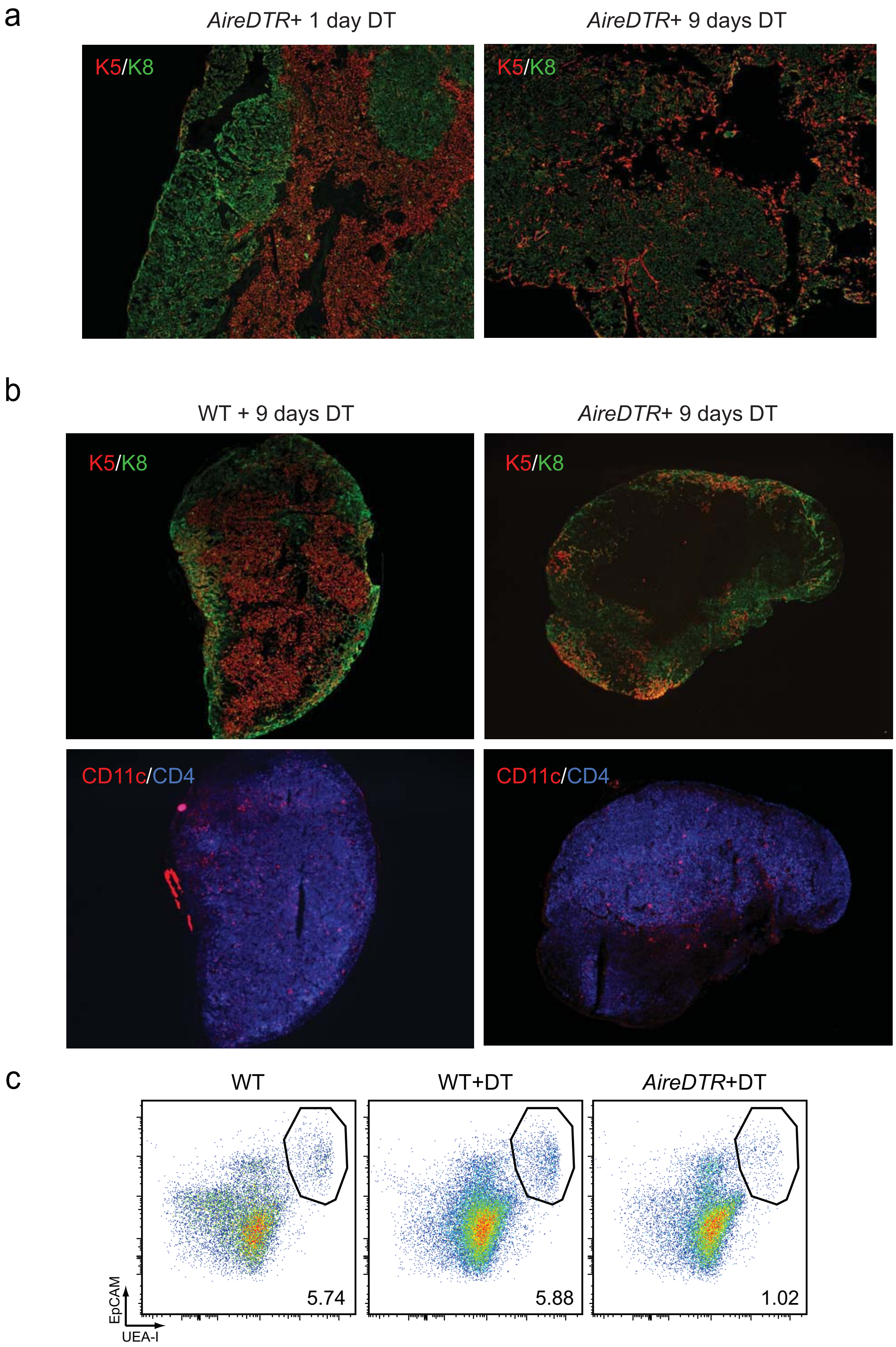
a
AireDTR+ 1 day DT
AireDTR+ 9 days DT
K5/K8
K5/K8
b
WT + 9 days DT
AireDTR+ 9 days DT
K5/K8
K5/K8
CD11c/CD4
CD11c/CD4
c
WT
WT+DT
AireDTR+DT
5.74
5.88
1.02
EpCAM
UEA-I

led us to question whether such architectural changes also had an impact on thymocyte maturation.

Thymocyte profile in "amedullary" *AireDTR* thymi is globally intact, with reduced percentages of FoxP3+ cells

The near-complete absence of medullary epithelium in *AireDTR* mice treated for nine days with DT led us to believe that thymocyte maturation might be impacted in these mice. Despite these massive architectural changes, however, to our surprise the global distribution of single-positive and double-positive CD4+ and CD8+ T cells was indistinguishable between wildtype and *AireDTR* mice treated with PBS or DT for this same period (**Fig. 4.5a**). Likewise, progression of thymocytes through the DN1-DN4 stages appeared unaltered (data not shown), although being a primarily cortical phenomenon *(12)*, this is perhaps expected. Despite these global similarities, thymocyte development in DT-treated *AireDTR* thymi was notably distinct from controls in that the percent of FoxP3+ regulatory T cells among single-positive CD4+ T cells was decreased (**Fig. 4.5b**). Consistent with this, the percentage of CD25+ cells among CD4 single-positive cells was also decreased (**Fig. 4.5b**). These data suggest that the absence of medullary epithelium may lead to a relative deficiency in thymic Treg frequency. Multiple factors could of course influence these ratios, including failure of Treg development, increased Treg death or egress, or increased retention, development, or proliferation of non-regulatory single-positive CD4 T cells. However given the existing evidence

Figure 4.5. Thymocyte profile is globally normal in “amedullary” *AireDTR* thymi, but shows decreased CD4+ Tregs. (**a**) Flow cytometric analysis of thymocytes from indicated mice stained for CD4 and CD8; treated mice had been treated continuously every other day for 9 days with 50ug/kg DT. Top and bottom rows are duplicate mice in each group. (**b**) Flow cytometric analysis of thymocytes in (a), pregated on CD4+, CD8- T cells and stained for FoxP3 (top) or CD25/CD44 (bottom). Numbers indicate percent of parent.

Figure 4.5

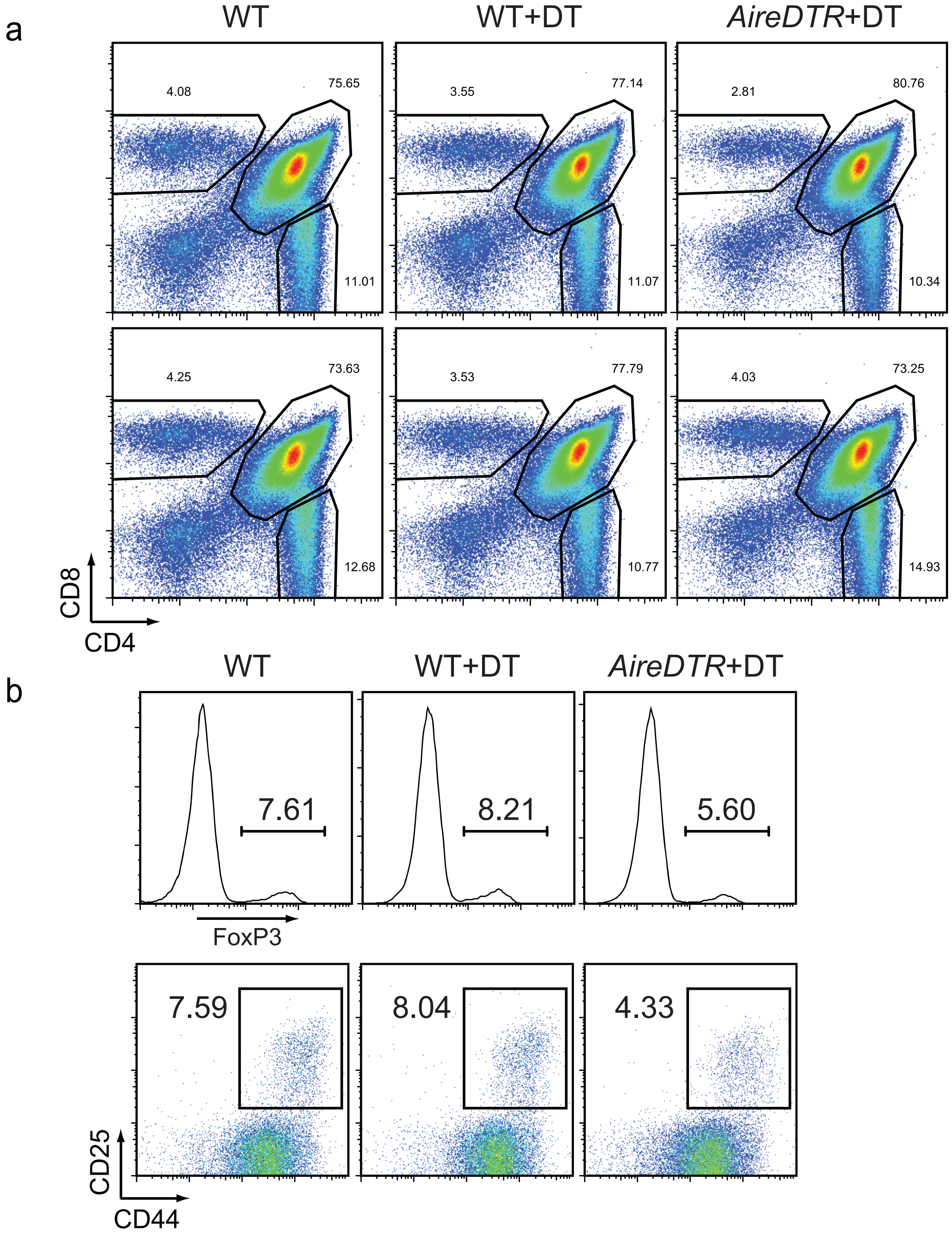
a
WT
WT+DT
AireDTR+DT
4.08
75.65
11.01
3.55
77.14
11.07
2.81
80.76
10.34
4.25
73.63
12.68
3.53
77.79
10.77
4.03
73.25
14.93
CD8
CD4
b
WT
WT+DT
AireDTR+DT
7.61
8.21
5.60
FoxP3
7.59
8.04
4.33
CD25
CD44

suggesting that self-antigen expression in *Aire*-expressing mTECs promotes Treg development *(13)*, it is conceivable that the complete lack of mTECs directly impedes Treg development. Further, because we have observed this phenomenon after only a short period of mTEC absence, it is possible that the phenotype will be more exaggerated after prolonged absence of these populations. With proper validation, we believe this system could serve as the first functional model to study thymocyte development in the absence of mTECs.

Treatment of *AireDTR* cohorts: preliminary data

We next investigated whether continuous treatment of *AireDTR* mice would predispose to autoimmunity. Because DT resistance appears to develop after approximately two weeks of treatment, because of the nonspecific DT toxicity, and because of the data suggesting that Aire's most significant role may be in the perinatal and neonatal time period *(14)*, we attempted to treat an initial litter of *AireDTR*+ and *AireDTR*- mice every other day from birth to weaning (day 21). However despite reports suggesting that this higher dosing (50ug/kg every other day) was tolerable in neonates *(2)*, this entire cohort rapidly lost weight after ~10 days regardless of genotype, and was euthanized by day 18 (data not shown). We then treated a second cohort of mice beginning at day 7 and continuing through day 21 with the same regimen, and these mice survived the treatment, although weight gain was uniformly and measurably retarded until treatment was discontinued (**Fig. 4.6a, arrows**).

Figure 4.6. *AireDTR* NOD mice treated with DT from weeks 1-3 do not show growth retardation or mortality but are predisposed to autoimmunity. (**a**) Mean weight values for cohorts of wildtype (blue) and *AireDTR* (red) mice treated as described. Arrows indicate the start and end of the treatment window. (**b**) Flow cytometric analysis of peripheral lymphocytes from the cohorts described in (a), pre-gated as lymphocytes (FSC/SSC) and CD4+, and stained for CD44 and CD62L (top) or CD4/FoxP3 (bottom). Numbers indicate percent of parent; bar graphs show mean and SD values for the entire cohort. (**c**) Hematoxylin and eosin-stained lacrimal glands from indicated mice and collected scores from the entire cohort assigned values 0-4 by trained and blinded observer.

Figure 4.6

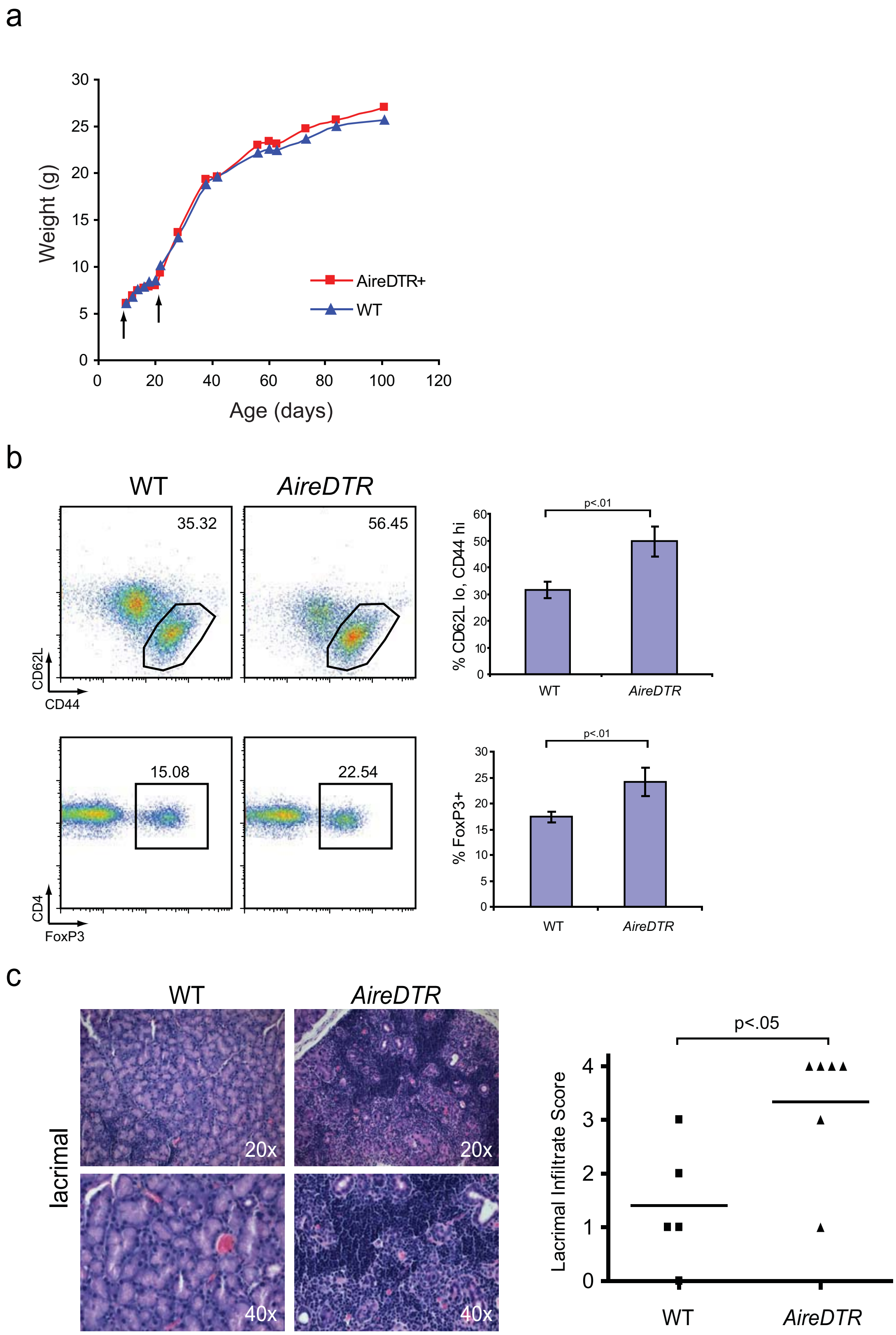
a
30
25
20
15
10
5
0
Weight (g)
0
20
40
60
80
100
120
Age (days)
AireDTR+
WT
b
WT
AireDTR
35.32
56.45
CD62L
CD44
p<.01
60
50
40
30
20
10
0
% CD62L lo, CD44 hi
WT
AireDTR
15.08
22.54
CD4
FoxP3
p<.01
30
25
20
15
10
5
0
% FoxP3+
WT
AireDTR
c
WT
AireDTR
lacrimal
20x
20x
40x
40x
p<.05
4
3
2
1
0
Lacrimal Infiltrate Score
WT
AireDTR

Treated wildtype and *AireDTR* mice remained indistinguishable with regard to weight gain even when aged to >100 days (**Fig. 4.6a**), but organs were harvested from these mice at 13 weeks, and lymphocytes stained for activation markers and for FoxP3 expression. Surprisingly, *AireDTR*+ mice uniformly showed elevation in the percentages of activated CD62L-low, CD44-high cells among total CD4+ populations, and also showed elevation in the percentage of FoxP3+ cells among CD4s (**Fig. 4.6b**). This suggested that perhaps these mice were experiencing some underlying autoimmunity not manifesting in weight loss or overall mortality. We did, however, notice erythematous inflammation around the eye of one *AireDTR* mouse. Consistent with this, preliminary examination of tissue histology confirmed that the *AireDTR* mice in this cohort experience significant lymphocytic infiltration and destruction of the lacrimal glands (**Fig. 4.6c**). Other organ histology has been unremarkable to date, but while the full range of tissue damage in this model is not yet clear, we will eagerly anticipate further phenotyping of the nature and spectrum of potential autoimmunity in these mice. Taken together, we believe these very preliminary findings suggest the *AireDTR* mouse may serve as a novel and informative model of autoimmunity, and may shed light on the contribution of both mTECs and eTACs to the maintenance of self-tolerance.

Discussion

Here we have described the development and initial validation of the *AireDTR* mouse, and while this work is still preliminary, we hope this tool will be useful in a broad range of future immunologic inquiry. Transgene expression in the *AireDTR* mouse appears to faithfully recapitulate *Aire* expression in mTECs and eTACs, and administration of DT leads to rapid and complete depletion of both populations.

In addition to the expected depletion of *Aire*-expressing mTECs, we were surprised to discover that prolonged DT treatment led to the complete loss of thymic medullary epithelium and a broad disorganization of thymic architecture. A wide range of possibilities could account for this phenomenon, some of which could be artifactual, while others might have significant implications for our understanding of mTEC development and biology. First, it is possible that this phenomenon is simply an artifact of the system. The synchronized death of 30-40% of the mTEC population in an adult thymus may interrupt thymic architecture, as mTECs interact with one another in a three-dimensional network that might be significantly interrupted by such absences. Similarly, the high local concentration of dying cells after DT treatment may be toxic to neighboring mTECs, causing bystander toxicity (though this seems less likely given that Aire expression itself may induce apoptosis in mTECs *(10)*, and moreover given the abundant thymocyte cell death normally occurring in the medulla). A related possibility is that Aire-negative mTECs may acquire functional DTR from dying Aire-positive mTECs, and thus acquire DT-sensitivity for the next treatment. In support of this, autophagy has been shown to play a significant role in mTEC biology *(15)*, but it is unclear that such a mechanism would be able to account for such a rapid and complete depletion of all mTECs, or that DTR acquired through autophagy would retain functionality. Likewise, the iterative depletion of *Aire*-expressing mTECs could also gradually eliminate all mTECs simply by depleting the precursor pool through repeated rounds of deletion and repopulation. For example, if loss of *Aire*-expressing mTECs induces transit-amplifying precursors to rapidly and repeatedly differentiate into *Aire*-expressing cells, and then these cells themselves are killed, this situation could eventually deplete earlier and earlier stages of mTECs. A more interesting possibility is that *Aire*-expressing mTECs may play some instructive role in organizing and specifying medullary epithelial differentiation or localization, either by direct cell-cell contact or by local secretion of organizing or trophic factors. Finally, it remains possible that *Aire* expression is not in fact a hallmark of terminally differentiated mTECs, but identifies a precursor population whose loss leads to the depletion of Aire-negative daughter mTECs. While it is beyond the scope of this chapter to fully pursue and distinguish such lines of inquiry into mTEC development, we believe these are interesting and important questions, and believe that a number of these possibilities might be readily differentiated through experiments ranging from description of the fundamental kinetics and phenotyping of mTEC populations that recover after DT withdrawal (and their relationship to Aire-reporter expression), to attempts at rescue by mixed reaggregate fetal thymic organ culture (RFTOC). The proper characterization of these phenomena could shed significant light on medullary epithelial development and its relationship to *Aire* expression, and we eagerly anticipate these developments.

These results also suggest that DT-treated *AireDTR* mice can progress to develop autoimmunity. However the nature of this autoimmunity, both in terms of its extent and its pathogenesis, remains obscure. "Amedullary" *AireDTR* thymi have a relative deficiency of CD25+ FoxP3+ regulatory T cells, indicating that in the absence of mTECs these regulatory populations may fail to develop properly. Further, the treatment of *AireDTR* mice from weeks 1-3 appears to predispose to autoimmunity, as revealed through increased peripheral lymphocyte activation (CD44hi, CD62Llow) and an increased frequency of regulatory T cells among CD4+ T cells. This is further supported by the preliminary finding that *AireDTR* mice display increased lymphocytic infiltration and destruction of the lacrimal glands, indicating that the loss of *Aire*-expressing cells directly or indirectly predisposes to autoimmunity. Moving forward, TCR-transgenic systems specific for Aire-regulated and non-regulated thymic antigens should be of significant future value in dissecting the impact of loss of mTECs on thymocyte selection. The use of Rag-GFP reporter mice might also be useful for future thymocyte selection experiments to identify and track recent thymic emigrants after mTEC ablation, particularly when combined with such TCR-transgenic systems.

While this novel mouse model clearly presents manifold tantalizing future directions for experimentation, we are specifically interested in examining the role of eTACs in normal immune homeostasis. The *AireDTR* transgene is currently being crossed to the NOD FoxN1-deficient ("Nude") mouse strain, which fail to develop endogenous thymi that can support T cell maturation. As we refine the autoimmune phenotype observed in DT-treated *AireDTR* mice, it will be useful to map this phenotype to specific *Aire*-expressing populations. Reciprocal transplantation of wildtype or *AireDTR*+ thymi into wildtype Nude or *AireDTR*+ Nude recipient mice will allow us to selectively deplete mTECs, eTACs, or both in selected mice. Similarly, thymectomy and simultaneous reciprocal thymic transplantation between wildtype and *AireDTR* mice is being employed to achieve similar results. As a technical note, in the latter experiment it will likely be useful after thymectomy and thymic transplantation to lethally irradiate and reconstitute these mice, and to DT-deplete during reconstitution, as a requirement for systemic Aire in adult mice can be revealed by irradiation-induced lymphopenia *(14)*. If prolonged DT depletion is required in this setting, it may also help to reconstitute these mice with IgH-/- bone marrow in place of wildtype. Finally, as we have not ruled out the possibility that eTACs are a radioresistant but hematopoietic population, reciprocal bone marrow chimeras could also be useful in such mapping studies. Given that DT-treated *AireDTR* mice develop a predisposition to autoimmunity, it will now be of interest both to try and extend treatment to exaggerate this phenotype, and to map this phenotype to specific populations of *Aire*-expressing cells.

Finally, the *AireDTR* mouse may provide a valuable tool for studying eTAC-mediated TSA expression and T-cell tolerance to such endogenous antigens. Recent evidence has suggested that a number of TCR-transgenic T cell lines become tolerized to self in the secondary lymphoid organs (*(16, 17)*, N. Wada, personal communication). While eTACs are a potential source of such tolerance induction, this has not yet been demonstrated and it remains possible that other populations are the source of these antigens. For those cognate antigens whose expression is detectable in eTACs, however, the *AireDTR* mouse may allow us to test whether tissue-specific self-antigen expression in the secondary lymphoid organs is dependent on the presence of eTACs, and moreover whether this population is necessary to maintain peripheral tolerance to such antigens.

Speculation regarding future research directions for this system could, of course, continue indefinitely. We are hopeful that the development and validation of this mouse as a model for mTEC and eTAC development, thymic selection, tissue-specific antigen-expression, and immune tolerance will afford significant future insight into immune homeostasis.

Methods

Transgene construction, BAC recombineering, and purification

Aire-driven Diphtheria Toxin Receptor-EGFP *(AireDTR)* transgenic mice were generated by standard cloning methods using a bacterial artificial chromosome (BAC) recombineering and transgenesis strategy. Briefly, the DTR-EGFP sequence was amplified from the pCD11c-DTR-EGFP vector using the primers 5'-TTAATTAAGGGACCATGAAGCTGCTGCCGT-3' and 5'-CGCGGCCGCTTTACTTGTA-3'. This PCR products was sub-cloned into pCR-Blunt II TOPO vectors (Invitrogen), sequenced, then digested with PacI and NotI and inserted into pAireFNF.

This targeting construct, pAireFNF-DTR-EGFP, was then inserted via standard recombineering *(18)* into a BAC clone from the Children's Hospital of Oakland Research Institute (CHORI) BACPAC Resource Center, clone 461e7 from the RPCI 23 Mouse BAC Library, as described in the previous chapter.

Highly purified Ii-BDC-Aire BAC DNA was carefully prepared as described in the previous chapter and evaluated for integrity by KpnI digestion and gel electrophoresis. Resuspended BAC DNA was injected into fertilized NOD oocytes by the UCSF Mouse Transgenic Core with the assistance of H. Lu and N. Killeen.

Mice and genotyping

AireDTR transgenic NOD mice were screened by real-time PCR using the primers 5'-CTGCTGCCCGACAACCA-3' and 5'-TGTGATCGCGCTTCTCGTT-3' and the probe Cy5-TACCTGAGCACCCAGTCCGCCCT-BHQ along with an endogenous control reaction for CD86 using the primers 5'-CTTGATAGTGTGAATGCCAAGTACCT-3' and 5'-TGATCTGAACATTGTGAAGTCGTAGA-3' and the probe FAM-CCGCACGAGCTTTGACAGGAACAACT-TAMRA. This same reaction was used to genotype *Adig* and *Adbig* mice, as it detects genomic GFP present in both transgenes. The *AireDTR* transgene was maintained in heterozygosity for all experiments.

Preparation of stroma and lymphocytes for flow cytometry

Preparation of lymphocytes and stroma, antibody staining, and flow cytometry were performed as described *(7)*. FACS data was acquired on LSR II and FACSCalibur flow cytometers (BD), and data was analyzed using FloJo 7.2.4 (TreeStar).

DT-Mediated Depletion of mTECs and eTACs

Depletion of *Aire*-expressing cells in *AireDTR* mice was achieved by intraperitoneal injection of diphtheria toxin (Sigma) at the doses indicated in each experiment (25-50ug/kg in PBS). Mice were monitored by weight during administration and were sacked or treatment was discontinued if they experienced significant weight loss.

Statistical Analysis

Statistical analysis of data was performed with Excel 2003 (Microsoft) and Prism 4.0 (GraphPad). Statistical comparisons were made using a Student's two-tailed T-test, and results with $p<0.05$ were considered statistically significant.

Histology, immunofluorescent staining and quantitation

All primary and secondary antibodies for histology were purchased from AbCam, BD Pharmingen, Invitrogen, Jackson, or eBioscience, with the exception of the anti-AIRE antibodies 5C-11 and 5H-12, which were gifts of H. Scott. For *AireDTR* mice, organs were harvested from experimental animals and embedded in Tissue-Tek Optimal Cutting Temperature (OCT) media (Fisher), then processed as described *(7)*. Slides were mounted in Vectashield mounting medium (Vector Laboratories) and visualized with an SP2-AOBS Confocal Microscope (Leica). Images were acquired using Leica Confocal Software (Leica), and analyzed and merged in Photoshop CS3 (Adobe). Linear contrast adjustment was applied equally to all samples and controls. For hematoxylin and eosin staining of pancreatic sections, tissues were fixed as described in Chapter III. Tissue infiltrate scores were assigned by a trained and blinded observer.

References

1. Bennett CL, Clausen BE. DC ablation in mice: promises, pitfalls, and challenges. Trends Immunol 2007;28:525-31.
2. Kim JM, Rasmussen JP, Rudensky AY. Regulatory T cells prevent catastrophic autoimmunity throughout the lifespan of mice. Nat Immunol 2007;8:191-7.
3. Stoneman V, Braganza D, Figg N, et al. Monocyte/macrophage suppression in CD11b diphtheria toxin receptor transgenic mice differentially affects atherogenesis and established plaques. Circ Res 2007;100:884-93.
4. Jung S, Unutmaz D, Wong P, et al. In vivo depletion of CD11c(+) dendritic cells abrogates priming of CD8(+) T cells by exogenous cell-associated antigens. Immunity 2002;17:211-20.
5. Kissenpfennig A, Henri S, Dubois B, et al. Dynamics and function of Langerhans cells in vivo: dermal dendritic cells colonize lymph node areas distinct from slower migrating Langerhans cells. Immunity 2005;22:643-54.
6. Yu W, Misulovin Z, Suh H, et al. Coordinate regulation of RAG1 and RAG2 by cell type-specific DNA elements 5' of RAG2. Science 1999;285:1080-4.
7. Gardner JM, Devoss JJ, Friedman RS, et al. Deletional tolerance mediated by extrathymic Aire-expressing cells. Science 2008;321:843-7.

8. Fletcher AL, Lowen TE, Sakkal S, et al. Ablation and regeneration of tolerance-inducing medullary thymic epithelial cells after cyclosporine, cyclophosphamide, and dexamethasone treatment. J Immunol 2009;183:823-31.
9. Buch T, Heppner FL, Tertilt C, et al. A Cre-inducible diphtheria toxin receptor mediates cell lineage ablation after toxin administration. Nat Methods 2005;2:419-26.
10. Gray D, Abramson J, Benoist C, Mathis D. Proliferative arrest and rapid turnover of thymic epithelial cells expressing Aire. J Exp Med 2007;204:2521-8.
11. Hubert FX, Kinkel SA, Webster KE, et al. A specific anti-Aire antibody reveals aire expression is restricted to medullary thymic epithelial cells and not expressed in periphery. J Immunol 2008;180:3824-32.
12. Takahama Y. Journey through the thymus: stromal guides for T-cell development and selection. Nat Rev Immunol 2006;6:127-35.
13. Aschenbrenner K, D'Cruz LM, Vollmann EH, et al. Selection of Foxp3+ regulatory T cells specific for self antigen expressed and presented by Aire+ medullary thymic epithelial cells. Nat Immunol 2007;8:351-8.
14. Guerau-de-Arellano M, Martinic M, Benoist C, Mathis D. Neonatal tolerance revisited: a perinatal window for Aire control of autoimmunity. J Exp Med 2009;206:1245-52.
15. Nedjic J, Aichinger M, Emmerich J, Mizushima N, Klein L. Autophagy in thymic epithelium shapes the T-cell repertoire and is essential for tolerance. Nature 2008;455:396-400.
16. Nichols LA, Chen Y, Colella TA, Bennett CL, Clausen BE, Engelhard VH. Deletional self-tolerance to a melanocyte/melanoma antigen derived from tyrosinase is mediated by a radio-resistant cell in peripheral and mesenteric lymph nodes. J Immunol 2007;179:993-1003.
17. Lee JW, Epardaud M, Sun J, et al. Peripheral antigen display by lymph node stroma promotes T cell tolerance to intestinal self. Nat Immunol 2007;8:181-90.
18. Lee EC, Yu D, Martinez de Velasco J, et al. A highly efficient Escherichia coli-based chromosome engineering system adapted for recombinogenic targeting and subcloning of BAC DNA. Genomics 2001;73:56-65.

Chapter V

Discussion

The maintenance of self-tolerance in the adaptive immune system requires the coordination of multiple overlapping mechanisms to prevent the escape and activation of autoreactive clones. While the notion of selective immune education as a component of self-tolerance is as old as clonal selection theory *(1)* the paradigm that centralized sites of T-cell education might be specifically engineered to express the diversity of an organism's entire transcriptome, and that such broad self-expression might be essential to the prevention of autoimmunity, is much more recent. Lines of evidence ranging from tissue-specific promoter expression studies *(2, 3)* to TCR-transgenic deletion data *(4, 5)* to real-time PCR analysis *(6)* had suggested for some time that the thymus was a site of immunologically relevant TSA expression, but the *Aire*-knockout mouse codified for the first time this idea that deficiencies of such thymic TSA expression could be directly linked to autoimmunity in both mice and humans *(7-9)*.

In this context, it is tempting to draw parallels with recent reports describing TSA expression in the secondary lymphoid organs. Preliminary studies employing tissue-specific antigen reporters *(10)*, TCR-transgenic systems *(11)*, and RT-PCR data *(12)* have now begun to suggest that TSA expression may also be a hallmark of the secondary lymphoid system. Likewise, *Aire* expression has been reported outside the thymus *(8, 10, 13)*, although the populations involved, the presence and role of Aire in these cells, and their potential function has remained unclear.

Here we have identified a population of extrathymic *Aire*-expressing cells in the secondary lymphoid organs. We have demonstrated that such cells express Aire and a host of Aire-regulated TSAs, and can interact with both CD4+ and CD8+ T cells. Further, we have shown that eTAC-T cell interactions lead to T-cell tolerance and prevent T cell-mediated autoimmunity, and that such antigen-expressing eTACs are uniquely resistant to conversion from tolerance to immunogenicity. Finally, we have recently developed a novel *AireDTR* mouse model which may help define the role of eTACs (and mTECs) in the normal maintenance of immunologic tolerance. In this discussion we will briefly summarize the findings described in the previous chapters, and then discuss some of the implications and complications of this work, as well as suggest future directions for this research.

eTACs exist in the secondary lymphoid organs and express diverse TSAs

In chapter two, we described the identification of extrathymic *Aire*-expressing cells (eTACs) that definitively express both *Aire* transcript and Aire protein, and found that as in the thymus, Aire protein in these cells was detected in characteristic nuclear speckles. By surface marker phenotyping this population appears broadly homogeneous, and shares some similarity with mTECs (MHCII-hi, CD45-low-intermediate, EpCAM+) but also some differences (absence of CD80, CD86 and presence of ICOS-L on eTACs). eTACs also appear to be distinct from other APCs like B cells (B220-negative), dendritic cells (CD11c-negative) , macrophages (CD11b-negative, F4/80 negative; data not shown), or from stromal populations like FRCs (gp38-negative) or FDCs (CD35-negative, FDC-

M2-negative; data not shown). This population is also radioresistant, though this does not preclude it being hematopoietic in origin as we will discuss.

Microarray analysis reveals that eTACs express a number of genes characteristic of antigen-presenting cells, and sorting eTACs from *Aire*-wildtype and -knockout animals identified a role for Aire in regulating gene expression in these cells. As in mTECs, the set of Aire-regulated genes in eTACs appeared significantly enriched for TSAs, though surprisingly this set of Aire-regulated TSAs in eTACs was unique from those seen in mTECs. Finally, the transgenic expression of a pancreas-specific autoantigen, IGRP, in eTACs allowed us to examine interaction of eTACs with autoreactive IGRP-specific CD8+ TCR-transgenic T cells, which engaged in immediate and prolonged contact with eTACs, causing T-cell proliferation followed by deletion.

These results suggested that eTACs were a distinct population of *Aire*-expressing cells capable of expressing a diverse repertoire of self-antigens, and that naïve autoreactive CD8+ T cells encountering such self antigen-expressing eTACs might be induced to die after aberrant activation. Despite these results, we wondered whether such self-antigen expression in eTACs would be sufficient to directly prevent autoimmunity. Further, we questioned whether such aberrant T cell activation was a distinct feature of eTACs per se or would be observed if the same antigen were expressed in any cell, and whether eTACs, expressing high levels of MHC II, could also interact with CD4+ T cells like other professional APCs. Thus we examined the ability of self antigen-expressing eTACs to directly prevent autoimmune disease mediated by both CD4+ and CD8+ T cells.

eTAC interactions with T cells are tolerogenic and prevent autoimmunity

To directly study eTAC-CD4+ interactions we generated transgenic *Adbig* mice expressing p31, a mimetope antigen for the BDC2.5 pancreas-specific CD4+ TCR-transgenic T cell, under transcriptional control of the *Aire* promoter. As in the eTAC-CD8+ system we observed direct interaction between eTACs and BDC2.5 CD4+ T cells which persisted even when mice were irradiated and reconstituted with MHCII-/- bone marrow. This interaction caused similarly rapid and antigen-specific proliferation, but unlike eTAC-CD8+ interactions, eTAC-BDC2.5 interaction led to the persistence of significant residual CD4+ T cell populations. These residual T cells were functionally unresponsive to secondary immunization, and were also enriched for FoxP3-expressing T cells. Importantly, this interaction also led to protection from BDC2.5-mediated adoptive transfer of diabetes in SCID mice.

Serial cotransfer experiments revealed that the tolerance induced among BDC2.5 T cells was stable and did not require continuous eTAC interaction or the presence of regulatory T cells, suggesting that functional inactivation of effectors may be a primary mechanism. Efforts to break this disease protection through perturbations known to convert other characterized peripheral tolerance mechanisms to immunogenicity (lymphopenia, CD40/TLR stimulus, PD-L1 blockade) were unsuccessful. This tolerance induction also appeared to be a cell type-specific function of eTACs, as antibody-mediated targeting of a BDC2.5 mimetope peptide to an independent APC population, DEC205+ DCs, resulted in similar T-cell proliferation in all secondary lymphoid organs but failed to induce T cell-unresponsiveness or prevent BDC2.5-mediated autoimmunity, and if anything seemed to prime these responses. Finally, returning to examine eTAC-CD8+ interactions in the *Adig* mouse, we found that IGRP-expressing eTACs induced deletion of endogenously developing 8.3 T cells, and that these interactions prevented 8.3-mediated diabetes. Together these results suggest that self-antigen expression in eTAC induces robust tolerance in both CD4+ and CD8+ T cells.

The *AireDTR* mouse: a tool for the study of immune tolerance

To help define the role of eTACs and mTECs in the immune system, we recently generated a novel *AireDTR* mouse which allows us to selectively deplete these populations by administration of diphtheria toxin (DT). Validation suggested that the transgene permits effective and specific depletion of these populations, though the window of depletion may be limited by nonspecific DT toxicity and by the development of anti-DT antibodies. Interestingly, prolonged depletion of *Aire*-expressing mTECs leads to a nearly complete absence of thymic medullary epithelium and a disruption of thymic architecture, along with a relative deficiency of FoxP3+ regulatory cells. Treatment of young *AireDTR* mice from weeks 1-3 of age also leads to a mild autoimmune phenotype still being characterized which includes increased lymphocyte activation and regulatory cell numbers, as well as lymphocytic infiltration and destruction of the lacrimal glands. These results suggest that the loss of *Aire*-expressing cells predisposes to autoimmunity, and it will be of significant future interest to define and expand this phenotype.

The apparent ablation of all mTECs in continuously treated DT-treated thymi could be instructive to rigorously define the stages of mTEC development (after DT treatment is stopped and these cells repopulate the medulla) and gain insight into the role that *Aire*-expressing mTECs play relative to the general medullary epithelium. Additionally, because these "amedullary" mice appear to exhibit a relative defect in FoxP3+ Treg development, this model could provide significant insight into the role of CD4+/mTEC interaction in this process. Finally, we believe it will be helpful to expand and define the nature of autoimmunity in these mice by treating younger mice and for longer periods of time with the properly titrated (25ug/kg) dosing. Given that we observed uniform T-cell activation and autoimmune destruction of at least one organ system after ablating from weeks 1-3, we expect that longer dosing might yield a more pronounced phenotype.

With regard to eTAC function, we are currently using both Nude (FoxN1-/-) and thymectomy/thymic transplant approaches to generate mice that selectively express the AireDTR construct only in mTECs or eTACs. Lethal irradiation and reconstitution of these mice with either wildtype, IgH-/- (if longer treatment is desired), or AireDTR (if depletion of hematopoietic cells is desired) bone marrow will allow us to map this autoimmune phenotype to specific compartments, and may also exaggerate the autoimmunity as such radiation-induced lymphopenia has been shown to reveal Aire-sensitivity in adult mice *(14)*. Finally, we hope to combine this *AireDTR* system with an appropriate TSA-specific TCR-transgenic model that undergoes negative selection in the secondary lymphoid organs, to determine whether eTACs play a role in this process. One such candidate system using T cells specific for desmoglein 3 (the autoantigen in pemphigus vulgaris, *(15)*) is currently being investigated for these purposes.

The mechanism of eTAC-mediated T-cell tolerance

While eTAC interaction appears to induce tolerance in both CD4+ and CD8+ T cells in this system, it remains unclear whether the same mechanism applies to both cell populations. One primary difference is the outcome of eTAC encounter for the T cell. Whereas CD8+ T cells appear to be largely deleted by two weeks post-transfer, significant residual populations of CD4+ T cells remain that are either functionally inactive or FoxP3+ regulatory T cells. This divergence may reflect the nature of CD4+ and CD8+ T cells themselves, the differential affinities for their relative ligands, or something fundamental about the nature of the signals delivered to CD4+ versus CD8+ T cells during eTAC interaction.

Another notable difference between these two cell types after eTAC encounter is the effect on CD90 expression. Unlike 8.3 CD8+ T cells, eTAC-experienced BDC2.5 CD4+ T cells undergo significant downregulation of the congenic CD90.1 marker during proliferation. This phenomenon appears to persist even two weeks post-transfer when BDC2.5 T cells have completely diluted CFSE, although the degree of downregulation is difficult to assess as we lose the ability to track cells that may have downregulated their congenic marker to the degree that they become indistinguishable from the general lymphocyte pool. However this phenomenon appears to be eTAC-specific, as BDC2.5 proliferation in response to anti-DEC1040-loaded dendritic cells does not produce similar CD90 downregulation, despite similarly rapid proliferation. The role of CD90 remains somewhat obscure, and the immunologic phenotype of the CD90 knockout mouse has been considered mild with only slight impairment in T-cell proliferation and cytokine production *(16)*. But the fact that this phenomenon is both eTAC-specific (i.e. not observed when BDC2.5 T cells interact with DEC205+ DCs) and preferentially seen in the non-regulatory, functionally inactive effector populations (i.e. not observed to the same degree in BDC2.5 T cells undergoing proliferation that express FoxP3) suggests that it could have some functional relevance. To our knowledge, this is a novel phenotype for proliferating T cells and we are not aware of the same phenomenon observed outside the context of eTAC encounter. It may be of significant future interest to further characterize this phenomenon.

The absence of the canonical costimulatory molecules CD80 and CD86 on eTACs may also contribute to this tolerance induction. TCR ligation in the absence of costimulation has classically been associated with T-cell anergy *(17, 18)*, has been speculated to play a role in tolerance mediated by tolerogenic, immature DCs *(19)* and could therefore certainly contribute to eTAC-mediated tolerance. Although we are unable to induce CD80 upregulation on eTACs through conventional DC-stimulatory means, *in vitro* culture of sorted eTACs from *Adig* or *Adbig* mice with cognate T cells in the presence or absence of anti-CD28, followed by a secondary culture with peptide-pulsed APCs, might suggest whether provision of an artificial second signal converts this primary interaction from tolerance to activation. However one preliminary result runs counter to this hypothesis. Reasoning that if eTAC-mediated CD4+ tolerance in the *Adbig* mouse was a result of absence of costimulation, we first *in vitro* activated BDC2.5 T cells prior to transfer believing that such activated T cells would bypass such a requirement. To our surprise, despite the clear evidence for successful *in vitro* activation by cell number, size, and activation markers, and the fact that activated BDC2.5 T cells transferred accelerated disease into wildtype SCID mice (2 mice) even more rapidly than naïve BDCs (~5 days vs. ~10), *Adbig* SCID mice (2 mice) were entirely protected from disease, and histology showed that their islets remained free of infiltrate (data not shown). While this does not rule out the possibility that absence of costimulation induces tolerance in this model, it also suggests that an independent mechanism might be operating to prevent such *in vitro* activated T cells from reaching the target organ or causing disease.

Finally, the complete lack of pancreatic T-cell infiltration in *Adbig* SCID adoptive transfer recipients despite the massive mobilization of BDC2.5 T cells into the blood also suggests that there may be a defect in leukocyte vascular adhesion or trans-endothelial migration after eTAC encounter. To this end it will be interesting to determine whether eTAC-stimulated BDC2.5 T cells show differential expression of relevant adhesion molecules (e.g. PSGL-1, CD18, VLA-4, CD44) relative to control (e.g. anti-DEC1040-stimulated) BDCs, or whether they might behave differently in *in vitro* or *in vivo* capture, rolling, firm adhesion, or transmigration assays. While the mechanism of eTAC-mediated tolerance in both the CD4+ and CD8+ T cell systems remains unclear, investigation of these phenomena may provide insight into novel pathways involved in T-cell tolerance.

eTACs and Tregs

Despite the clear results indicating that FoxP3+ cells are not required for eTAC-mediated tolerance induction of BDC2.5 T cells, the relationship between eTACs and regulatory T cell development remains of significant interest. Particularly given the enrichment for FoxP3+ cells after eTAC encounter among Treg-depleted BDC2.5 T cells, and the selective lack of CD90 downregulation on these regulatory populations, such interactions may be of physiologic significance. Much work is needed, however, to define the nature of these interactions. For example, it is currently unknown whether the FoxP3+ BDC2.5 cells that emerge after eTAC interaction in the *Adbig* mouse have acquired functional suppressive ability, and whether they otherwise resemble genuine regulatory T cells. BDC2.5-FoxP3GFP mice might be employed in adoptive transfer into *Adbig* mice to track and sort these populations so that *in vitro* and *in vivo* suppressive activity could be assessed in these populations. Likewise, simple phenotypic analysis, for example GITR upregulation, CD127 downregulation, and CpG methylation of the FoxP3 promoter, which have been used to distinguish the condition and functionality of FoxP3+ regulatory T cells from associated populations *(20)*, might shed some light on whether these cells represent true regulatory T cells with suppressive activity.

It also remains unclear whether such FoxP3+ cells in this setting are induced from FoxP3-negative effector populations or represent expanded natural Treg contaminants from the original population. Despite effective CD25-pre-depletion of transferred cells (data not shown), some contaminating FoxP3+ cells are certainly cotransferred in these experiments, and could be the cells ultimately constituting this pool of residual FoxP3+ cells. A more rigorous approach would be appropriate before concluding that eTAC interaction directly promotes the peripheral development of induced Treg populations. That said, one appealing possibility for the role of a tolerogenic self-antigen expressing population like eTACs in the secondary lymphoid organs would to promote the selective survival and/or development of regulatory T cells. To this end, the *AireDTR* mouse may provide a valuable tool to characterize the role of eTACs in this process.

The role of Aire in eTACs

Our results suggest that Aire regulates a set of tissue-specific antigens in eTACs that is distinct from the set regulated in the thymus. Suggestively, this set of TSAs includes a number of autoantigens relevant in human autoimmune diseases, including Dsg1a (pemphigus foliaceus *(21)*), and Lad1 (linear IgA dermatosis *(22)*). However the functional significance of Aire in this population remains unclear. To date we have not found an appropriate model antigen/TCR transgenic system to study Aire-regulated peripheral T cell selection in eTACs in a manner similar to work done in the thymus *(23, 24)*. The future study of Aire's role in eTACs would be significantly facilitated by such model systems.

Looking more broadly at the role extrathymic Aire may play in maintaining immunologic tolerance, the significant experimental difficulty in directly evaluating the relevance of extrathymic *Aire* is the challenge of knocking it out selectively outside the thymus. In the absence of a genetic means to target one population (mTECs or eTACs) specifically, we have pursued two transplant-based approaches. The first involved backcrossing the FoxN1 mutation onto the autoimmune-prone NOD background, and then intercrossing with the Aire mutation to generate FoxN1-/- Aire -/- and FoxN1-/- Aire+/+ mice, which could receive thymic transplants. The difficulty in this approach has been purely in breeding, as neither gene will breed as a knockout, and NOD FoxN1-/- mice have not been successfully generated in significant numbers in our colony. Such an approach has clear advantages, however, and may be worth pursuing in a more directed fashion or in collaboration with a mouse colony successfully producing Nude mice.

A parallel strategy has been to attempt to achieve the same ends through thymectomy and thymic transplantation. This approach has significant drawbacks, including considerations of incomplete thymectomy and artifacts related to differences in the pre-thymectomy thymic selection environments, but the former can be partly addressed by controls and by careful technique, and the latter minimized by crossing *Aire*-knockout mice onto a T-cell deficient strain (e.g. TCRα-/-), doing thymectomy and thymic transplantation of TCRα-/- Aire+/+ and TCRα-/- Aire-/- mice, and then irradiating and chimerising these mice with wildtype (TCRα+/+) bone marrow only after thymic exchange. While we have been unable to do this experiment in any significant numbers to date, short of a genetic mechanism it may be the most successful way to directly study this phenomenon, particularly as irradiation-induced lymphopenia has been shown to reveal a requirement for functional Aire in adult mice *(14)*. Naturally, demonstration of a physiologically relevant role for extrathymic *Aire*, particularly related to the set of peripherally Aire-regulated TSAs, would be of significant interest.

The identity and origin of eTACs

While we have shown eTACs to be a distinct, radioresistant population of cells that partially resemble mTECs, the precise identity and origin of these cells remains unknown. As noted in chapter two, we have also seen evidence that some hematopoietic (or at least bone marrow-derived) cells can express these *Aire* reporter transgenes (Fig. S2.3), and it may be that eTACs are both radioresistant in nature and hematopoietic in origin. Given the existing data regarding their potential relevance in immune tolerance, it will be of real interest to more thoroughly map the ontogeny and precise identity of these cells. Reciprocal *Adig*/WT NOD bone marrow chimeras and surface marker phenotyping should be informative to determine whether transgene-expressing bone marrow-derived cells express characteristic eTAC surface proteins, and immunofluorescent staining should help determine if Aire protein can be detected in any such cells. Similarly, adoptive transfer of congenically labeled 8.3 T cells should demonstrate whether the transgene-expressing cells of bone marrow origin are able to induce deletion of cognate CD8+ T cells. Likewise, experiments in *Adbig* and *Adbig* SCID mice should demonstrate whether such hematopoietic cells can induce functional inactivation of BDC2.5 T cells and protect such mice from T-cell mediated autoimmune diabetes. Further characterization of the origin and identity of these cells will be of great interest.

Why eTACs?

More broadly, is there a place for specific TSA-expressing cell populations in the secondary lymphoid organs? On the one hand, the immune system clearly requires overlapping systems to prevent the escape and activation of autoreactive T cells. Furthermore, as the thymus involutes in early adulthood, mTEC-mediated selection presumably begins to play a less significant role in maintaining tolerance among the circulating lymphocyte pool. Thus eTACs might play a role in preventing the development or emergence of autoreactive clones that emerge later in life. Likewise, the secondary lymphoid organs are certainly sites supporting the generation of receptor diversity through B cell somatic hypermutation, and it is of course possible that eTACs play a role in preventing the emergence of autoreactive clones from this process. Indeed their selective localization to T-B boundary regions suggests that interacting with B cell-T-cell conjugation might play a relevant role in their function.

Alternatively, the unique set of Aire-regulated antigens in eTACs suggest that they may play a continuously important role throughout life, presenting a complementary version of "self" to that displayed by mTECs and eliminating those T cells that evade thymic selection for lack of antigen exposure. It is not clear, however, what the advantage of such an organization would be, and why T-cell reactivity to some antigens would be corrected during thymic development, while in other cases it would happen in the periphery. A simpler solution might seem to simply unify this process by presenting as complete a version of the peripheral self as possible in one centralized location. Conversely, it is also not clear that the secondary lymphoid organs need promiscuous gene expression to expose T cells to a diverse picture of self at all; the secondary lymphoid organs drain nearly all of the body's tissues, and many tissue-specific antigens along with them. It seems equally likely that tolerogenic antigen-draining DCs might fill this role in the secondary lymphoid organs by simply acquiring antigen in the end organs and then trafficking back to the draining lymph nodes *(25)*.

Further, even if we accept that such cells may play a contributory role in tolerance and operate by the mechanisms described here, such a mechanism of CD4+ tolerance would lead to the persistence of significant numbers of residual, functionally autoreactive CD4+ T cells after eTAC encounter. This seems to be a highly inefficient mechanism for disposing of such clones, though perhaps the induction or maintenance of regulatory

CD4+ populations contributes more significantly *in vivo*. Alternatively, however, such pools of functionally inactive but antigen-specific T cells might serve as competitive inhibitors of other autoreactive clones simply by occupying available MHC-antigen complexes and preventing functional T cells from finding similar sites for activation.

Finally, it is worth speculating on the potential hazards that this population might pose. Indeed, might not a self antigen-expressing tolerogenic population in the secondary lymphoid organs be a significant risk to the organism? On the one hand, if certain stimuli were able to convert this population from tolerance to immunogenicity, they might rapidly become a potent source for priming a diverse array of autoreactive T cells. Avoidance of such risk is at least consistent with the data suggesting that eTACs are in fact uniquely difficult to convert to immunogenicity, and indeed we been unable to do so. Conversely, however, might not such a permanently tolerogenic cell also present significant risk to host defense if such populations themselves ever became infected? If even activated T cells fail to break tolerance induced by eTACs, much less to directly attack this population, eTACs might offer a highly attractive target for infection.

Therapeutic self-antigen expression in eTACs?

The robust nature of eTAC-mediated tolerance induction, in concert with the recent report of detection of Aire protein in human secondary lymphoid organs, raises the attractive possibility that such cells might serve as appropriate therapeutic targets in the prevention of autoimmunity. One potential approach might be via identification of unique surface markers for antibody-mediated antigen targeting, similar to the approach that has been used to target antigens to DEC205+ dendritic cells *(19, 26)*. Microarray data for eTACs could be screened relative to other characterized APC populations to generate candidate eTAC-specific cell-surface markers, which could then be validated by FACS. An alternative approach would be try and generate eTAC-specific antibodies by direct immunization with eTACs, although the amounts of tissue required for such procedures are currently well beyond our capacity to isolate purified eTACs. Such antibody-mediated approaches present significant challenges including the need to target a receptor that leads to correct processing and presentation of the desired antigen, and also confirm that antibody treatment does not lead to depletion or inactivation of the target population. Regardless, such avenues might have significant future clinical promise if antibody-conjugated antigens targeted to eTACs could induce tolerance that resembled the tolerance generated by *Aire*-driven TSA expression in eTACs.

As a more speculative proof-of-principle experiment, it would also be of interest to test transgenic lymph node transplantation as a mechanism of tolerance induction. Based on the idea that eTACs are resident or long-lived constituents of the secondary lymphoid architecture, and that most lymphocytes circulate continuously throughout the secondary lymphoid system for extended periods before encountering cognate self-antigen and undergoing activation, theoretically even a single transplanted lymph node in which eTACs expressed a cognate autoantigen might be sufficient to impact autoimmunity. One simple test of this using existing mice would be to transplant *Adig* or wildtype lymph nodes (possibly pre-depleted of replicating cells via incubation in 2-deoxyguanosine) into young 8.3 mice to determine whether *Adig* lymph nodes specifically reduced the total number or tetramer-reactivity of IGRP-specific 8.3 T cells, and whether such intervention could impact diabetes incidence in this model. If successful, such lymph node transplantation might have the added benefit that tolerance induction would not require targeting to every lymph node but could even be accomplished in *ex vivo* tissue. While speculative, such antigen targeting to eTACs in single *ex vivo* lymph nodes followed by re-transplantation might be a relatively simple means of generating an "immunologic sieve."

The recent evidence that eTACs are detectable in human secondary lymphoid organs *(27)* also raises further interesting questions about their roles in disease tolerance. It would be interesting to determine, for instance, whether eTAC numbers increase or decrease in particular disease states, or in response to inflammation, age, or autoimmunity. Such correlative data in patients could suggest a potential role for these populations in human disease.

Clearly, the description of this discrete population of extrathymic *Aire*-expressing cells in the secondary lymphoid organs raises many more questions than it answers. Hopefully the further study of this novel population will provide some insight into the mechanisms that maintain self-tolerance in the immune system, and perhaps identify useful tools to more precisely manipulate such systems in the context of autoimmunity.

References

1. Burnet FM. A Modification of Jerne's Theory of Antibody Production using the Concept of Clonal Selection. The Australian Journal of Science 1957;20:67-9.
2. Jolicoeur C, Hanahan D, Smith KM. T-cell tolerance toward a transgenic beta-cell antigen and transcription of endogenous pancreatic genes in thymus. Proc Natl Acad Sci U S A 1994;91:6707-11.
3. Antonia SJ, Geiger T, Miller J, Flavell RA. Mechanisms of immune tolerance induction through the thymic expression of a peripheral tissue-specific protein. Int Immunol 1995;7:715-25.
4. Kappler JW, Roehm N, Marrack P. T cell tolerance by clonal elimination in the thymus. Cell 1987;49:273-80.
5. Kisielow P, Bluthmann H, Staerz UD, Steinmetz M, von Boehmer H. Tolerance in T-cell-receptor transgenic mice involves deletion of nonmature CD4+8+ thymocytes. Nature 1988;333:742-6.
6. Derbinski J, Schulte A, Kyewski B, Klein L. Promiscuous gene expression in medullary thymic epithelial cells mirrors the peripheral self. Nat Immunol 2001;2:1032-9.
7. Anderson MS, Venanzi ES, Klein L, et al. Projection of an immunological self shadow within the thymus by the aire protein. Science 2002;298:1395-401.
8. Nagamine K, Peterson P, Scott HS, et al. Positional cloning of the APECED gene. Nat Genet 1997;17:393-8.
9. An autoimmune disease, APECED, caused by mutations in a novel gene featuring two PHD-type zinc-finger domains. Nat Genet 1997;17:399-403.
10. Lee JW, Epardaud M, Sun J, et al. Peripheral antigen display by lymph node stroma promotes T cell tolerance to intestinal self. Nat Immunol 2007;8:181-90.
11. Nichols LA, Chen Y, Colella TA, Bennett CL, Clausen BE, Engelhard VH. Deletional self-tolerance to a melanocyte/melanoma antigen derived from tyrosinase is mediated by a radio-resistant cell in peripheral and mesenteric lymph nodes. J Immunol 2007;179:993-1003.
12. Yip L, Su L, Sheng D, et al. Deaf1 isoforms control the expression of genes encoding peripheral tissue antigens in the pancreatic lymph nodes during type 1 diabetes. Nat Immunol 2009;10:1026-33.

13. Heino M, Peterson P, Sillanpaa N, et al. RNA and protein expression of the murine autoimmune regulator gene (Aire) in normal, RelB-deficient and in NOD mouse. Eur J Immunol 2000;30:1884-93.

14. Guerau-de-Arellano M, Martinic M, Benoist C, Mathis D. Neonatal tolerance revisited: a perinatal window for Aire control of autoimmunity. J Exp Med 2009;206:1245-52.

15. Karpati S, Amagai M, Prussick R, Stanley JR. Pemphigus vulgaris antigen is a desmosomal desmoglein. Dermatology 1994;189 Suppl 1:24-6.

16. Haeryfar SM, Hoskin DW. Thy-1: more than a mouse pan-T cell marker. J Immunol 2004;173:3581-8.

17. Schwartz RH. A cell culture model for T lymphocyte clonal anergy. Science 1990;248:1349-56.

18. Norton SD, Zuckerman L, Urdahl KB, Shefner R, Miller J, Jenkins MK. The CD28 ligand, B7, enhances IL-2 production by providing a costimulatory signal to T cells. J Immunol 1992;149:1556-61.

19. Hawiger D, Inaba K, Dorsett Y, et al. Dendritic cells induce peripheral T cell unresponsiveness under steady state conditions in vivo. J Exp Med 2001;194:769-79.

20. Zhou X, Bailey-Bucktrout SL, Jeker LT, et al. Instability of the transcription factor Foxp3 leads to the generation of pathogenic memory T cells in vivo. Nat Immunol 2009;10:1000-7.

21. Lin MS, Fu CL, Aoki V, et al. Desmoglein-1-specific T lymphocytes from patients with endemic pemphigus foliaceus (fogo selvagem). J Clin Invest 2000;105:207-13.

22. Marinkovich MP, Taylor TB, Keene DR, Burgeson RE, Zone JJ. LAD-1, the linear IgA bullous dermatosis autoantigen, is a novel 120-kDa anchoring filament protein synthesized by epidermal cells. J Invest Dermatol 1996;106:734-8.

23. Liston A, Lesage S, Wilson J, Peltonen L, Goodnow CC. Aire regulates negative selection of organ-specific T cells. Nat Immunol 2003;4:350-4.

24. Anderson MS, Venanzi ES, Chen Z, Berzins SP, Benoist C, Mathis D. The cellular mechanism of Aire control of T cell tolerance. Immunity 2005;23:227-39.

25. Scheinecker C, McHugh R, Shevach EM, Germain RN. Constitutive presentation of a natural tissue autoantigen exclusively by dendritic cells in the draining lymph node. J Exp Med 2002;196:1079-90.

26. Mukhopadhaya A, Hanafusa T, Jarchum I, et al. Selective delivery of beta cell antigen to dendritic cells in vivo leads to deletion and tolerance of autoreactive CD8+ T cells in NOD mice. Proc Natl Acad Sci U S A 2008;105:6374-9.

27. Poliani PL, Kisand K, Marrella V, et al. Human Peripheral Lymphoid Tissues Contain Autoimmune Regulator-Expressing Dendritic Cells. Am J Pathol.

Appendix:
Selected Protocols

Thymectomy/Thymic Transplant/Bone Marrow Chimerism

(A) Thymic harvest

(1) One week before transplantation, select donor mice. The donor mice should be neonatal (pink and furless, ~1-2 days old… see image below), so if genotyping is required it should be done in the intervening week. In this case, we used 2 d.o. pups, all wt NOD.

(2) Bring mice up to lab. They will not survive too long (more than a few hours) away from mother, so only bring them up when you are ready to proceed. Prepare materials:

Dissecting Scope
Styrofoam dissecting board with paper towels and pins
Scissors and two pair of tweezers
Sterile Complete DMEM-hi
2-Deoxyguanosine
12-well plate
Transwell Plate (Costar 12-well)

(3) Fill 12-well plate, 1 well/mouse, with 1mL of sterile complete DMEM. Harvest is done on the benchtop, then transferred to the hood when putting in the transwell plate, so the procedure overall is semi-sterile.

D10F:

General mouse lymphocyte cell culture medium (D10F), 500 mL

reagent	**amount**
DMEM with high glucose (4.5 g/L)	429.5 mL
HEPES (1M)	5 mL
heat inactivated FCS	50 mL
GlutaMax-I (200mM)	5 mL

NEAA (100X)	5 mL
2-mercaptoethanol **prediluted to 50mM** (1000X)	0.5 mL
Penn/Strep (100x)	5 mL

Vacuum filter through a 0.22 um membrane to ensure sterility.

(4) Cover dissecting board with paper towels. Quickly decapitate mice with scissors above the shoulders, so forelimbs remain attached.

(5) Pin the back side of the shoulders with two pins and the hindquarters with one pin. Make two cuts with scissors along the sides of the ribcage, cutting from the trachea outward to just inside the forelimbs and down the length of the ribcage (but cutting outside the ribcage itself).

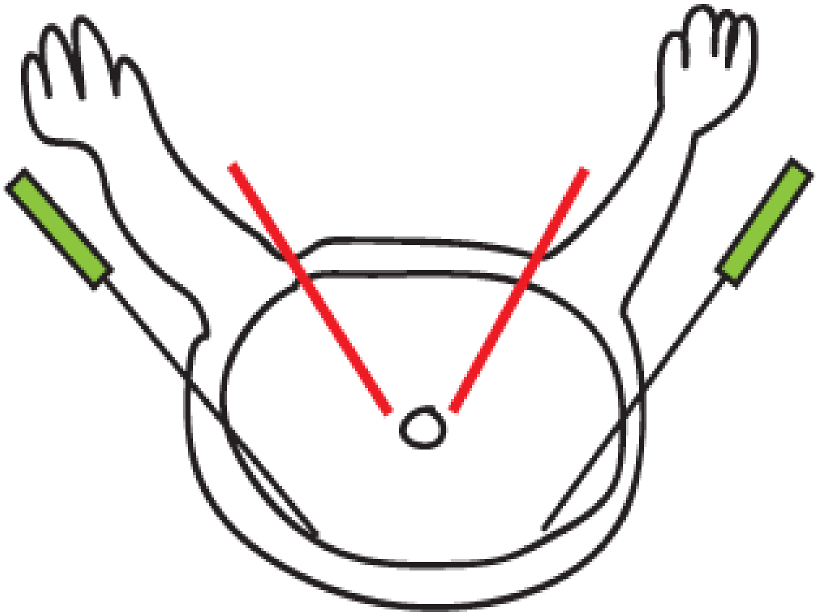

(6) Using foreceps, pull open the ribcage, exposing the thorax. Under the dissecting scope (or not), the two thymic lobes should be obviously visible as large white ovals sitting on top of the heart. Remove the thymi intact with foreceps, trying not to tear them in the process. Place both thymic lobes in one well of DMEM in the 12-well plate. Also if you want to genotype, remember to **CUT THE TAIL** into a PCR tube labeled to correspond to the thymic well, and get the tail processed for genotyping. In this case there is no need, as they are all wildtype NOD mice.

(7) Once all thymi are removed, make up 2-DG media for depletion of lymphocytes in the hood:

1.35mM 2-deoxyguanosine in complete DMEM-10.
(2-DG: 285.26g/mole, so 36mg/100mL)

Sterile-filter using a steriflip.

(8) In the hood, pipette 2mL/well of 2-DG media into the BOTTOM wells of the 12-well transwell plate. Place 1-2 drops of media in top well just for your own peace of mind (although it will equilibrate on its own). Transfer thymic lobes onto the mesh of the upper well, 1 well/donor.

(9) Culture at 37 degrees for 7 days.

(10) The evening before transplant, replace 2-DG media with regular complete DMEM.

(B) Thymectomy/kidney capsule thymic transplant

A surgical procedure for thymectomy of mice followed by transplantation of thymi under the kidney capsule. We are using wt thymi that have been cultured for a week in 2-deosyguanosine-containing media (see above).

(1) Prepare necessary reagents:

Sterile drape
Autoclaved or sterilized tools (fine foreceps, stapler, foreceps with teeth, scissors)
Fine silicone tubing
Alcohol Prep Pads
Heating pad
Thymi in 12-well Costar transwell plate in DMEM
Fine-gauge Corning Silastic tubing (to push thymus under capsule)
Electrocautery

Anesthetic/Analgesic
Sterile suture (6-0 silk is good)
Nair
Sterile Q-tips
Vial of sterile PBS
25-gauge needle tip
Ehrlenmeyer flask and surgical tubing to hook up to vacuum apparatus
Clean styrofoam operating board
Rubber Bands (4-6 large)
Insulin syringes (3-4)
Alcohol Prep Pads
Razor Blades (2-3)
5mL pipettes (4-5)
P1000 tips, NON-barrier

(2) Prepare appropriate drug formulations for anesthesia and analgesia:
Anesthetic: Ketamine /Xylazine (80mg/kg/ 10mg/kg)
Analgesic: Buprenorphine/Flunixin (0.05mg/kg)

Average mouse weight ~0.025kg, so want to inject 2mg Ket and 0.25mg Xyl per mouse in 100uL. For smaller mice, adjust dosage (70uL works well for ~50do mice; 100uL works well for ~90do mice) Thus, final concentrations should be:
20mg/mL Ket
2.5mg/mL Xyl

Stock solutions of both at 100mg/mL. Thus, in 1mL final solution, should have:
200uL Ket
25uL Xyl
775uL sterile saline

(3) Bring all materials down to procedure room. Select recipient mice

(4) Prepare a 5mL pipette to accept P1000 tips for suction. Break 5mL pipette in half, discard the front (tapered) half, and remove cotton plug from back half. Attach one end of this pipette to the surgical tubing connected to the Ehrlenmeyer vacuum flask.

In order to fit inside a P1000 tip, the new tip of this pipette must be “shaved” down slightly using a razor blade:

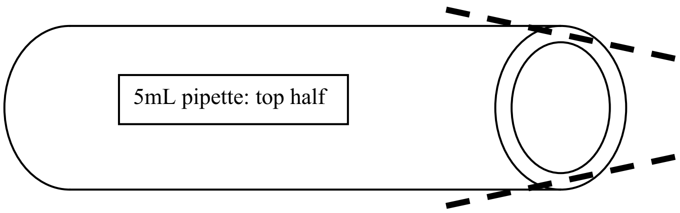

It’s also helpful to **CUT A SMALL HOLE** in the side of the 5ml pipette tip with the razor blade that can be occluded with your finger during suction. This allows for much greater control of the amount of suction at the appropriate times.

(5) Prepare P1000 tips for thymic suction by cutting a larger opening with a sterile razor blade on a sterile drape.

For immunosufficient thymi, you need a relatively large-diameter tip opening to suck the thymus, but apparently you don’t want it to be either too large or too small—based on Helene’s cuts, the hole should be large enough that the end of a P20 Pipetman can just fit inside. Cut enough to have at least one per animal, with some to spare. Store these tips in a sealed container until use. However, for SCID mice, which have a very small thymus, you need a much smaller-diameter tip, small enough that a P10 Pipetman can just fit inside. A small-diameter tip can also be useful for thymectomy of replete hosts, if you want to use the suction to “grab” the thymus and then pull it out manually with foreceps.

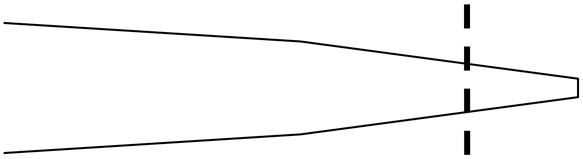

(6) Bring all reagents in plastic sheath down to the mouse house.
Need to use a procedure room with a vacuum attachment, and the only one accessible on our floor is in the first hallway, all the way down near the end of the hall on the left. This room is communal, so if you want to use it a specific time you should **SIGN UP** in advance on the sheet of paper on the room's door.

(7) Put down sterile drapes on bench. Set up styrofoam surgery board covered with a sterile drape and three rubber bands to restrain the mice as displayed below (only after removal of hair on left flank; restrain before step 12). Note there is an error in diagram below—horizontal rubber band (head restraint) should be ABOVE vertical restraint bands.

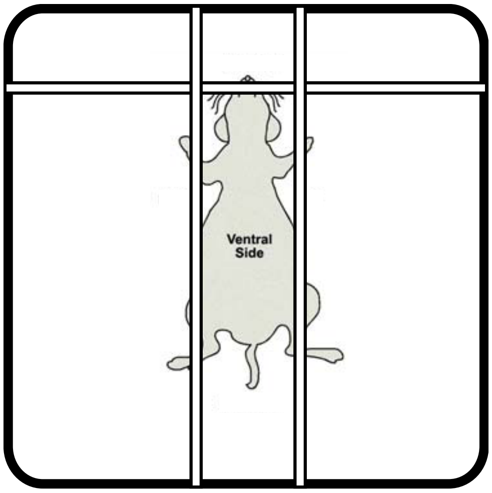

(8) Anesthetize mice using Ketamine/Xylazine mixture, 100ul/~25g mouse. Inject INTRAMUSCULAR or SUB-Q, not IP, as this has faster onset and longer duration. Wait until mouse is completely anesthetized before proceeding. Test paw withdrawal reflex after light pinch on all four limbs.

(9) Set up "sterile" field. Turn on lamp above field reasonably close to provide additional heat. Wash hands with EtOH

(10) Order of operations is as follows: Shave and Nair left flank, then thymectomize, then thymic transplant. Begin by removing hair around left-side flank and back region using clippers and then Nair, making sure the Nair gets rubbed into the follicle bases to completely remove hair from the field. Flank should be just clean pink skin on the mouse's left side in an area about the size of a quarter, stretching from the bottom of the ribage down to the innominate bone, and stretching back to almost the vertebra.

(11) Wash area with EtOH and clean up remaining Nair.

(12) Wet chest and neck area thoroughly with alcohol prep pad. Using scissors, make a 2cm-incision from middle of neck to middle of chest, below the 3rd rib line (see both diagrams below). Spread the incision on either side by cutting away at the subcutaneous connective tissue:

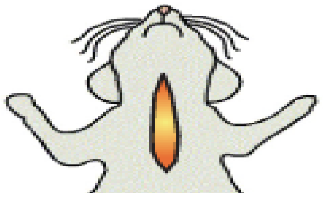

(13) This will expose the salivary glands on the rostral side of the incision, and the rib cage on the caudal side of the incision. Cut the connective tissue away from the bottom of the salivary glands and reflect them up and out of the incision toward the head. Some small amount of bleeding may occur during this cutting. Use a sterile q-tip to blot away any blood.

(14) Using a pair of sharp scissors, make a single cut in the ribcage down the midline to the 3rd rib. This point is defined by a small white line or chevron pointing rostrally:

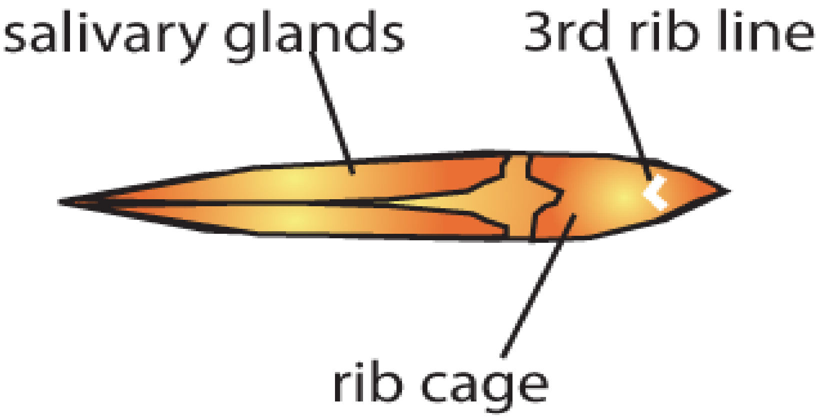

(15) Prepare other reagents needed for actual thymectomy: curved dull foreceps, curved sharp foreceps, active (1/2 strength) vacuum with cut tip, stapler with staples.

(16) Using dull curved foreceps, pull up on the left side of the rib cage. Insert the vacuum tip into the chest cavity deep enough to draw out the thymus, being careful to avoid vessels and the heart, and not completely occluding the opening so as to prevent a pneumothorax. The SCID thymus is very small, while wt thymi at this age are quite large. Depending on preference, you can either use vacuum to suck out thymus or can remove manually with foreceps after "grabbing" it with suction. For SCIDs you must grab it and manually remove, for wt animals you can do either. Make sure you get BOTH LOBES INTACT out of the chest, and spread them out on a paper towel to confirm. Also vacuum the opening again after you think it's out to make sure nothing else comes out when you apply suction. **It's better to have a dead mouse than an incomplete thymectomy.**

(17) Once thymus is removed, mouse should still be breathing normally or slightly more rapidly. Immediately after thymus is out, cover the chest opening as best as possible with the salivary gland "flap," then staple the skin closed with three staples proceeding from caudal to rostral. Check that mouse is still breathing normally, then rotate it onto its side to gain access to the shaved lateral flank.

(18) Clean the bare flank with EtOH. Using scissors, make an incision near the back, beneath the spleen and the rib cage, about 1cm long. Then make a similar but slightly shorter incision in the peritoneum beneath.

(19) Wash hands again with EtOH.

(20) Using gloved hands, palpate for the kidney within the abdomen. Should feel hard and bean-like, and be near the spine. Slowly move it up toward the incision, wiggling it past any fat if possible. Squeeze the kidney out of the incision, situating it so that it stays exposed outside the body. It may be easier to first pull out the perirenal fat, and let the kidney come with it. Using locking pickups, grab a bit of perirenal fat or connective tissue near the kidney and clamp it to keep the kidney from sliding back into the body.

(21) Wet the surface of the kidney with a PBS-moistened (or sterile media-moistened) q-tip to prevent drying.

(22) Choose thymus to transplant and place it on the kidney surface. Using sharp foreceps, grab the kidney capsule and make a short incision using the tip of the 25-gauge needle to cut. Place the thymus at the edge of the incision and use the plastic tubing to push it under the capsule and away from the incision. It is best to do this process on the FLAT SIDE OF THE KIDNEY, not on the curved apex, as this makes it easier to tear when you push the thymus under.

(23) Once thymus is inserted and pushed far enough away from the incision site, cauterize the incision on the kidney lightly.

(24) Re-insert the kidney and any other externalized viscera into the body. First tuck it through the outer skin layer, then through the peritoneum.

(25) Suture the peritoneum closed using 6-0 silk sutures. Staple the skin back together.

(26) Place the mouse on a few paper towels on the heating pad. Check it's not too hot.

(27) Document the thymi transplanted into each mouse, and any notes on each procedure:

(28) Once surgery is complete, provide preventative analgesia for pain control:

Buprenorphine/Flunixin sub-q (0.05mg/kg)

(29) Once mice begin to wake, remove them from the heating pad and place them in the cage, on the heated section of the cage. Do not put anesthetized animals in a cage with awake animals, as the awake mice may become aggressive toward the sleepers. Best to have a "recovery cage" that is also on the heating pad.

(30) Remain with animals until they awaken. Provide additional analgesia at 24 and 48 hours post-operatively. Also put some food pellets in the cage in case they can't reach the food dispenser in the first day or two.

(31) Remove staples at TWO WEEKS post-surgery.

(C) Bone marrow chimerism of thymectomized/ transplanted mice

Mice are suitable for irradiation and BM chimerism as soon as surgical wounds have healed; since staples are removed at two weeks, this is often a good earliest time point to consider irradiation.

Primary irradiation

1. For NODs, want to give ~1300 rads of radiation in two doses, ~900 rads now and then another ~400 rads after at least three hours have passed. First, go to irradiator room on 4th floor of the LARC (near the gowning room) and get the irradiation pie. Bring it back to the mouse room and spray it down with bleach thoroughly.

2. Transfer desired RECIPIENT mice (not donor, obviously) into pie wedges, one or two per wedge. Stuff a paper towel into the open hole to block it and prevent the mice from moving the divider once you are done. Tape the lid down

3. Take the mice down to the irradiator in the pie. Sign in on the irradiator log.

4. Remove the key from the wall safe by pressing “1248.” Turn the key to activate the system.

5. Turn on the compressor switch.

6. Place the mice in the irradiator chamber, checking of course that the source is not raised (door will not open if it’s raised, but check anyway). To open the door, press the red button atop the door and give it a bump with your hip to open it. Put the pie onto the turn wheel, seating it in the outer holes.

7. Turn on the turntable switch, and watch to make sure it is turning. Close the door firmly.

8. Set the irradiation time using the timer. Currently source production is posted on the wall of the irradiator room. To set the timer, first press the R button to reset to zero. Then press the P1 button, and then adjust the digits using the buttons below each digit. Then press E to enter. Then press P1 again to make sure your time was entered. Also check that the SECOND number that cycles through the timer says 0.00. The first should be your time, and the second should be at 0. If not, hit reset and try again. Bring a watch down so you can time it to confirm, and manually lower the source if necessary.

9. Once the time is entered, press Source Raise. Irradiation will begin. **Time the exposure** to make sure the timer is working. If it exceeds the time, you can stop by pressing Source Lower. Remove mice and return them to cages to rest.

Initial isolation of bone marrow

1. Take selected donor mice back to lab for harvesting. Wash out pie with bleach and return it to the irradiator room.

2. On benchtop, remove all long bones from the donor mice (femurs, tibia, humeri) and strip muscle from bone using scissors and kimwipes. Place appendages containing bones into a Petri dish containing DMEM (nonsterile at this point).

3. Transfer bones in dish to the hood, along with another sterile Petri dish of DMEM poured in the hood for each sample group. Clean bones further if necessary and separate them from one another. Once clean, take each bone and cut off the two ends. Then transfer the shaft (along with the two ends if large enough) to the sterile dish, draw up DMEM from the dish into an insulin syringe and flush the marrow from the bone. Do the same with the ends. The shaft should bleach white when it is clean. Discard the empty bones.

4. When all bones have been cleaned, use a 10mL pipette tip to dissociate all the clumps by pipetting up and down a few times, then transfer the media containing the BM cells into a 50mL Falcon tube, passing through a cell-strainer cap. Wash the dish with an additional 10mL of sterile media (or appropriate amount to balance tubes) and transfer this wash to the tube.

5. Centrifuge at 1200rpm for 5 min at 4 degrees. Decant supernatant and resuspend the cells in 2mL per mouse of DMEM (6mL in this case). Keep cells on ice.

Complement depletion of CD4/CD8 cells

1. Add 1uL of anti-CD4 (clone GK1.5, 4mg/ml) per mouse. Then add 1uL of anti-CD8 (clone YTS 164.5, 4mg/ml) per mouse. Incubate **15 minutes** on ice, mixing every 5 minutes.

2. During incubation, warm 10mL of sterile DMEM in 37 degree water bath. Also remove one tube of rabbit complement **per up to three mice** and thaw on ice. For larger cohorts, split into multiple samples of three mice or less each.

3. Once incubation is complete, add pre-warmed DMEM to each sample. Then add 1mL of rabbit complement and incubate at 37 degrees for **30 minutes,** in rotator inside incubator.

4. Add 30mL DMEM, spin for 5 min at 1200rpm at 4 degrees, and wash again with 30mL DMEM, spinning again. Resuspend pellet third time in 20mL sterile HBSS, filter through a 70um mesh into a new tube to remove clumps, and count cells while the tubes are spinning a final time (1200rpm, 5 min, 4 deg.).

5. Need to inject a **minimum of 5 million cells per recipient, preferably 10 million, in a volume of 200uLof sterile HBSS.** This means a desired concentration of 5e7 cells/ml. Also if possible, want to have a significant excess for making mistakes during injection (not that mistakes ever happen).

6. Spin cells at 1200rpm for 5 min at 4 degrees and resuspend in the appropriate volume of Hank's BSS to achieve 5e7 cells/mL. Transfer cells to a 1.5mL eppendorfs, place in a small ice container (50mL conical) and transport them down to the LARC.

Secondary irradiation

1. Return the mice to the irradiator and repeat steps from primary irradiation, but in this case 400 rads.

2. Bring mice back to the room and transfer back to cages. Wash the pie and return it to the irradiator room.

Injection of BM

1. Remove injection restraint from drawer and clean it thoroughly. Attach it to the hood surface. Place a food pellet in the back of the restraint for the mouse to rest on; prevents them from jumping as much. Select a group of mice and warm them with the heat lamp, being careful not to overheat them. Mice should show whisker-cleaning behavior when they are warm.

2. Select an appropriate syringe: should have the bevel oriented in such a way that it is faced up when the syringe is comfortably in your hand ready to inject. Bevel orientation is random on the syringes, so if you have one with a bad orientation, throw it away and try another.

3. Using one insulin syringe per BM sample (or until it gets cloggy), draw up BM solution after flicking tube to resuspend. Select the appropriate mouse and place it securely in the restraint. Do not use plunger. Inject 200uL of solution into the tail vein. Approach the vein at a shallow angle with the tail slightly bent over your finger and rotated to access the lateral veins… otherwise it's easy to go through it. It is very superficial. Don't try to force it, as this means you're not in the vein. Also, if you're in the vein, you'll see it flush all the way up when you inject.

4. Clean the wound site and return the mice to their cages. In mice where the donor cells don't take, the mice should die after about ten days. Those mice that survive should be completely reconstituted by eight weeks.

Stromal Preparation for FACS

Digestion Media:

DMEM (Hi Glucose)	**15 mL**	**30 mL**	**50 mL**
2% HI FBS	300 uL	600 uL	1 mL
0.125% Collagenase D	18.75 mg	37.5 mg	62.5 mg
100 ug/mL DNase I	15 uL	30 uL	50 uL
100 ug/mL Collagenase/Dispase	15 uL	30 uL	50 uL

Percoll Densities:

1.124

Percoll Stock	9 mL	27 mL	45 mL	
10x PBS	1 mL	3 mL	5 mL	

1.115

1.124 Percoll	9.274 mL	18.548 mL	27.822 mL	37.096 mL
1x PBS	0.726 mL	1.452 mL	2.178 mL	2.904 mL

1.065

1.124 Percoll	5.24 mL	10.48 mL	15.72 mL	20.96 mL
1x PBS	4.76 mL	9.52 mL	14.28 mL	19.04 mL

Tissue Isolation and Digestion

1) Collect thymi, pooled LNs, and spleens from each animal place into separate small Petri dishes with 5 mL digestion media (RT). Mince organs with new, clean razor blades until small enough to easily be sucked through tip of glass Pasteur pipette.

2) Transfer minced organs and media to labeled 15 mL conical tubes using glass Pasteur pipette tips. Use 3 mL of digestion media to rinse remaining tissue from Petri dishes and then add to the conical tubes.

3) Place conical tubes containing minced organ tissue and 8 mL digestion media into a 37° C water bath for 40-50 minutes with periodic mixing of contents via glass pipettes (every 10 minutes).

4) When sufficient time has passed and only clumps of connective tissue (esp. in the LNs) remains, spin down cells at 1200 rpm for 5 min at 4° C.

5) Resuspend thoroughly in 5 mL cold AutoMACS buffer (1x PBS, 0.5% BSA, 2mM EDTA) to remove clumps and stop digestion, and leave on ice for 10 minutes.

6) Spin down cells at 1200 rpm for 5 min at 4°C. During spin, coat 15ml conicals with FCS.

Stromal Cell Isolation

7) Resuspend cells in 4 mL dense (1.115) Percoll and transfer through 100um cell-strainer into new FCS-coated tubes.

8) Create a Percoll gradient by gently layering 2 mL of light (1.065) Percoll onto the heavy fraction, followed by 2 mL of 1x PBS.

9) Spin the tubes for 30 minutes at 2700 rpm, 4° C, with the break set to 0 and the acceleration set to 5. During the spin, the stromal cells will settle at the boundary between the light Percoll and 1x PBS, while the lymphocytes will be between the light and heavy Percoll fractions.

10) Remove the stromal fraction with a disposable transfer pipette, and save the dense lymphocyte fraction of a GFP- sample for compensation controls. Resuspend in FACS buffer to a net volume of 5 mL for stromal cells and 10 mL for lymphocytes.

11) Count cells.

FACS Staining

12) Identify the antibodies to be used for staining:

- [GFP] (in cells from transgenic animals)
- CD45 PerCP
- MHC Class II (I-Ag^7 or pan-MHC in A647)

13) Make a master mix with each antibody at 1 uL per 100 uL FACS buffer. Split lymphocyte fraction into necessary compensation control tubes.
14) Add 2.4G2 at 1:100 in FACS buffer to cells at 100 uL per 10 million cells with a minimum of 100 uL volume per tube (it is likely that all tubes will have 100 uL). Incubate on ice for 10 minutes.
15) Add an equal volume of the master mix to the tubes, and add 1 uL comp Ab to appropriate tubes. Incubate covered on ice for 20 minutes.
16) Wash 2-3 x in FACS buffer.

Publishing Agreement

It is the policy of the University to encourage the distribution of all theses, dissertations, and manuscripts. Copies of all UCSF theses, dissertations, and manuscripts will be routed to the library via the Graduate Division. The library will make all theses, dissertations, and manuscripts accessible to the public and will preserve these to the best of their abilities, in perpetuity.

I hereby grant permission to the Graduate Division of the University of California, San Francisco to release copies of my thesis, dissertation,or manuscript to the Campus Library to provide access and preservation, in whole or in part, in perpetuity.

Author Signature

03/25/10

Date